

https://dspace.org/

Production of Nano silicon particles from sugarcane bagasse ash for solar cell application

Farirai, Fortunate

2020
https://hdl.handle.net/10539/30078

Downloaded from a DSpace repository. https://dspace.org/



UNIVERSITY OF THE
WITWATERSRAND,
JOHANNESBURG

PRODUCTION OF NANO SILICON PARTICLES FROM SUGARCANE BAGASSE ASH FOR SOLAR CELL APPLICATION

Fortunate FARIRAI

(1660060)

A Thesis Submitted to the Faculty of Engineering and the Built Environment, University of the Witwatersrand, Johannesburg, South Africa, in fulfillment of the requirements for the degree of Doctor of Philosophy in Engineering.

Main Supervisor: Professor Michael DARAMOLA

Co-Supervisor: Dr. Mathew MUPA

April 2020

Candidate's Declaration

I declare that this dissertation is my own unaided work. It is being submitted for the degree of Doctor of Philosophy in Engineering to the University of the Witwatersrand, Johannesburg, South Africa. It has not been submitted before for any degree or examination to any other University

. …….. 02nd …… day of…April ……../2020…….



Signature of Candidate

Dedication

I dedicate this thesis to the True Living God Almighty, the God of Abraham, Isaac, Jacob and Professor Ezekiel Handinawangu Guti, God have been faithful to me. This thesis is also dedicated to my loving, caring, supportive husband, Wisdom Tatenda Farirai, my loving sons, Tanatswa, Tatenda, Tinodaishe, my late mother (Mary Mlilo), my late grandparents (Langeni and Soneni Mlilo), my parents in-law (Lazarus and Mable Farirai) and finally to all the Mlilo and Farirai families.

Abstract

Beneficiation of solid waste like agricultural waste materials as renewable sources of energy for sustainable and renewable energy production is well applauded. Silicon (Si), a major semiconductor material used in the production of solar cells has been obtained from sugarcane bagasse ash, a solid waste product from sugarcane processing industries. Currently, pure silicon is obtained from quartz via a high energy-intensive carbothermal process, translating into a huge operating cost, and consequently, the high cost of the solar cells produced thereof.

Sugarcane bagasse ash, a waste product from sugar and bio-ethanol processing industries, has been conventionally used as an additive to cement due to its good pozollanic properties and high silica content. For valorization of wastes, the complete characterization of the materials is necessary for potential applications. Therefore, the first investigation of this study was to carry out the composition analysis of sugarcane bagasse and its ash to ascertain its suitability for the production of nano silicon. The chemical composition, surface chemistry, degree of crystallinity, calorific value, and morphology were checked by XRF, FTIR, XRD, bomb calorimetry, SEM and TEM. The results showed that sugarcane bagasse ash contains silica and other oxides. The sugarcane bagasse bottom ash contained 71.49 wt. % silica. The FTIR results revealed the presence of polymerized silica between the wave number 1011 cm^{1} and 1080 cm^{-1}. The ash content of raw sugarcane bagasse obtained was 5.2 wt. %. The moisture content, volatile matter and fixed carbon were 6.4, 58.54 and 29.86 wt%, respectively.

Optimization by citric acid leaching was conducted prior to extraction. The optimum conditions obtained for acid concentration, temperature and time were 2 M, 90 ^{o}C and 60 minutes,

respectively. In this study, sol-gel coupled with adsorption, using activated carbon was used to then extract high purity amorphous silica from the sodium silicate solution produced. in the leaching process.

Physicochemical characteristics of the extracted silica samples were checked using XRF, XRD, FTIR, N_2 adsorption-desorption method, SEM and TEM. Most metal impurities which included iron, manganese, magnesium, calcium, potassium, titanium and chromium were adsorbed by the activated carbon due to its large specific surface area of 1308 m^2/g which enhances the physical adsorption of dissolved or dispersed substances from the solution. Amorphous nano-silica of 98.92% purity with a particle size range of 6-24 nm was obtained. From the N_2 adsorption-desorption analysis, the silica powder exhibited the following properties: 240 m^2/g for specific surface area, 0.58 cm^3/g average pore volume, and 10 nm for average pore diameter.

The extracted silica was used as the precursor in the production of nano silicon by a magnesiothermic reduction for 4 h at 700 ℃, followed by acid leaching of unreacted magnesium and silica. The physicochemical properties of the as-produced silicon sample were checked using Raman spectroscopy, Fourier Transform Infrared spectroscopy and N_2 physisorption at 77 K. A strong peak around 520 cm^{-1} were observed from the Raman spectrum, confirming the presence of crystalline silicon. The FTIR analysis reveals a sharp peak between 1010 - 1050 cm^{-1}, indicating the presence of Si-O-Si functional group. N_2 physisorption at 77 K reveals that the surface area, pore volume and pore diameter of the as-produced silicon was 30.14 m^2/g, 0.19 cm^3/g and 25 nm, respectively. The produced silicon nanoparticles were incorporated into the hole transport layer poly(3,4- ethylene dioxythiophene)-poly(styrene sulfonate) (PEDOT:PSS) of an organic solar cell

based on a blend of poly(3-hexylthiophene) (P3HT) and [6:6]-phenyl-C61butyric acid (PCBM). Consequently, 4 solar cell devices were fabricated: F1 (reference cell), F2 (with SiO_2NPs), F3 (with SiNPs) and F4 (with p-type SiNPs) in the hole transport layer (PEDOT: PSS). The current-voltage (J-V) characteristics of the solar cells were analyzed to establish the performance of the P3HT: PCBM organic solar cells. The power conversion efficiency (PCE) of the fabricated cells achieved 0.83% (F1), 0.001% (F2), 0.14% (F3) and 0.63% (F4). From this study, a proof of concept for the application of SiNPs in solar cells has been established. However, this work opens an area for future work to improve the PCE.

Acknowledgements

To the Great God, the God of Abraham, Isaac, Jacob and the Apostle of my time Professor Ezekiel Handinawangu Guti. Glory and Honor be unto You Lord Jesus Christ. It was not an easy road, but I am grateful that I have reached this far. Good health and strength to work anytime during this research is worth appreciating.

My sincere appreciation and gratitude go to my supportive advisor/supervisor, Professor Michael Olawale Daramola, for mentoring, directing, training and teaching me waste valorization into useful materials. I am appreciative of your support, patience, kindness and constructive criticism which have shaped me to be from a mere researcher into an independent researcher. The touching event when you requested to meet with my family when they visited me here in South Africa, I felt your unconditional love towards me and my family. It showed that you want a complete person and you support academics who also prioritize family. I was deeply moved and motivated to keep on keeping on. Thank you, Professor. I will continue to look up to you as a mentor and seek collaboration in future projects.

When I applied for PhD, Professor Iyuke was to be my supervisor, however when I came early 2017 for registration that was when I learnt he was no longer with the school. I am sincerely grateful for how you had the faith in me to take me as your student. Thank you very much Professor for your selflessness to share knowledge with me.

You trained me in many ways, I got a chance to be a daily supervisor for two 4th year students Lufuno, Rinae**,** and an MSc student**,** Precious Ntombikhayise Bhengu. Prof, this really was a great experience for me. Thank you very much for the opportunity. Furthermore, I would want to thank you for the support you gave me when I told you that I was going to contest at the 10th Wits Cross-

Faculty Research Symposium doing Grad Flash. Indeed, I contested and was awarded second place Grad Flash in the Faculty of Engineering and the Built Environment. I appreciate your support.

Special gratitude goes to my co-supervisor Dr. Mathew Mupa from Bindura University of Science Education in Zimbabwe. He assisted me to access the laboratories to conduct part of my experimental work and gave constructive criticism which helped me to reach where I am now. I also appreciate him for being a fatherly figure and helping a lot in this work. In the same thread, I would like to express gratitude to Engineer Fungai Mutandwa of Green Fuels Zimbabwe, for assistance in the form of technical advice and necessary raw materials.

I wish to express my special mention and gratitude to Professor Nosipho Moloto, Professor Daniel Wamwangi, Dr. Mildred Airo and Dr. Francis Otieno from the Wits School of Chemistry and Physics for their support and selflessness in allowing me to fabricate my solar cells in their laboratories. Dr Mildred and Dr Francis, we are like family now. Thank you very much for your immense contribution in this work. For sure, we are going to have future collaborations.

Also, I would like to extend thanks to Mr. Sancho Nkosilathi Nyoni, Dr. Olawumi Sadare, Miss Chenai Mlandu, Miss. Olayile Ejekwu, Mr. Maxwell Ozonoh, Mr. Thomas Aniokete, Dr. Chipo Shonhiwa, Mr. Mothlatsi, Ms Janet Smith, Ms. Ntokozo Dube, Mr. Hardlife Rambawasvika, Mr. V. Chiduku, Mr. T. Chayamiti, Mr. Godfrey Mawire, Nyasha Machakaire and many others from either the Wits School of Chemical and Metallurgical Engineering and the Department of Chemistry at Bindura University. You indeed made the time spent in this study and laboratories enjoyable and unforgettable. Thank you for your kindness and assistance.

I wish to thank the Sustainable Energy and Environment Research Unit (SEERU) research group colleagues and the School of Chemical and Metallurgical Engineering for the moral support. Wits University for the Post Graduate Merit Award which helped me on my tuition and quarterly stipend which was of importance to me for my welfare.

Regarding my family, my personal team, I run short of words. When I think of the difficult time I went through leaving my husband with the kids, I cry. These become tears of joy when I see that the sacrifice was for a good cause. I would like to give a special thanks to my loving, caring husband, Wisdom Tatenda Farirai, for his selflessness, sacrifice, love, and understanding; the list is endless. You are a great supporter, team player, great father to our boys. To our three boys Tanatswa, Tatenda and Tinodaishe, thank you boys for allowing mom to go to school leaving you behind. Love you my family.

To Sekuru Lazarus and Mbuya Mable Farirai you are gifts from God to have such parents (inlaws) like you. I usually say mom and dad in-love not in-law. I thank you my mother, Ms Alice Mlilo. To Gogo Getrude Mudodo words won't be enough to say thank you for the work you did taking care of the kids in my absence. May God bless you. To all the Mlilo and Farirai families, I say thank you all for your support.

To my ZAOGA FIF family I want to thank you for the prayers and moral support through this journey. A special mention to the Great Apostle of my time Prof. E. H. Guti and Dr. E. Guti for introducing me to the faithful and true God, to Overseers S and S Musiza, Overseers G and W Musvipa, Pastors E and H. Musiza, Pastors R and S Madzivanyika, Pastors S and N Mangwende, Pastor S. Siwela, Pastors K and B Mudamburi and Pastors P and A Supu. Elders Mr. and Mrs. Murimba, Elders Mr. and Mrs. Govo, Elders Mr. and Mrs. Mandevere, Elder Mrs. Magwehere,

Elders Simbarashe and Chipo Mutizwa. I thank you. To my friends Tofara, Tonderai, Rumbidzai, Natsayi, Angela, Loveness and Rutendo I would like to thank you for the moral support.

I also want to thank the Scientific and Industrial Research and Development Centre management and staff for their continuous support throughout the studies. To TWAS-OWSD International (UNESCO) for providing funding to visit the Department of Physics at University of Catania in Sicily, Italy and Abdus Salam International Centre for Theoretical Physics in Trieste, Italy.

Special thanks goes to Organization for Women in Science for the Developing World Zimbabwe National Chapter for the encouragement we were giving each other on our platform. It really helped me a lot.

To Wise Petroleum, Genesis Energy management and staff, I would want to thank you.

It was not going to be possible to get where I am now without you all.

Publications and Presentations

The following is a list of submitted papers and papers under review related to this work.

Book Chapter and Journals:

1. **Farirai, F**., Shonhiwa, C., Mupa, M. and Daramola, M.O. (2019) Compositional Analysis of Zimbabwean Sugarcane Bagasse Ash towards Production of Nano Silicon for Solar Cell Application. *In* Valorization of Biomass to Value-Added Commodities. M.O Daramola and A.O Ayeni, Eds. Springer Nature Publisher (In press)
2. **Farirai, F**., Ozonoh, M., Aniokete, C.T., Eterigho-Ikelegbe, O., Zeyi, B., Mupa, M. and Daramola, M.O.(2020) Methods of Extracting Silica and Silicon from Agricultural Waste Ashes and Application of the Produced Silicon in Solar Cells, A mini-review. International Journal for Sustainable Engineering, DOI: 10.1080/19397038.2020.1720854.
3. **Farirai, F**., Mupa, M., Daramola, M.O. (2020) An improved method for the production of high purity silica from sugarcane bagasse ash obtained from a Bioethanol Plant Boiler. Particulate Science and Technology, DOI: 10.1080/02726351.2020.1734700
4. **Farirai, F**., Airo, M.A., Otieno, F.O., Mupa, M. and Daramola, M.O., Sugarcane bagasse ash derived nano silicon for application in organic-inorganic hybrid solar cell (submitted).

Peer Reviewed Conference Proceedings:

1. **Farirai, F**., Shonhiwa, C., Mupa, M. and Daramola, M.O., Sol-gel Coupling Adsorption Method for Extraction of High Purity Silica from Sugarcane Bagasse Ash for Solar Cell Application. Poster Presentation. 27th European Biomass Conference and Exhibition, p.1436-1438. ISBN 978-88-89407-19-6, DOI: 10.5071/27th EUBCE 2019-3DV.4.17. 27-31 May 2019. Lisbon, Portugal.

2. **Farirai F**., Airo, M.A., Sadare, O., Mupa, M. and Daramola, M.O., Magnesiothermic reduction of silica from sugarcane bagasse ash into silicon for solar cell application: A Preliminary Investigation. 6th Southern Africa Solar Energy Conference. 25-27 November 2019. East London, South Africa.

Presentations:

1. **Farirai F**., Shonhiwa, C., Mupa, M. and Daramola, M.O., Compositional Analysis of Zimbabwean Sugarcane Bagasse Ash towards the Production of nano silicon for solar cell application. Oral Presentation. 12th Zimbabwe International Research Symposium. 13-15 February 2019. Harare, Zimbabwe.
2. **Farirai, F**., Mupa, M., Daramola, M.O., Sol-gel Coupling Method for Extraction of High Purity Silica from Sugarcane Bagasse Ash for Solar Cell Application. Grad Flash Presentation. 10th Cross Faculty Postgraduate Research Symposium. 3-4 September 2019, University of Witwatersrand, Johannesburg, South Africa (2nd Prize Faculty of Engineering and the Built Environment).
3. **Farirai, F**., Airo, M.A., Otieno, F.O., Mupa, M. and Daramola, M.O., Sugarcane bagasse ash derived nano silicon for application in inorganic-organic hybrid bulk heterojunction solar cells. Oral Presentation. Seminar. 21 November 2019, Department of Physics, University of Catania, Sicily, Italy.

Table of Contents

Chapter 1 : Introduction 1

1.1 Introduction 1

1.2 Background and Motivation 1

1.3 Problem Statement 9

1.4 Research Aim, Questions and Objectives 10

1.5 Research Benefits and Novel Contribution to Knowledge 11

1.6 Thesis Layout 12

Chapter 2 : Literature Review 14

2.1 Introduction 14

2.2 Overview of Agricultural Waste and the Disposal Techniques 18

2.2.1 Disposal of Agro Waste 18

2.2.2 Agro-Waste Reuse 20

2.3 Agro Waste Sources for Nano Silica and Silicon 22

2.3.1 Rice husk ash 23

2.3.2 Corn cob ash 24

2.3.3 Wheat straw ash 25

2.3.4 Sugarcane bagasse ash 28

2.3.5 Demerits of bio-sourced ash from biomass-firing heaters 31

2.4 Production of Silicon Nanoparticles 34

2.4.1 Pulsed laser ablation (PLA) 35
2.4.2 Heating degradation 36
2.4.3 Ball milling 37
2.4.4 Physicochemical methods 37
2.4.5 Chemical techniques 38
2.4.6 Electrochemical techniques 40
2.4.7 Surface modification 40
2.5 Drawbacks and Benefits of Different Methods 42
2.6 Methods of Characterization of Silicon Nanoparticles 45
2.7 Characterization of Si NPs 47
2.8 Solar Cell Technologies 52
2.8.1 Current trends in solar cell technology 55
2.8.2 Methods of silicon solar cell fabrication 57
2.8.3 Nano Photovoltaics (Silicon Nanoparticles in Solar Cells) 59
2.8.4 Bulk heterojunction organics solar cells (OSCs) 60
2.8.5 Silicon nanoparticles enhancing properties of OSCs 62
2.8.6 Challenges of producing nano silicon from agro waste 63
2.9 Concluding Remark 64
Chapter 3 : Methodology 66
3.1 Introduction 66

3.2 Chemicals and Chemical Reagents 66
3.3 Sugarcane Bagasse Ash Availability and Sampling Procedure 67
3.3.1 Assumptions 67
3.4 Sampling Method 68
3.4.1 Sugarcane bagasse ash (SCBA) 69
3.4.2 Comprehensive characterization of sugarcane bagasse ash 69
3.4.3 Leaching and thermal treatment of sugarcane bagasse ash (SCBA) 70
3.4.4 Extraction of nano silica from sugarcane bagasse ash 70
3.5 Magnesiothermic Reduction of Nano Silica into Nano Silicon 72
3.6 Instrumental Characterization of Nano Silica and Nano Silicon 73
3.6.1 X-ray fluorescence spectrophotometry 74
3.6.2 X-ray diffractometry 74
3.6.3 Fourier transform infrared spectrophotometry 74
3.6.4 Nitrogen physisorption 75
3.6.5 Scanning electron microscopy 75
3.6.6 Transmission electron microscopy 75
3.7 Fabrication of Organic Solar Cell 75
3.7.1 Doping of nano silicon particles 76
3.7.2 Organic solar cell fabrication 76
3.7.2.1 Substrate cleaning 76

3.7.3 Thermal Evaporation 79
3.8 Solar Cell Characterization Techniques 80
3.8.1 Raman spectroscopy 80
3.8.2 Atomic force microscopy 80
3.8.3 Optical properties and I –V characteristics 81
3.9 Concluding Remark 81
Chapter 4 : Chemical and Physicochemical Analysis of SCB, SCBBA and SCBFA 82
4.1 Introduction 82
4.2 Experimental 84
4.3 Results and Discussion 84
4.3.1 XRF analysis 84
4.3.2 Ash content, calorific value and elemental composition 86
4.3.3 FESEM-EDX analysis 88
4.3.4 FTIR analysis 91
4.3.5 XRD analysis 93
4.3.6 Thermogravimetric analysis 94
4.4 Concluding Remark 96
Chapter 5 : Extraction of Silica from SCBA 97
5.1 Introduction 97
5.2 Experimental 99

5.2.1 Investigation of the effect of leaching condition on the pre-treatment of SCBA with citric acid 99

5.2.2 Enhancement of silica purity using sol-gel coupling adsorption method 100

5.3 Results and Discussion 101

5.3.1 Characterization of SCBA 101

5.3.2 Enhancing purity of extracted silica using sol-gel coupling adsorption method .. 107

5.3.2.1 Chemical composition of silica-A and silica-B 107

5.3.2.2 Degree of crystallinity of silica-A and silica-B 109

5.3.2.3 Surface nature of silica-A and silica-B 110

5.3.2.4 Textural properties of silica-A and silica-B 111

5.3.2.5 Morphology of silica-A and silica-B 113

5.4 Concluding Remark 116

Chapter 6 : Production of Nano Silicon and Hybrid Organic Solar Cell 118

6.1 Introduction 118

6.2 Experimental 120

6.2.1 Production and characterization of nanosilicon from SCBA-derived silica using magnesiothermic reduction 120

6.2.2 Production of hybrid organic solar cell and performance evaluation 120

6.3 Results and Discussion 123

6.3.1 Production of nanosilicon 123

6.3.1.1 Degree of crystallinity of produced nanosilicon 125

6.3.1.2 Determination of level of impurity in waste water produced after washing of nano silicon 126

6.3.1.3 Surface chemistry of produced nanosilicon 128

6.3.1.4 Raman spectroscopy for nano silicon..... 129

6.3.1.5 Textural properties of nanosilicon..... 131

6.3.1.6 Morphology of the nanosilicon 132

6.3.2 Fabrication and performance evaluation of hybrid organic solar cell 135

6.3.2.1 Scanning electron microscopy (SEM)..... 135

6.3.2.2 Atomic force microscopy/ surface roughness 136

6.3.2.3 UV-vis spectroscopy 138

6.3.2.4 J-V characterization..... 139

6.4 Concluding Remark..... 142

Chapter 7 : General Conclusions and Recommendations 144

7.1 Conclusions 144

7.2 Recommendations 145

References 147

Appendices 188

8.1 Appendix 1 188

List of Figures

Figure 2-1 Industrial process to produce single crystalline Si cells from quartz (Tao, 2008) 17

Figure 2-2 Scheme depicting some methods of agricultural waste disposal 19

Figure 2-3 Percentage of silica in selected agro-waste ashes (Kazmi et al., 2016; Bhagiyalakshmi et al.,..... 22

Figure 2-4 Schematic of mechanism of ash formation and deposition on a super heater tube (Shao et al., 2012) 33

Figure 2-5 Silicon nanoparticles characterization techniques..... 46

Figure 2-6 XRD patterns of nanosilicon at different sintering temperatures. Adapted from Venkateswaran..... 47

Figure 2-7 Particle size distribution of nano silicon at different sintering temperatures Venkateswaran et al. (2013) 48

Figure 2-8 FTIR spectrum of nano silicon at different sintering temperatures. Adapted from 48

Figure 2-9 TEM images of nano silicon at different sintering temperatures Venkateswaran et al. (2013)..... 49

Figure 2-10 UV–Vis Absorption Spectra of Nano Silicon at Different Sintering Temperatures . Adapted..... 49

Figure 2-11 Solar cell working mechanism. Adapted from Kumar et al. (2016) 53

Figure 2-12 NREL data on the progress in efficiency of thin film based solar cells from 1975-2020 (National Renewable Energy Laboratory, 2020)..... 54

Figure 2-13 Stages to produce crystalline silicon solar cells from quartz. Adapted from Goetzberger et al. (2003) 58

Figure 2-14 Quantum-confined Si-NPs Can Be Used as a High Bandgap Layer in Lieu of Other Materials, Allowing for a Multi-Bandgap Solar Cell Composed Entirely of Silicon (Adapted from Klafehn, 2016). 60

Figure 2-15 Operational sequence of an organic solar cell (Adapted from Otieno et al. (2018*)*.. 61

Figure 3-1 Overview of the methodology employed in this study 66

Figure 3-2 Sugarcane bagasse ash (a) and the source plant at Green Fuels, Chisumbanje (b)..... 67

Figure 3-3 As received (a) sugarcane bagasse bottom ash (b) sugarcane bagasse fly ash (c) sugarcane bagasse 69

Figure 3-4 Experimental flow diagram for the extraction of nano silica from sugarcane bagasse ash 72

Figure 3-5 Synthetic steps in the magnesiothermic reduction of SCBA nano silica into nano silicon 73

Figure 3-6 Chemical structures of (a) poly (3, 4-ethylene dioxythiophene (PEDOT), (b) poly(styrene sulfonate) (PSS), (c) [6,6]-phenyl-C61-butyric acid methyl ester (PCBM), and (d) poly(3-hexlythiophene) P3HT) (Otieno et al., 2016)..... 78

Figure 3-7 (a) Illustration of spin coating procedure (b) Cross-sectional area of an organic solar cell incorporated with SiNPs (b) (adapted from Otieno (2015) with minor modifications)..... 79

Figure 3-8 Thermal evaporation set-up for application of aluminum cathode to the device..... 80

Figure 4-1 a) Morphology b) Spectrum of SCB 88

Figure 4-2 Morphology b) Spectrum for SCBBA 89

Figure 4-3 a) Morphology b) Spectrum of SCBFA 89

Figure 4-4 FTIR spectra for the (SCB), (SCBBA) and (SCBFA) 92

Figure 4-5 XRD pattern for SCB, SCBBA and SCBFA (Q-quartz, Cri-cristabolite & Tri-Tridymite) 93
Figure 4-6 Thermogravimetric curve of SCB, SCBBA and SCBFA samples..... 94
Figure 5-1 Summary of the enhancement of the purity of sodium silicate before precipitation of silica. 101
Figure 5-2 3D response surface plot for the effects of temperature (A), time (B) and acid concentration (C) on the extraction of SiO_2..... 106
Figure 5-3 XRD pattern for SCBA, commercial grade silica, silica (A) and silica (B) 109
Figure 5-4 Surface chemistry of SCBA, commercial grade silica, silica (A) and silica (B) 110
Figure 5-5 Nitrogen adsorption-desorption isotherm for A-SCBA, B-commercial grade silica, C-silica (A) and D-silica (B)..... 111
Figure 5-6 SEM images for (A) SCBA (B) commercial SiO_2 (C) silica-A (D) silica-B..... 113
Figure 5-7 TEM images and corresponding particle size distribution for A) commercial grade SiO_2, B) silica-A and C) silica-B..... 115
Figure 6-1 Schematic diagram of the hybrid organic solar cell..... 121
Figure 6-2 The J-V characteristics of a solar cell in the dark and under illumination; The equivalent circuit diagram. 122
Figure 6-3 Nano silica (A), nano silicon (B) and fabricated solar cell devices (C)..... 123
Figure 6-4 XRD pattern for commercial grade silicon, nano silicon washed with aquaregia and nano silicon washed with 2 % HF..... 125
Figure 6-5 Trace elements in wastewater after washing nano silicon with aquaregia and 2% HF 127
Figure 6-6 Surface chemistry for commercial grade silicon, Nano-Si_{AQ} and Nano-Si_{HF} 129

Figure 6-7 Raman spectrum for the synthesized nano silicon (Nano-Si_{HF})..... 130

Figure 6-8 BET isotherms and pore size distribution curves for A) commercial grade silicon B) Nano-Si_{AQ} and C) Nano-Si_{HF}..... 131

Figure 6-9 SEM micrographs for A) commercial grade silicon B)nano-Si_{AQ} and C) Nano-Si_{HF}. 133

Figure 6-10 (a) TEM micrograph of nano-Si_{AQ} and (b) corresponding particle size distribution 134

Figure 6-11 (a) TEM micrograph of nano-Si_{HF} and (b) corresponding particle size distribution 134

Figure 6-12 (a)TEM micrograph of commercial-grade silicon and (b) particle size distribution 135

Figure 6-13 Surface morphology of fabricated solar cell devices A) reference cell, F1, B) F2, C) F3, D) F4..... 136

Figure 6-14 AFM images of A) reference B) F2 C) F3 D) F4..... 137

Figure 6-15 Solid-state uv-vis measurements of the thin films F1, F2, F3 and F4..... 139

Figure 6-16 J–V characteristics, recorded under illumination at 100 mW cm^{-2} (AM 1.5G) of reference device F1 and devices with SCBA-derived SiO2 NPs and p-type SCBA-derived SiNPs incorporated into the PEDOT: PSS layer..... 140

Figure 6-17 J–V characteristics, recorded under illumination at 100 mW cm^{-2} (AM 1.5G) of devices with SCBA SiNPs incorporated into the PEDOT:PSS layer. 141

Figure 6-18 Energy-level diagram of a hybrid organic solar cell structure 142

List of Tables

Table 1-1 Renewable energy potential capacity in Zimbabwe 2

Table 1-2 The chemical composition of sugarcane bagasse ash (SCBA) from selected countries 8

Table 2-1 Renewable energy resources and their application (Panda et al., 2006) 15

Table 2-2 Composition of selected agricultural wastes 21

Table 2-3 Synthesis of nanoparticles from selected agro waste sources using various processing routes 26

Table 2-4 Physicochemical composition of sugarcane bagasse ash from different countries 30

Table 2-5 Methods of producing silicon nanoparticles starting with different precursors 43

Table 2-6 XRF results for SiNPs produced by Venkateswaran et al. (2013) 50

Table 2-7 Conversion efficiencies of selected thin film solar cells 56

Table 3-1 Annual estimated quantity of sugarcane bagasse ash produced 68

Table 4-1 Chemical composition of SCB, SCBBA and SCBFA 85

Table 4-2 Physicochemical characterization of sugarcane bagasse samples 87

Table 4-3 EDX elemental composition of SCB, SCBBA and SCBFA 90

Table 5-1 Levels and coded factors of parameters for 2-3 design 100

Table 5-2 The designed experiment and responses 103

Table 5-3 Analysis of variance (ANOVA) 104

Table 5-4 Chemical composition of raw ash, silica-A and silica-B 108

Table 5-5 Textural properties of the samples 112

Table 6-1 Device structures 120

Table 6-2 Elemental composition of commercial grade silicon and synthesized nano silicon 124

Table 6-3 Textural properties of commercial grade silicon, Nano-Si_{AQ} and Nano-Si_{HF} 132

Table 6-4 Summary of tapping mode AFM analysis 137

Table 6-5 Summary of the performance of devices with different structures 140

List of Symbols and Abbreviations

a-Si	amorphous silicon
AFM	atomic force microscopy
AM	1.5G solar spectral irradiance: air mass
BET	Brunauer–Emmett–Teller method
BJH	bulk heterojunction
c-Si	crystalline silicon
CH	coffee husk
CSP	concentrated solar power
CVD	chemical vapor deposition
CZ	Czochralski
DSS	directional solidification system
EDX	energy-dispersive x-ray spectroscopy
Eg	energy band gap
EMC	electromagnetic casting
eV	electron Volt
FTIR	Fourier transform infrared spectroscopy
FWHM	full width at half maxima
GS	ground nut shell
GW	gigawatt
GWh/a	gigawatt hours per annum
HEM	heat exchange method
ITO	indium tin oxide

MG-Si	metallurgical grade silicon
MW	megawatt
Nano-Si_{AQ}	silicon nanoparticles washed with aquaregia
Nano-Si_{HF}	silicon nanoparticles washed with hydrofluoric acid
OSCs	organic solar cells
P3HT	poly (3-hexylthiophene-2, 5-diyl) regioregular
PCE	power conversion efficiency
PLA	pulsed laser ablation
PCBM	[6, 6]-phenyl-C61-butyric acid methyl ester
P Si	porous silicon
PSD	particle size distribution
PV	photovoltaic
RE	renewable energy
RHA	rice husk ash
RH	rice husk
R_{ku}	kurtosis
R_{ms}	root mean square
R_{sk}	skewness
SCB	sugarcane bagasse
SCBA	sugarcane bagasse ash
SCBBA	sugarcane bagasse bottom ash
SCBFA	sugarcane bagasse fly ash
SEM	scanning electron microscopy
Si	silicon

SiO_2	silicon dioxide
SiNPs	silicon nanoparticles/ nano silico particles
Si QDs	Silicon quantum dots
TEM	transmission electron microscopy
UV	ultra violet
UV-Vis	ultra violet – visible spectroscopy
VHF	very high frequency
XRF	x-ray fluorescence
XRD	x-ray diffraction

Chapter 1 : Introduction

1.1 Introduction

In this chapter, the motivation for this research and the research objectives are clearly explained. The benefits of the research effort to the scientific and industrial community are also highlighted.

1.2 Background and Motivation

Zimbabwe is located in Southern Africa and it covers an area of over 390 000 km^2. It is a landlocked country bordered by Zambia, Botswana, Mozambique and South Africa. The country has sub-tropical climatic conditions, with one rainy season, between December and April (Muzari et al., 2016). Currently, the country is experiencing acute electricity shortages which are primarily met through the insufficient generation of electricity at the country's hydropower and thermal power plants (Makhanda et al., 2019). In addition, the country imports all its petroleum fuels at great cost resulting in increased costs of business activities (Makonese et al., 2018).

The electricity energy need of Zimbabwe is approximately 2000 MW, but generation statistics given by the power generation monopoly the Zimbabwe Power Company indicate that less than 800 MW are produced (ZPC., 2020). National access to electricity is estimated at 40%, but access is much lower in rural areas, at approximately 19% (Muhumuza et al., 2018). The rural communities meet 80- 90% of their energy needs from traditional fuels, mainly wood fuel while approximately 15- 30% of urban households use wood as the main cooking fuel (Makonese et al., 2018). However, the country has abundant renewable energy resources which can be sustainably exploited for the benefit of her citizens. These resources include biomass, hydropower along the

country's rivers and dams, wind energy, geothermal, and solar energy (Somorin et al., 2019). Table 1-1 presents an overview of the renewable energy potential capacity in Zimbabwe.

Table 1-1 Renewable energy potential capacity in Zimbabwe

Renewable Energy Resource	Estimated Capacity	Reference
Wind	40 GW	(Chigumira et al., 2019)
Solar	Photovoltaic (PV) 109 GW Concentrated Solar Power (CSP) 40 GW	(Chigumira et al., 2019)
Hydro	90-120 GWh/a	(Makonese, 2016)
Biomass/Biogas	1000 MW	(Makonese, 2016)
Geothermal	50 MW	(Makonese, 2016)

The potential capacity of solar photovoltaics in Zimbabwe is estimated at 109 GW. Therefore, it is important to explore the feasibility of harnessing the energy source to benefit the citizens. Globally, solar photovoltaics has vast potential as a clean, abundant and economical energy resource but the technology faces the challenge of low power conversion efficiency in existing solar cell materials (Armaroli and Balzani, 2007). Silicon has an optimum bandgap for sunlight absorption (Zhao et al., 2019) but this is not a necessary and sufficient condition since it has an indirect bandgap A high photo-conversion efficiency of about 25% has been achieved in silicon solar cells. The major advantages relevant for photovoltaic application, such as low toxicity, abundant raw material and scalable solar cell fabrication processes (Yoshikawa et al., 2017). In

recent years, research has focused more on new photovoltaic systems that incorporate optically active nanostructures such as nanoparticles, quantum dots, nanotubes, nanorods and nanowires, which offer great potential for new device structures (Peng et al., 2010). Nayfeh et al. (2007) reported a 60% improvement in power performance when using silicon solar cells in the ultraviolet range of the electromagnetic spectrum by integrating high film of silicon nanoparticles directly onto the solar cell. Silicon (Si) is a valuable metalloid whose applications range from being an additive in aluminum and ferrous alloys in structural applications to produce solar panels for renewable energy and to semiconductors for electronics (Zulehner et al., 2000). Metallurgical grade silicon (MG-Si) with purity usually at 99% is processed from quartz sand (SiO_2) (Islam et al., 2011). The conventional method used to obtain silicon from quartz involves high energy to melt the quartz (50 kWh/kg) (Tao, 2008). Silicon is then produced through the reduction of silica using carbon but the reaction also results in the formation of a by-product (carbon dioxide) that is detrimental to the environment (Adebisi et al., 2017).

The incorporation of silicon nanoparticles into solar cells promises advantages such as improvement in the power conversion efficiency (Lopez-Delgado et al., 2016). This may result in cheaper solar power in the future and reduce manufacturing costs since (printing-like) technology can then be used to produce solar panels as flexible rolls rather than discrete panels, making them easier to install (Hermann, 2004). Klafehn (2016) states that the main source of interest in silicon nanoparticles (Si-NPs) arises from the unique effect that quantum confinement has on silicon. The bandgap possessed by silicon is normally 1.12 eV, allowing it to collect light with energy above the bandgap efficiency, while absorption of higher energy photons leads to excess energy above the bandgap being lost as heat. As the size of SiNPs decreases below 10 nm in diameter, the

bandgap can be increased to 1.8 eV, allowing for efficient collection of radiation of higher energy wavelengths.

Solar cells can be categorized based on their materials of construction. Inorganic solar cells use elements such as silicon and gallium while organic solar cells use organic molecules and polymers. The former is more popular due to their relatively higher power conversion efficiencies (PCE) (~ 25%) and comparative longer lifespan (25-30 years). In contrast, organic solar cells have lower efficiencies (~5%) and shorter lifespan (5 years) (Orgil, 2018). To commercialize organic solar cells, the major focus area is the improvement of the PCE.

Several studies have been conducted to improve the PCE, such as the tuning of certain parameters like optical properties of the blend (P3HT: PCBM) (Zhu et al., 2015), donor material absorbance through mixing energy band-engineered polymers to increase the absorption bandwidth (Yang et al., 2015), optimization of formation of domain and size (Ding et al., 2018; Dowland et al., 2013; MacLachlan et al., 2015; Morgenstern et al., 2016), and engineering the interfacial area (Pfadler et al., 2014).

Another approach which has gained interest among researchers is the introduction of inorganic semiconductor particles in the active ingredient of the organic solar cells resulting in the advent of hybrid solar cells (Zhou et al., 2011). Several inorganic particles such as ZnO (Bhat et al., 2011; Hames et al., 2010; Takanezawa et al., 2008), TiO_2 (Kuo et al., 2008), PbS (Tsang et al., 2009), PbSe (Tan et al., 2009), SnO_2 (Kudo et al., 2007), $CuInS_2$ (Arici et al., 2003), CdTe (Gur et

al., 2006), CdS (Lee et al., 2008; Wang et al., 2007) , CdSe (Yang et al., 2011) have been utilized and reported.

The utilization of elemental silicon nanoparticles in hybrid bulk heterojunction solar cells was first explored by Liu et al. (2008). The SiNPs was incorporated in poly-3-(hexylthiophene) and the results were a maximum power conversion efficiency of 1.15% (Liu et al., 2008). With further optimization of the processing parameters, electrode selection and choice of active material, the PCE of the hybrid solar cell improved to 1.47% (Liu et al., 2010). According to Zhao et al. (2016), the PCE improved by incorporating SiNPs into P3HT: PCBM solar cells, creating a cascade band structure.

Size reduction and doping are some of the effective ways to fine-tune the energy levels of semiconducting nanoparticles. To understand the utilization of doped SiNPs in hybrid solar cells, silicon nanoparticles with various dopants (n-type and p-type) have been synthesized and subsequently used with active material. The preferred reference material in such fundamental studies in hybrid solar cells is the material blend P3HT:PCBM (Chi et al., 2014). Hemaprabha et al. (2018) reported the use of n-type and p-type nano silicon in P3HT: PCBM at various weight percentages and their effect on solar cells parameters. The PCE obtained using doped p-type silicon nanoparticle was 3.46%. The team proposed that the addition of nanoparticles could improve the energy levels through doping and mixing with optimized weight ratios in addition to reducing the size of SiNPs.

In the same view, the profitability of the solar cell manufacturing industry can also be boosted when a low-cost waste material such as sugarcane bagasse ash is used to produce silicon (Lund et al., 2000). Sugarcane is grown commercially in the Lowveld of Zimbabwe which includes Chisumbanje, Nyanyadzi and Chiredzi (Scoones et al., 2017), and it is the second-largest export earner in the agricultural sector after tobacco in Zimbabwe. Tongaat Hullets, located in Chiredzi is one of the key players in the production of raw sugar in Zimbabwe. Sugar production creates waste by-products, such as sugarcane bagasse, that can still be used for added profitability (Aigbodion et al., 2010).

Currently, sugarcane bagasse is used as a fuel in power-generation boilers which supply electricity to these industries (Pandey et al., 2000). However, the use of sugarcane bagasse in boilers results in an ash residue called sugarcane bagasse ash (SCBA). SCBA is used as a filler to reinforce building materials and as a fertilizer in sugarcane fields (Jose et al., 2019). One of the potential elements present in this solid waste, SCBA is silicon (Norsuraya et al., 2016). Sugarcane is known to absorb more silicon than any other mineral nutrient in the soil in the form of silicic acid (H_4SiO_4) and accumulates to approximately 380 kg/ha of Silicon (Si) in a 12-month-old crop (Savant et al., 1999). Silicon in this solid waste is in the form of silica (SiO_2). Natural silica is alleged to be safe to handle, cheap and can be extracted from cheap sources (Norsuraya et al., 2016).

Researchers worldwide have reported on the potential applications of silica obtained from biowaste, including sugarcane bagasse ash (Ferreira-Leitao et al., 2010). However, the silica content in sugarcane bagasse ash is highly dependent on the geographical location, environmental conditions, as well as the farming practices. From a study that was conducted by Du Preez (1970)

in South Africa, treatment of soil with silicate-containing fertilizers resulted in an increase in cane yield as the silica concentration increases in the plant (Du Preez and others, 1970). Sugarcane in Hawaii is normally a two-year crop while in most countries it is a one-year crop. Both soluble and total silicon reflected differences in soil and irrigation water silicon (Haynes, 2019)**.** Mauritius was one of the first countries to adopt the use of silicate materials as soil amendments in sugarcane plantations. The result was an increase in yield due to the increased number of millable stalks and increased plant size (Savant et al., 1999). The chemical composition of a typical sugarcane bagasse ash is shown in Table 1-2. The variations observed from country to country, as shown in Table 1-2, call for the need to explore its extraction as reported in this study. The extracted silica could be converted into silicon via environmentally benign and energy-efficient processes as shown in this thesis. Consequently, the produced silicon could be explored in the production of solar cells as a renewable source of energy.

Table 1-2 The chemical composition of sugarcane bagasse ash (SCBA) from selected countries

% Constituents in Sugarcane bagasse Ash (SCBA) from Selected Countries							
Constituents	Brazil		Columbia	Nigeria	Uganda	Zimbabwe	
in SCBA	A	B					
SiO_2	31.41		96.2	72.8	60.98	62.1	71.49
Al_2O_3	7.57		0.2	6.4	7.39	5.54	6.2
Fe_2O_3	6.02		1.7	5.5	6.07	5.42	3
CaO	16.06		0.1	3.8	12.66	1	3.3
MgO	1.07		<0.1	2.3	2.51	1.12	1.37
K_2O	1.58		0.3	2.7	3.53	2.22	4.79
Na_2O	0.14		-	1.2	0.15	0.81	-
SO_3	0.78		0.1	-	1.23	-	-
TiO_2	2.09		0.2	-	-	-	-
MnO	0.1		-	-	-	-	0.14
Chloride	0.14		-	-	-	-	-
P_2O_5	-		0.1	-	-	-	0.61
LOI	32.2		1.04	3.7	4.8	-	0.31
Reference	(Castaldelli et al., 2013)		(Sales and Lima, 2010)	(Torres Agredo et al., 2014)	(Otuoze et al., 2012)	(Basika et al., 2015)	Current Study

Against this background, this thesis concentrated on the characterization of sugarcane bagasse and its ash, extraction of silica from the ash, conversion of the extracted silica into silicon; and application of the produced silicon in the production of organic solar cells. (Lund et al., 2000) reported that there is potential to produce high purity silicon from biomass which is as a cheap alternative source to quartz sand.

1.3 Problem Statement

Bioethanol and sugar-producing industries are found in the Lowveld region of Zimbabwe**.** The bagasse produced by these companies is used as fuel in biomass-firing boilers, producing bagasse ash which is used, to a limited extent, in the sugarcane plantations as fertilizer. The disposal of bagasse ash waste, therefore, poses a dumping challenge to the environment. Currently**,** there is very little published information available on the production of silicon nanoparticles from sugarcane bagasse ash for solar cell application. Furthermore, quartz is at present the main source of silicon for solar cell application. It is obtained by sand mining, which has detrimental effects on the environment such as land degradation, erosion, fissures, and adverse effects on water supply and quality. Metallurgical-grade silicon (MG-Si) (600 000 tons/year) is produced through high-temperature carbothermal reduction of the quartz which requires an energy input of 50 kWh/kg and is then beneficiated into solar-grade silicon using the Siemens process which requires an additional energy input of 200 kWh/kg. The first stage is represented by Equation 1.1:

$$SiO_2(s) \xrightarrow[\text{charcoal}]{1900\,^{\circ}C} Si(s) + CO_2(g) \qquad \textit{Equation 1.1}$$

The process strongly contributes to environmentally unfriendly greenhouse gas emissions because of the several million tons of CO_2 that are released into the atmosphere per annum to meet the targeted production of MG-Si. The use of plant biomass as the source of silicon instead of quartz sand may address this environmental concern. The extraction of high purity silicon from sugarcane bagasse ash will not only add economic value to this bio-waste material but also increase process efficiency for the ethanol and sugar industries and promote environmental care by being an alternative process to sand mining activities.

Organic solar cell production, however, still faces challenges primarily related to a low power conversion efficiency (PCE) which reduces their commercialization. The incorporation of nanosilicon to the organic solar cells is hypothesized to be potentially capable of improving the PCE while concurrently retaining, to an extent, the desirable lightweight and flexibility of organic solar cells.

1.4 Research Aim, Questions and Objectives

Based on the above problem statement, the aim of the study was to produce nano silicon particles from sugarcane bagasse ash for solar cell application. To provide a logical direction to the study, the questions below were posed:

1. Can silica of desirable quality usable in producing high purity silicon nanoparticles be extracted from sugarcane bagasse ash via an environmentally benign and energy-efficient process?
2. Can high purity silicon nanoparticles be obtained based on the outcome of (1)?
3. Can a hybrid organic solar cell with reasonable power conversion efficiency (PCE) be produced using high purity silicon obtained in (2)?

Based on the research questions highlighted above, the specific objectives of the study were;

1. To characterize the sugarcane bagasse ash (SCBA) obtained from an ethanol-producing company in Zimbabwe and extract the silica from the SCBA using environmentally friendly process.
2. To propose and apply an energy-efficient process for the conversion of the extracted silica into pure silicon nanoparticles.
3. To fabricate a hybrid organic solar cell using the produced pure silicon and evaluate its performance.

1.5 Research Benefits and Novel Contribution to Knowledge

Previous research has primarily reported on nano silicon production from rice husk ash, corn cob ash and wheat straw ash but this research focuses more on the utilization of sugarcane bagasse ash as a potential source of silicon nanoparticles. It led to the production of high -purity nano silicon particles using sugarcane bagasse ash waste. The source of nano silicon particles is renewable and low-cost and has potential to be a substitute for quartz. The process was found to be potentially energy-efficient in contrast to the commercial process utilizing quartz as the precursor material. Solar cell development was a topical issue in this research since there is a need to increase the power conversion efficiency (PCE) if solar energy is to reach parity with grid electricity. A hybrid organic solar cell of improved PCE resulted from the approach used in this experiment.

From the literature survey, most researchers have reported on the utilization of sugarcane bagasse ash as a substitute to cement in concrete because of its high silica content with good pozollanic properties. This work opened a new area for sugarcane bagasse ash valorization as a source of

silicon for solar cell application. The novel contribution has been communicated to the researchers working in a similar research area and other related areas through the publication of articles in international journal and conference proceedings.

1.6 Thesis Layout

Chapter 1: This chapter gives the background introduction, motivation on the reason the research was conducted. Its originality and novelty contribution to the body of knowledge is presented. The research questions, aims and objectives are also stated. The outline of the whole thesis is highlighted.

Chapter 2: This chapter contains detailed literature review presenting the current methods for the extraction of silica from various agro waste, the preparation of nano silicon from different precursors, and methods that have been used to characterize the nano silicon. It also highlighted the methods for the fabrication of solar cells, current trends and the challenges in the field. A review paper based on this chapter has been submitted to a journal.

Chapter 3: This chapter presents the general methodology of the research study. The materials and methods used in this research are described. This chapter also describes the synthesis of the nano silicon particles from sugarcane bagasse ash waste. The fabrication of the solar cell material. Characterization techniques used to analyze the sugarcane bagasse ash waste, nanosilica; nano silicon and the solar cell material produced are also detailed in this chapter.

Chapter 4: Compositional analysis and organic acid leaching of SCBA is presented in this chapter. Based on the former, a manuscript in the form of a book chapter has been produced and submitted for publication.

Chapter 5: The extraction of silica by the sol-gel coupling adsorption method is reported and discussed in this chapter.

Chapter 6: In this chapter, the preparation of nano silicon particles by magnesiothermic reduction and the fabrication of the organic solar cell incorporating the synthesized nano silicon particles is discussed and reported.

Chapter 7: This chapter discussed the overall findings and the overall conclusion and recommendations of the research. Suggested future work is also presented in this chapter. References to all articles accessed in this study are presented at the end of all chapters of this thesis.

Chapter 2 : Literature Review

This chapter brings together published information on agro-waste availability, characterization techniques, conversion of silica into nano silicon, and its application in production of solar cells.

2.1 Introduction

The beneficiation of agricultural waste is a topical issue in the field of sustainable and renewable energy production. Literature on recent methods applied to extract silica from different agricultural waste ashes and silicon (Si), a major semiconductor material, from the silica and its application in solar cell technology will be in review. Specific attention is given to such methods as relating to sugarcane bagasse ash, a waste product from the sugarcane processing industry. Also reviewed is the current carbothermal process through which silicon is obtained from an inorganic source, quartz. The chapter also highlights current challenges and opportunities associated with present solar cell production technologies.

Globally, the daily energy demand is increasing with the increase in population, civilization and industrialization. The estimated number of people who totally do not have access to electricity worldwide is 1.1 billion of which 84% of the number lives in the rural communities and 95% are in Sub-Saharan Africa and developing Asia (International Energy Agency, 2017). Some communities only have limited access to electricity and continue to depend on traditional biomass fuel to supplement their energy needs. Such is the case in the rural areas where traditional biomass fuel is still depended on by about 2.7 billion people with the number projected to increase to 2.8 billion by 2030 (Kaygusuz, 2012). However, there are different energy systems and sources from which energy could be produced for the use of mankind. Different sources of energy and methods of production and conversion to other forms to suit different applications are given in Table 2-1.

Table 2-1 Renewable energy resources and their application (Panda et al., 2006)

Energy Sources	Conversion and Applications
Direct Solar	Photovoltaic cells, Thermal power generation
Biomass	Heat and power generation, pyrolysis, gasification, digestion.
Geothermal	Urban heating, power generation, hydrothermal, hot dry rock
Wind	Power generation, wind generators, windmills, water pump
Hydropower	Electrical power generation
Wave and Tides	Numerous designs, barrage, tidal stream, and electrical power generation

Solar photovoltaics have vast potential as the clean, abundant and economical energy source. Armaroli and Balzani, (2007) reported a conversion efficiency range of between 17 to 25 % for silicon-based solar cells. A later report by VonderHaar (2017) places the conversion efficiency of silicon-based single crystalline solar cells above 25% and that of multi-crystalline solar cells above 20%. He et al. (2019) states that the theoretical power conversion efficiency can improve to above 29% for thin crystalline Si solar cells if surface passivation and light-harvesting can both approach their ideal limits**.**

Silicon solar cells have higher photo-conversion efficiency due to the presence of an optimum bandgap for sunlight absorption. Silicon solar cells have major advantages relevant for photovoltaic applications, such as low toxicity, abundant raw material, scalable solar cell

fabrication processes (Yoshikawa et al., 2017). Peng et al., (2010) reported that research is currently focused on new photovoltaic systems that incorporate optically active nanostructures such as nanoparticles, quantum dots, nanotubes, nanorods and nanowires, which offer substantial potential for new device structures. Silicon solar cells power performance improved by 60 % in the ultraviolet range of the electromagnetic spectrum by integrating high film of silicon nanoparticles directly onto the solar cell (Nayfeh et al., 2007). Silicon nanoparticles are promising materials that can be incorporated into solar cells and possess competitive advantages such as flexibility in shape, easy to install, the use of print-like manufacturing process to improve the conversion efficiency (Ludwig et al., 2004).

According to Klafehn (2016), the main interest in silicon nanoparticles (SiNPs) arises from the unique effect that quantum confinement has on silicon. For instance, the band gap possessed by silicon is normally 1.12 eV, allowing it to collect light with energy above the band gap efficiency. However, as the size of SiNPs decrease below 10 nm in diameter, its band gap increases to 1.8 eV, allowing for the efficient collection of higher energy wavelength without significant loss in energy as heat.

Silicon (Si) is the second-most abundant element after oxygen in the earth's crust (Matichenkov and Calvert, 2002). The element is a valuable metalloid and is the primary component of highspeed optical fibres, semiconductors, photovoltaic cells, thin-film transistors, silicon carbide and silicon nitride, among many other applications (Gupta and Gupta, 2016). Silicon is produced by carbothermic reduction of quartz sand at 1900 ^{o}C as shown in Equation 2.1 (Bernardis, 2012):

$$SiO_2(s) + C(s) \rightarrow Si(s) + CO_2(g)$$ *Equation 2.1*

Metallurgical grade silicon (MG-Si) is produced and is approximately 99 % pure and the energy input for this process is about 50 kWh/kg (Tao, 2008). The current global production of MG-Si is approximately 600 000 tones/year , and the production process releases a million tons of greenhouse gases into the atmosphere (Tao, 2008). About 5 % of the 600 000 tons of (MG-Si) is further purified to produce electronic-grade silicon (EG-Si) for the semiconductor industry. The purity of EG-Si is above 99.9999 %. For solar grade silicon (SG-Si), the required impurity level is below ~0.001% (Tao, 2008). A schematic representation of the production of silicon solar cells from quartz/ sand as the source of silicon is summarized in Figure 2-1.

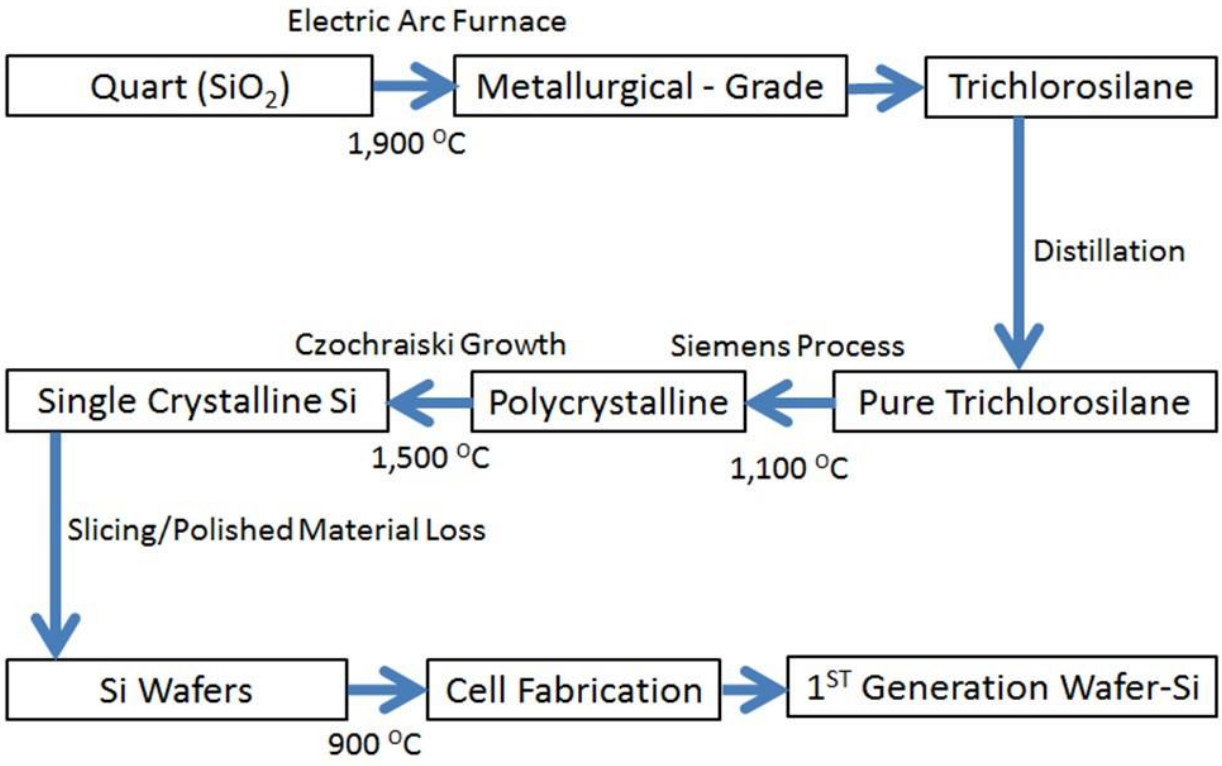


Figure 2-1 Industrial process to produce single crystalline Si cells from quartz (Tao, 2008)

The electric arc furnace requires approximately 1900 ^{o}C to melt sand which translates to 50 kWh of energy to melt a kilogram of sand. Since 600 000 tons of MG- Si are estimated to be produced annually, the approximated energy required could be 30 TWh/kg. It is obvious that the process described above is energy intensive as well as environmentally unsustainable. Based on these findings, there is enough motivation to investigate alternative sources for silicon for solar cell production. Thus, this review specifically concentrates on methods of extracting silica from the agro-waste ashes, methods of converting the extracted silica to silicon and the application of the produced silicon in solar cells. In addition, the review highlights current challenges in the field and proffers suggestions to overcome the challenges as a way of provoking the thoughts of researchers, scientists and stakeholders in the energy sectors.

2.2 Overview of Agricultural Waste and the Disposal Techniques

2.2.1 Disposal of Agro Waste

The conventional system of disposal of agricultural waste is dependent on the chemical and physical properties of the agro waste materials generated. It is pertinent to point out that waste disposal and pollution are inextricably related (Duhan et al., 2017). Under this context, the attention of the world focuses on how best the wastes generated can be disposed of such that they will not pose any threat to the environment. Currently, a few environmental protection laws and regulations have been adopted worldwide under the direction of the United Nations and enacted by local governments to guide various systems of waste or agricultural waste disposals. Momentarily, some of the disposal systems are practiced more than the others, and this may be

attributed to certain factors including cost of disposal, environmental friendliness, properties of the waste, basic needs for the future utilisation of the waste, and many other factors. Figure 2-2 presents the various systems that can be applied to agricultural waste disposal.

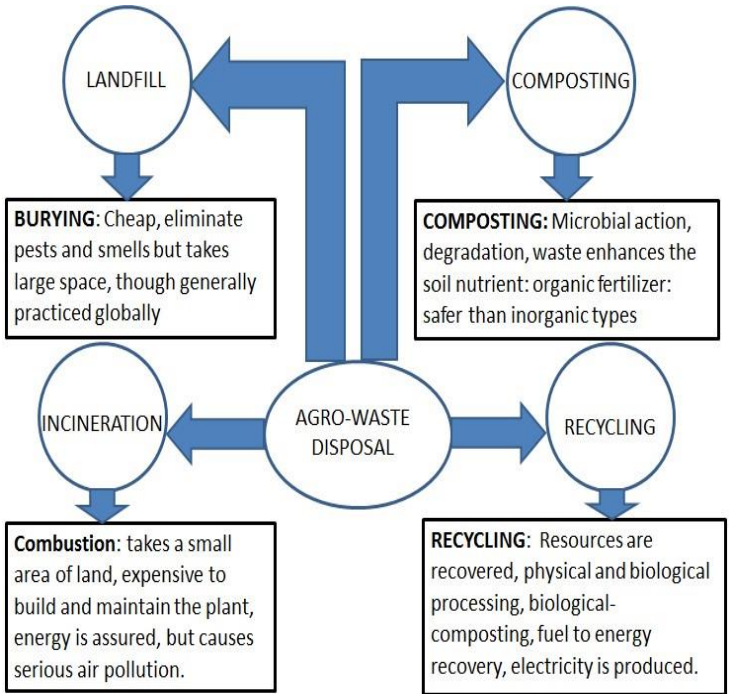


Figure 2-2 Scheme depicting some methods of agricultural waste disposal

It can be observed that land-filling of agro waste is considered a cheap technique of agro waste disposal, however there are environmental challenges associated with this. The most common challenge is ground water pollution. Although combustion is categorised under incineration, the process takes a small area which is an advantage, but it requires expensive equipment however, results in serious air pollution and generates solid waste in the form of ash (Drosg et al., 2015). Composting is another option of agro waste disposal; it involves microbial action that enhances the soil nutrient and preferable to inorganic methods of disposing waste. Recycling is the current

topical issue worldwide. Agro waste recycling is an attractive strategy of waste disposal because useful materials can be recovered (Duhan et al., 2017).

2.2.2 Agro-Waste Reuse

An agricultural waste is referred to as waste generated because of activities such as the harvesting of farm produce and its processing into different products for the intended applications (Iacovidou et al., 2018; Yadav and Samadder, 2018; Murillo and Cristina, 2014; Drosg et al., 2015). However, there is a need to comprehensively characterize the wastes by investigating the physical and chemical properties of these residues before their utilization (Adriano et al., 1980). The availability of agricultural residues determines their reuse or utilization. The major drawback in the utilization of these residues is limited information concerning fuel feeding, combustion and emission characteristics (Werther et al., 2000). The composition of some selected crop residues is shown in Table 2.2. Meanwhile, understanding the chemical constituents of crop residues or wastes will enhance their selectivity and utilisation for fuel or energy production. Most agricultural wastes are considered suitable and favorable for energy production depending on their availability and chemical compositions.

Table 2-2 Composition of selected agricultural wastes

Substrates	Cellulose	Hemicellulose	Lignin	Protein	Ash	References
Rice Straw	32-47	19 -27	5 -24	-	12.7	(Teghammar et al., 2012)
Wheat Straw	35-45	20 -30	8 -15	3.1	10.1	(Kabel et al., 2007)
Corn Straw	42.6	21.3	8.2	5.1	4.3	(Saha and Cotta, 2006)
Sugarcane Bagasse		165*	18.4	3	2.4	(Georgieva et al., 2008)

*Total carbohydrates

Several researchers have reported various compositions of agro waste as depicted in Table 2.2. It is seen that rice straw have high ash content of 12.7 w% and, is in affirmation with the high silica content in rice. However, Georgieva et al.(2008) reported 2.4 % ash content in sugarcane bagasse. The various bio-waste materials have different silica contents (Demirbas, 2011). Similarly, some authors have worked on the characterization of the silica contents of agro waste materials as presented in Figure 2-3.

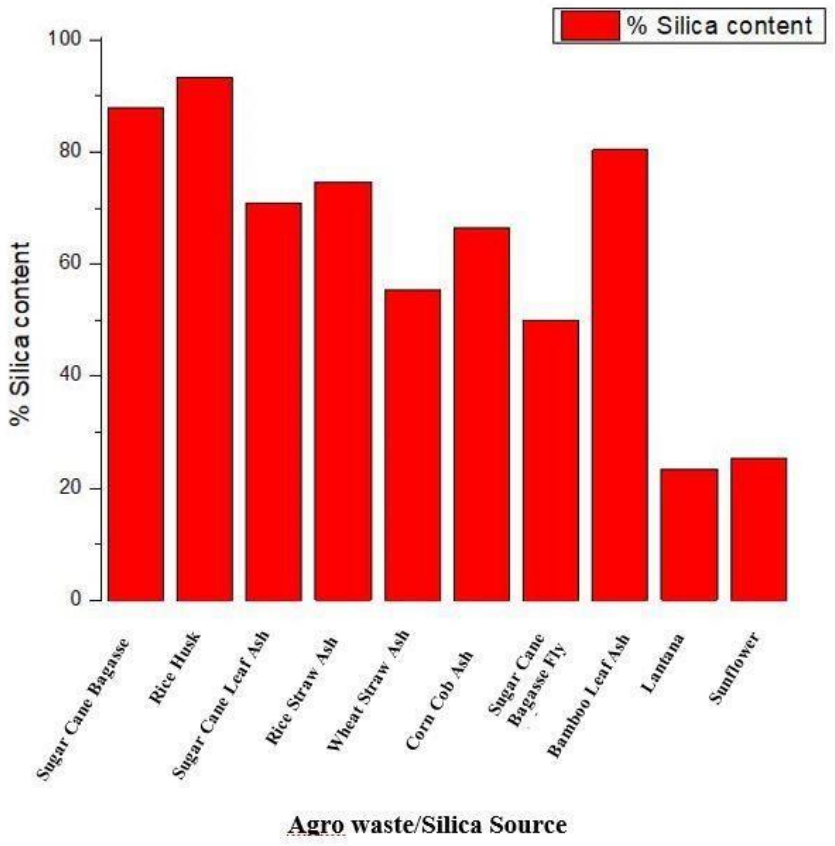


Figure 2-3 Percentage of silica in selected agro-waste ashes (Kazmi et al., 2016; Bhagiyalakshmi et al., 2010; Frias et al., 2007; Binod et al., 2010; Adesanya and Raheem, 2009; Purnomo et al., 2012; Villar-Cociña et al., 2011)

2.3 Agro Waste Sources for Nano Silica and Silicon

In recent years, agricultural waste products have gained recognition as a potential raw material for preparing silicon composites. Agricultural waste is one of the cheapest sources of silica production (Zhang et al., 2010). Natural silica has many benefits including; safe to handle and cost-effectiveness (Norsuraya et al., 2016). Several potential methods and reasons for the use of agro-wastes to generate silica have been offered by numerous authors (Adebisi et al., 2017; Falk et al.,

2019; Mor et al., 2017; Patel et al., 2017; Zamani et al., 2019).The reasons include: (i) cheap cost of raw materials; (ii) high percentage silica content in the agricultural waste; (iii) comparable silica quality; (iv) the fine size of the amorphous material; (v) high energy content; and (vi) low energy consumption.

It can be recalled from Table 2-2 and Figure 2-3 that rice husks have the highest silica content from the physio-chemical analysis of the samples. A review of some high waste volume generating and silica-rich agro-wastes namely rice-husk ash, wheat straw, corn cob ash, and sugarcane bagasse ashes is given.

2.3.1 Rice husk ash

Rice husk ash is one of the most abundant natural resources rich in silica (SiO_2). It is one of the agricultural by-products from rice milling industries. Rice husk ash consists of more than 90% amorphous silica (Li et al., 2011). To produce nano silicon crystalline particles from rice husk ash a magnesiothermic reduction method which involves the activation of the ash with an alkali, Sodium hydroxide solution is applied. The process involves boiling the mixture for an hour to yield a sodium silicate solution (Na_2SiO_3). The nano silica was then precipitated by sulphuric acid. Vacuum filtration was done in conjunction with hydrofluoric acid and distilled water washing to obtain solid nano silicon particles and remove other impurities as a waste filtrate. Washing of the nano silicon for many times yielded the solid silicon, and it was followed by drying of the solid nano silicon particles at 110 ^oC (Venkateswaran et al., 2013).

Liou and Yang (2011) reported an alkali-leaching method for the extraction of nano silica from rice husk ash. Rice husk samples were treated with hot hydrochloric acid to remove metallic

impurities; the samples were washed with distilled water and dried. The dried samples were placed in a muffle furnace to eliminate the organic matter. The ash was then mixed with 1.5 M NaOH solution and boiled at 100 ^{o}C with stirring for one hour to produce sodium silicate solution. Nano silica was then produced by neutralizing sodium silicate solution with hydrochloric acid, sulphuric acid, citric acid and oxalic acid to ascertain the best performing acid in the precipitation process. Carmona et al. (2013) extracted nano silica from rice husk ash by acid leaching method and subsequently the ash was subjected to thermal treatment. (Lee et al., 2017), carried out a series of experiments each with sulphuric acid, hydrochloric acid, oxalic acid and an ionic liquid to investigate the possibility of enhancing the purity of silica from rice husk. After the chemical treatments, the residue was pyrolyzed at 800 ^{o}C in a muffle furnace for 48 hours the resulting product was nano silica. Mor et al. (2017) produced nano silica particles by hydrothermal activation of rice husk ash (RHA) in 2 M NaOH. Product was a supernatant solution which was sodium silicate.

2.3.2 Corn cob ash

Another agricultural waste for production of nano silica is corn cob ash. Globally, large amount of corn cob ash is generated after eating separating the grains annually. Many of the rural communities consume the corn and burn the cobs into ashes usually found in heaps or mounds. Several articles have been published on the utilization of corn cob ash for nano silica production. Okoronkwo et al. (2013) and Venkateswaran et al. (2013) used corn cob ash to produce nano silica. The reaction was carried out using 1 M NaOH solution as an activating agent, after thermal treatment of corn cob at 650 ^{o}C treatment for 3 hours. The ash was cooled and treated with 1M sodium hydroxide to produce sodium silicate solution. This was titrated with 3M HCl with stirring

until pH of 7. The precipitate was washed and dried. Shim et al., (2015) reported the extraction of nano silica from corn cob ash at variable pH conditions via sol-gel method. Okoronkwo et al. (2013) also reported synthesis of nano silica through the sol- gel method and nanostructured with templating concept. The Hexadecyltrimethylammonium bromide (CTAB) was dissolved in distilled water and stirred for five minutes to obtain a homogeneous transparent solution. With continuous stirring ammonium hydroxide was added with continuous stirring, the extracted silica was then added slowly with stirring and was left to age for 20 hours. The nano silica was washed, dried and then calcined in a muffle furnace at 550 ^{o}C.

2.3.3 Wheat straw ash

Wheat straw is another abundant agro waste which have been explored by several authors because of its high silica content. Globally, over 500 million tons of wheat straw are produced. Most of these are burnt in the field causing significant environmental and health hazards and traffic accidents (YaNing et al., 2012). About 2.45 billion people, approximately 35% of the world population, rely on wheat as their staple food. Chen et al. (2010) extracted nano silica from wheat straw by two methods namely combustion and acid leaching. Wheat straw which had been washed clean and dried was burnt in a muffle furnace at 500 ^{o}C for 8 hours. The ash obtained was cooled and 88.09 wt.% silica was obtained. Acid treatment involved mixing of 10 g wheat straw at 60-70 ^{o}C for 24 hours in 100 ml of a 4:1 concentrate of HNO_3 and H_2SO_4 aqueous solution followed by centrifugation and washing for several times. The silica powder obtained was 91.33 wt% pure. Table 2-3 summarizes other various methods for the synthesis of nano silica and nano silicon from selected agro waste sources.

Table 2-3 Synthesis of nanoparticles from selected agro waste sources using various processing routes

Starting Material	Procedure Sequence	Products	Particle size(nm)	Reference
Rice Husk	Pyrolysis, leaching. sol-gel, reduction, leaching	Silicon	70-100	(Venkateswaran et al., 2013)
Rice Husk	Acid leaching, combustion, Leaching, pyrolysis, sol-gel. Maximum temperature 500 ^{o}C, 700 ^{o}C, 1 000 ^{o}C	Silica	6	(Rafiee et al., 2012)
Rice Husk (from 2 different sources)	Leaching calcination Maximum temperature 650 ^{o}C	Silica	181,2 -294.7	(Carmona et al., 2013)
Rice husk, rice straw (RS), Sylvan horsetail, scouring horse tail and larch needles	Hydrolysis, calcination, metallothermic reduction Maximum temperature 700 ^{o}C	Amorphous silica	50-200	(Zemnukhova et al., 2012)
Corn cob	Precipitation. Maximum temperature 750 ^{o}C	Amorphous silica	25	(Mohanraj et al., 2012)

Rice husk	Sol-gel, supercritical carbon dioxide drying Maximum temperature 600 ^{o}C	Nanoporous silica aerogel	10-60	(Tang and Wang, 2005)
Rice husk, coffee husk, sugarcane bagasse	Biotransformation, calcination, leaching. Maximum temperature 700 ^{o}C	Silica	152-254	(Espíndola-Gonzalez et al., 2010)
Maize Stalk	Pretreatment in dilute hydrochloric acid and treatment of sodium silicate in ethylene glycol	Silica	26.9	(Adebisi et al., 2019)
Cassava periderm	Pyrolysis, sol-gel, calcination. Maximum temperature 600 ^{o}C	Silica	62	(Adebisi et al., 2019)
Silica, Mg	Magnesiothermic reduction Maximum temperature 650 ^{o}C	Silicon	Less than 2	(Bao et al., 2007; Yermekova et al., 2010)

2.3.4 Sugarcane bagasse ash

Another interesting agro waste material is sugarcane bagasse a waste product from sugar milling and ethanol industries. It has been reported that agricultural activities reduce silicon from the soil due to its utilization by plants (Savant et al., 1999). For instance, sugarcane is known to absorb more silicon than any other mineral nutrient from the soil in the form of silicic acid (H_4SiO_4), accumulating approximately 380 kg/ha of silicon (Si), in a 12-month-old crop plantation period (Savant et al., 1999). Sugarcane bagasse ash (SCBA) is another waste from sugar and bioethanol industries, potentially used as the cheap source of natural silica. Researchers worldwide have dedicated effort to investigate potential applications of silica from bio-waste including sugarcane bagasse ash (Ferreira-Leitão et al., 2010). However, the silica content in sugarcane bagasse ash is highly dependent on the geographical location and the environment where the sugarcane is grown as well as the farming practices. From a study that was conducted by Preez (1970) in South Africa, on the treatment of soil with silicate-containing fertilizers, there was an increase in cane yield with an increase in the silica concentration in the plant. Sugarcane in Hawaii is normally a two-year crop while in most countries it is an annual crop (Fox et al., 1969).

Sugarcane bagasse ash has good pozzolanic properties and could be used in place of cement but to around 10% to retain the desired strength and increase the characteristics of the concrete (Maheswari et al., 2017). The chemical composition of sugarcane bagasse ash and specifically the level of silica is of major interest to the quality of concrete formulations. The chemical compositions of a typical sugarcane bagasse ash with reference to geographical locations are

shown in Table 2-4. It can be observed that the silica content and other compositions of the ash vary in accordance with the geographical locations and climatic conditions.

Table 2-4 Physicochemical composition of sugarcane bagasse ash from different countries

SiO_2	Fe_2O_3	Al_2O_3	CaO	MgO	SO_3/SO_4	K_2O	LOI	Country	References
44.70	2.90	2.40	14.9	3.50	NA	4.40	16.7	Iran	(Abbasi and Zargar, 2013)
72.85	6.96	1.08	9.97	6.49	NA	6.71	4.23	Nigeria	(Abdulkadir et al., 2014)
77.25	4.21	6.37	4.05	2.61	0.11	2.34	1.40	Sudan	(Asma Abd Elhameed Hussein et al., 2014)
41.15	2.70	7.00	3.20	0.12	0.03	8.75	17.7	Nigeria	(G R Otoko, 2014)
66.89	29.18	29.18	1.92	0.83	0.56	NA	0.72	India	(Asma Abd Elhameed Hussein et al., 2014)
62.43	6.98	4.28	11.8	2.51	1.48	3.53	4.73	India	(Mrs.U.R.Kawade et al., 2013)
87.59	0.67	0.57	2.59	1.65	0.00	3.64	NA	India	(Modani and Vyawahare, 2013)
67.82	2.56	6.33	1.54	2.03	-	2.87	2.31	Thirukovikur	(Hariharan et al., 2014)
31.41	6.02	7.57	16.06	1.07	0.78	1.58	32.2	Brazil	(Castaldelli et al., 2013)
96.2	1.7	0.2	0.1	0.1	0.1	0.3	1.04	Brazil	(Sales and Lima, 2010a)
72.8	5.5	6.4	3.8	2.3	-	2.7	3.7	Columbia	(Torres Agredo et al., 2014)
84.0	1.7	1.1	0.5	0.6	-	0.5	3.1	South-Africa	(Aboyade et al., 2011)
62.1	5.42	5.54	1.0	1.12	-	2.22	-	Uganda	(Basika et al., 2015)

Researchers have indicated the use of sugarcane bagasse ash (SCBA) in different applications, and equally specifically investigated the influence of SCBA on the surface characteristics of silica for silicon production. Sol-gel and bio-digestion methods could be used to produce the nano silica. Similarly, Vaibhav et al. (2015), demonstrated in their work a successful production of silicon nanoparticles using precipitation technique and silica extracted from sugarcane bagasse, groundnut shell, rice husk and bamboo leaves.

2.3.5 Demerits of bio-sourced ash from biomass-firing heaters

Despite the potential applications of ash sourced from combustion of agro-waste, there are significant process challenges that result from the firing of biomass prior to the extraction of silicon. Several researchers have reported on the negative impacts of bio-sourced ashes from fuel-feeding on process equipment and complications related to their deposition into the environment. In a study by Yao et al. (2020) on co-firing anthracitic coal with woody biomass (pine sawdust), it was observed that mitigating slagging and fouling tendencies of ash which related to the ash fusion temperature (AFT) requires careful temperature control. Yao et al. (2019) found that there were less acidic oxides (SiO_2) and amphoteric oxides (Al_2O_3) in soybean straw compared to coal while basic oxides were much higher. The higher basic oxides resulted in lower AFT, thus requiring that the process operates at lower temperatures. An advantage of the co-firing strategy is the reduction in ash volume per unit volume of fuel-feed due to the presence of less inorganic materials in the biomass component.

The challenge with utilising biomass fuels lies in the abundance of alkali/alkaline earth metals (K, Na and Ca) and chlorine (Cl) and low sulphur content which has been proven to adversely impact combustion and significantly alter the properties of the ash product (Shao et al., 2012). Due to the

high activity of the alkali/alkaline earth metals present, particularly the readily volatilized forms of potassium (K) in biomass, vapour compounds and ions of chlorine are formed. Because of the low melting temperatures (<800℃) of the vapour phase K-constituting compounds and ions of chlorine, deposits form adhesive layers on heat transfer surfaces. This problem is more complex in agro-waste with an abundance of silica combined with alkali/alkaline earth metals (rice husk, sugarcane bagasse etc.) which readily cause slag and fouling within the temperature range 800-900℃, the normal temperature ranges for biomass firing boilers. Therefore, co-deposition of alkali silicates and alkali chlorides resulting in corrosion/fouling is difficult to avoid at a low AFT (typically <700℃) (Shao et al., 2012).

Despite the low-S content of biomass fuels or co-firing fuels which significantly reduces emission of SO_x gases, ash deposition is negatively affected particularly due to the high Cl content of biomass. The work of Nielsen et al. (2000) and Yao et al. (2019) concurred that intense volatilization of sylvinite, KCl, a typical fluxing agent, which happens between 750900ºC is responsible for ash fusion and agglomeration. Sulphur is known to reduce corrosion and such challenges related to chloride deposits through the following sulphation mechanism (Nielsen et al., 2000). Equations 2.2 and 2.3 give mechanisms through which this happens.

$$2Cl\,(s) + SO_2(g) + \frac{1}{2}O_2\,(g) + H_2O\,(g) \rightarrow K_2SO_4\,(s) + 2HCl\,(g)\quad \Delta H^\circ = [-646.5\ kJmol^{-1}\ ]$$

Equation 2.2

$$2KCl\,(s) + SO_2\,(g) + O_2\,(g) \rightarrow K_2SO_4\,(s) + Cl_2\,(g)$$

Equation 2.3

Therefore, due to low-S, combustion of biomass of co-fired fuels can lead to increased Cl-related deposition and corrosion problems. Despite the focus on the process challenges concomitant with biomass-firing, another challenges to be considered is the environmental penalties of chlorine-bearing ash deposits. Figure 2-4 gives a schematic of the ash formation deposition mechanisms on a superheater tube surface.

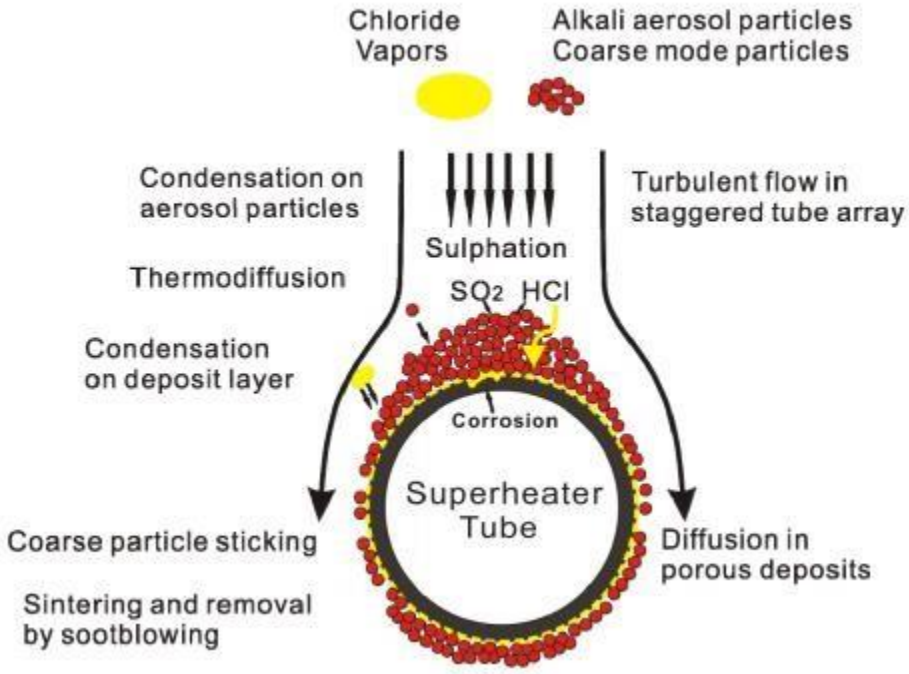


Figure 2-4 Schematic of mechanism of ash formation and deposition on a super heater tube (Shao et al., 2012)

Since the global community moves towards CO_2 emission free society, thus it becomes more pertinent that more-sustainable approaches to the harvesting of silica from agro-waste be investigated. However, the use of bio-sourced ash finds its significance not as a long-term method

for extraction of silica but a mitigating method to reduce the environmental impact of ash deposits from biomass-firing activities.

2.4 Production of Silicon Nanoparticles

Nanoparticles are fundamental building blocks of nanotechnology (Nagarajan, 2008). Synthesis often follows a bottom-up or top-down approach (Kulkarni et al., 2010; Overney and Jeanneret, 2010; Yadav and Samadder, 2018). The first approach relates to when the material is made from elemental basis through chemical processes and the latter to reduction from the bulk state via mechanical milling or chemical attrition processes. Nanotechnology has improved the manufacturing of high efficiency products due to the ability to control and modify the properties of the materials of construction starting from the nanoscale. Bottom-up synthesis of nanoparticles is achieved through pyrolysis, hydro (solvo) thermal reaction, inert gas condensation, sol-gel fabrication and structured media methods whereas; top-down methods are largely achieved by milling and attrition (Overney and Jeanneret, 2010).

Nano-silicon produced from silica can be produced to suit different applications in biotechnology and electronics among others. In electronics applications, it is used for fabrication of transistors, solar cells, semiconductor detectors. Solar modules made from high-quality crystalline silicon layers on glass substrates have the potential of making photovoltaic electricity substantially cheap (Venkateswaran et al., 2013). Solar energy exploitation has spurred research and scientific attention in renewable alternative energy primarily to address energy shortages. On the grounds of these energy shortages, silicon nanoparticles for solar cell applications have gained international recognition as a promising option (Huan and Shu-Qing, 2014).

Production of silicon nanoparticles based on synthetic and analytical size-selected techniques offers a comprehensive understanding of the properties, morphologies and dimensions of silicon nanoparticles (SiNPs). There are quite a few routes for the synthesis of SiNPs such as pulsed laser ablation, heating degradation and ball milling, chemical and electrochemical etching syntheses (Eisenhawer et al., 2011). Guiding strategies include the understanding of the surface chemistry, size distribution and dimensions of particles, and its scalability. Above the others, the chemical synthesis method has the advantage of size and shape control, as well as purity improvement. A few select methods of silicon nanoparticle synthesis are given in the subsections that follow;

2.4.1 Pulsed laser ablation (PLA)

Pulsed laser ablation (PLA) which uses PLA vaporization of the greater amount of the metal in a pulsed supersonic nozzle to render ultra-cold metal cluster of copper (Cu(II)) (Powers et al., 1982) and high-melting molybdenum (Mo(II)) (Hopkins et al., 1983). This method is most advanced for semiconductors such as SiNPs. Production is facilitated by the application of argon fluoride excimer laser ablation (ArF laser) at constant helium (He) gas atmosphere as demonstrated by Yoshida et al. (1996). The authors correlated a relationship indicating that the increase in helium (He) pressure from the kinetic energy of the material which collided with that of the surrounding gas particles has a link with the cohesive energy as shown in Equation 2.4:

$$d_m \propto \sqrt[3]{\rho} \propto \sqrt[3]{P} \qquad \textit{Equation 2.4}$$

Where d_m the diameter of the ultrafine crystallite, P is the ambient pressure and ρ is the density of the surrounding gas.

2.4.2 Heating degradation

Thermal decomposition has extensively been used to produce SiNPs using silane as starting materials. For example, Ho et al. (1994) has shown the possibility of producing the elemental silicon atom by chemical decomposition via two chemical equations coupled to a rotating chemical vapor deposition (CVD). Further work by Swihart and Girshick. (1999) resulted in a plausible yield of 20 silicon atoms and rendered a kinetic mechanism for the formation of silicon hydride. These earlier works have garnered more inspiration for more researchers including English et al. (2002) proposing production of sterically stabilized silicon nanostructures thereby enthroning the freedom of environmental contamination using heating and pressurized solvents in an elevated temperature greater than their critical points (400-500 ^{o}C) for decomposition of organosilane feedstock. However, Shafeev et al. (2004) have demonstrated that microwave-assisted thermal decomposition can affect organosilane precursors at certain microwave powers. In another effort, Knipping et al. (2004), achieved Si single crystals ranging from 6-11 nm through microwave-induced decomposition of silane. This result has shown that the particle size was proportional to the precursor concentration whereas, the gas pressure proved an inverse relationship with the microwave power. The use of thermal degradation in Si nanostructures are currently applied in SiNPs featuring blue emission, great PL yield, high pH stability and favorable size with the use of a facile one-pot aqueous production technique (He et al., 2009; Panda et al., 2006). This process shows that the use of microwave supported the nucleation or Oswald ripening (He et al., 2009).

2.4.3 Ball milling

Nano-crystalline materials can be successfully produced from ball milling and this method is popular because of its simplicity, relatively inexpensive equipment and can take on a wide range of other materials. (Lam et al., 2000) used ball milling to synthesize large-scale ultrafine SiNPs with an average diameter of 5nm using solid graphite (C) in conjunction with silicon dioxide (SiO_2) in a planetary ball miller for 7-10 days. 1:1 graphite-SiO_2 molar ratio was applied and the mixture was loaded into a stainless-steel vial together with stainless-steel balls (7.5 mm in diameter). The content was sealed with a Viton O-ring. However, before sealing, argon was passed through the vial to repel other gases while the remaining argon was set at atmospheric pressure. After the period was past, the milled powders were annealed in a hydraulic press for 48 h at 150 ^oC under a loading of 30 kgf/mm^2. The annealed powders were put back into the vial and milled for another 2 h to break up the pressed tablet into powder form.

The resulting NPs were covered with an amorphous SiO_2 layer 1nm in thickness and this produced a multi-peak PL spectrum due to the wide range of particle sizes. Apart from the size distribution, another issue arises from the aggregation which presented a complex and coarse shape. This tends to limit the ball milling synthetic strategy despite its convenience and inexpensiveness.

2.4.4 Physicochemical methods

In this category of silicon nanoparticles production technique, photothermic aerosol synthesis is popular. This utilizes a laser-induced decomposition of gas phase materials and is carried out in three stages. At the onset, the silicon powders are synthesized by CO_2 laser-induced heating of

silane followed by H_2 and a photosensitizer (e.g. sulfur hexafluoride) to a degree that can be effectively dissociated. The product of this synthesis is in the range of SiNPs from 5nm to 10 nm or even larger than 10nm (Ehbrecht and Huisken, 1999). Subsequently it does not manifest serious size confinement effect which implies a much lower PL efficiency. This, therefore, calls for a post-treatment for size selection and to reduce particle dimension as required. However, it was of importance to select the neutral clusters using cluster size, slotted molecular beam chopper wheel based on the correlation suggested by Ehbrecht and Huisken, (1999). Etching of the obtained SiNPs by chemical etching with HF/HNO_3 would induce bright visible luminescence (Li et al., 2003; Erogbogbo et al., 2010).

A physical route to SiNPs production usually encounters low product yield, but in the physicochemical case, a gram scale yield of silicon quantum dots (Si QDs is) obtained (Zhang et al., 2007). This results in non-aggregation, and a well-controlled nanoparticle size incidentally deposited on the desired substrate or liquid medium. Huisken et al., (2002) demonstrated a successful particle injection through a nozzle into a high vacuum device and then deposited a molecular beam of Si clusters on a suitable substrate.

2.4.5 Chemical techniques

Production of SiNPs takes on the solution phase synthesis which received plausible efforts (JR Heath, 1992). The starting materials were silicon halides. These were systematically reduced by sodium naphthalenide (K. Baldwin et al., 2002; JR Heath, 1992; Zou et al., 2006), lithium naphthalenide (Kornowski et al., 1993), lithium aluminum hydride (Hapala et al., 2013; Sudeep et al., 2008) or zinc salts (Bley and Kauzlarich, 1996) These reactions were carried out in a variety

of surfactant solvent environments resulting in small-sized, free-standing SiNPs which were hydrogen capped (Hapala et al., 2013; Wilcoxon et al., 1999) . Recently, Chang and Sun, (2014) used allyltrichlorosilane as both the surfactant and the functionalization reagent and silicon tetrachloride in a ratio of 1:3, to explore a simple approach to the synthesis of morphologycontrolled hexagonal silicon nanocrystals modified with allyl in the range of 20-50 nm.

The Si-Cl bonds were reduced by lithium tetrahydridoaluminate to Si-Si which promotes the growth of Si crystals (Chang and Sun, 2014). To control the size dispersion, Tilley et al. (2005) found that the narrow size distribution could be obtained by using powerful hydride reducing agents and selective surfactants in micelles, which termed, “micro-emulsion synthesis”. In this process, the surfactant plays a critical role in restricting the core growth and finally resulted in uniform particle dimensions.

Chang and Sun, (2014) have successfully demonstrated a one-step technique to produce highly monodispersed, alkyl-capped, brightly luminescent nanocrystals using hexyltrichlorosilane as both surfactant and the reactant. When the hexyltrichlorosilane was not used, the product of reaction showed smaller Si QDs with diameters 2±0.5 nm implying a narrow size distribution and excitation wavelength-dependent PL performance. The PL was shown to peak-range from 350-450 nm as the excitation state wavelength red-shifted (Wang et al., 2011). Several authors including McMillan et al. (2005) and Zhang et al. (2007) have utilized different precursors to synthesize silicon nanoparticles. For example, zinc salt was used with ammonium bromide, nanoparticles with bright

blue emission in the size range of 3.9±1.3 nm could be obtained with resultant by-products such as ammonia, hydrogen and sodium bromide.

2.4.6 Electrochemical techniques

This method appears to be one of the versatile approaches to SiNPs synthesis when looking at it from the fundamental perspectives. An example is the synthesis of porous silicon (PSi) otherwise known as silicon nanocrystal thin film that transcended photoluminescent SiNPs which was developed through galvanostatic anodization. Traditionally, its preparation involved filling of a Teflon cell with a blend of aqueous HF and ethanol followed by etching a silicon wafer under steady current supply. A fracturing treatment is carried out on the fleshly etched PSi layer for sonication in order to achieve quantum confined colloidal silicon nanoparticles (SiNPs) (Ahire et al., 2012). Bley et al (1996) note that electrolyte composition, etching time, silicon dopant type and dopant concentration exert irreversible effect on the surface morphology and properties of the PSi thin film. The ethanol used has the advantage of preventing bubble break up and annulment of the hydrophobicity leading to effective pore formation (Sailor and Wu, 2009) and consequently results in a more uniform hydrogen-terminated silicon nanocrystals.

2.4.7 Surface modification

SiNPs synthesis through surface modification is achievable through an understanding the surface chemistry of the nanoparticles. For example, from the fact that chemical reactions take place at the surface much higher than they do at the bulk mass, pristine Si nanocrystals with hydrogen termination show meta-stability due to its surface hydrophobicity to oxygen and water. This shows that surface modification of Si nanocrystals which have functional molecules would significantly

improve their stability, optical performance and solubility in some solvents (Sato and Swihart, 2006; Zhu et al., 2005).

Some authors (Bent, 2002; Duke, 1996; Neergaard Waltenburg and Yates, 1995) have suggested the existence of dangling bonds on the surface of SiNPs which enhance chemical reactivity at the surfaces with other organic molecules. There is one instead of two spin-paired electrons responsible for the tendency of minimizing the free energy that removes the dangling bonds. The resulting energy minimization was a trade-off between that gained in forming new local bonds and the energy lost during bond strain from its new configuration. The result is a complex reconstruction of the surface that leads into termination with certain molecules. Presently, different types of water-soluble SiNPs with bioconjugation are available in the areas of in-vivo and in-vitro applications. In Si-H bonding, it can easily be oxidized while Si-Si linkage produces a weaker bond. However, in order to avoid surface oxidation an inert atmosphere must be incorporated (Ruizendaal et al., 2011 ; Ahire et al., 2012).

The seemingly chemically stable Si-C bond emerges as a suitable medium for further chemical compound passivation such as acrylic acid, octylamine (Zhang et al., 2007), 4-bromo-1-butene (Ruizendaal et al., 2011) and epoxide-1-heptene (Tilley et al., 2005). This is so because the Si-C has low polarity and high bond strength through hydrosilylation and if a further modification was necessary, the small organic molecules with a C=C end group would produce hydrophobic and hydrophilic SiNPs (Ahire et al., 2012) .

Polarization effect has been investigated on the scale of in-situ oxidation under high temperature yielding SiO_2 that aided particle to become water-soluble for easy surface functionalization (Hu et al., 2009). The commonly used approaches these days to achieve hydrosilylation of silicon nanocrystals are metallic catalysis, UV irradiation, heating treatment and microwave-assisted functionalization.

2.5 Drawbacks and Benefits of Different Methods

Physical methods have the capacity to achieve size controllability of the synthesized SiNPs. The SiNPs produced can be zero dimensional (0D), 2D or 3D. The major disadvantage with this method is that production is not scalable, and the Si QDs generated must be stabilized. Essentially, quantum dots (QDs) are nanosized semiconductor particles which have unique optical and electrical properties compared to larger-sized particles due to quantum mechanics. Under mild conditions chemical synthesis techniques of SiNPs have been shown to achieve surface modification and controllable particle size distribution of Si QDs, but the question of contamination of the residual side products which are reducing agents are compromised (Hapala et al., 2013; Zou et al., 2006). The need for a high yield and uniformity in essential properties has attracted much research attention to porous silicon as a source of Si QDs through use of electrochemical techniques under certain conditions (Ahire et al., 2012 ; Wilson et al., 1993). Many methods have been applied by several researchers to study the production of nanoparticles using different feedstocks. Table 2-5 presents some of the methods used by different authors in the production of silicon nanoparticles.

Table 2-5 Methods of producing silicon nanoparticles starting with different precursors

Feedstock	Method of operation	References
Silane (SiH_4)	Ultra-sonification; involving porous silicon fractioning	(Belomoin et al., 2002)
Silane (SiH_4)	Microwave-induced/laser-induced decomposition	(Barth et al., 2010)
Si	Pulsed-laser ablation	(Espíndola-Gonzalez et al., 2010)
Silane (SiH_4)	Low-temperature solution route	(Neiner et al., 2006)
Silane (SiH_4)	Plasma-enhanced chemical vapor deposition	(Izdebska and Thomas, 2015; Mercaldo et al., 2009; Pi et al., 2006)
Silane (SiH_4)	Low-pressure vapor deposition	(Boulos et al., 2013)
Si	Spark discharge process	(Kim et al., 2011; Won et al., 2011)
SiO_2	Metallothermic process and hydrometallurgical process of combustion product	(Nagai et al., 2012; Yang et al., 2014)
SiO_2	Vacuum directional solidification	
$SiCl_4$	Halidothermic reduction (sub halidy reduction)	(Bley and Kauzlarich, 1996)
RH, SCB, CH	Vermicomposting, with annelids	(Espíndola-Gonzalez et al., 2010)

Paddy Straw	Pretreated with dilute H_2SO_4 to remove polysaccharides and other impurities followed by delignification with alkaline mixture ($NaOH - H_2O_2$) for the extraction of silica in nano form and lignin	(Kauldhar and Yadav, 2018)
Cassava Periderm	Modified sol-gel method and metallothermic reduction of silica nanoparticles	(Agunsoye et al., 2018)

Basically, silicon nanoparticles have necessary physical characteristics for solar cell fabrication. These include an active surface state, outstanding photoluminescence and biocompatibility among other desirable features (Chang and Sun, 2014).

2.6 Methods of Characterization of Silicon Nanoparticles

In the production of silicon nanoparticles, different characterization techniques are applied to allow for a proper understanding of the nature of the nano material produced. If the properties of the materials are identified, it will be possible to project the material for a suitable application. Cho et al. (2013) studied the synthesis of luminescent silicon nanoparticles from the reaction of magnesium silicide and ethylene diammonium chloride in a low-temperature condition. Two important parameters; the amount of reducing agent and reaction time on the synthesis process were investigated. The nanoparticles were optically characterized by FTIR (Nicolet 5700), photoluminescence spectroscopy (Perkin- Elmer, LS 55 luminescence spectrophotometer) and uv-vis absorption (Shimadzu, UV-2401 spectrophotometer). The size of silicon nanoparticles was obtained by TEM (Hitachi, H-7600).

Similarly, Odo et al. (2012) investigated the production of silicon nanoparticles from single crystalline silicon wafers and polycrystalline bulk using a vibrating disc mill in a top-down synthesis route. The authors applied scanning electron microscopy (SEM), transmission electron microscopy (TEM), and energy dispersive x-ray spectroscopy (EDX) to study the elemental composition and morphology of the silicon-particles produced, whereas, the structural characteristics of the particles were studied using XRD. On the other hand, the silicon

nanoparticles synthesized from a thin section of porous silicon in an organic solvent were characterized by Bley and Kauzlarich, (1996) using high-resolution transition electron microscopy (HRTEM) and FTIR. The two techniques were used to determine the mono-dispersion and the composition of the amorphous surface layer of the nanoparticles, respectively. The authors stated that the average particle diameter, size distribution and the charge of the nanoparticles influences both the in-vivo distribution and physical balance of the nanomaterial. Many authors including Bhatia (2016); Pal et al. (2011); Patra and Baek (2015) and Polakovič et al. (1999) have also reported about nanoparticles characterization. A schematic representation of the methods of characterizing silicon nanoparticles is shown in Figure 2-5.

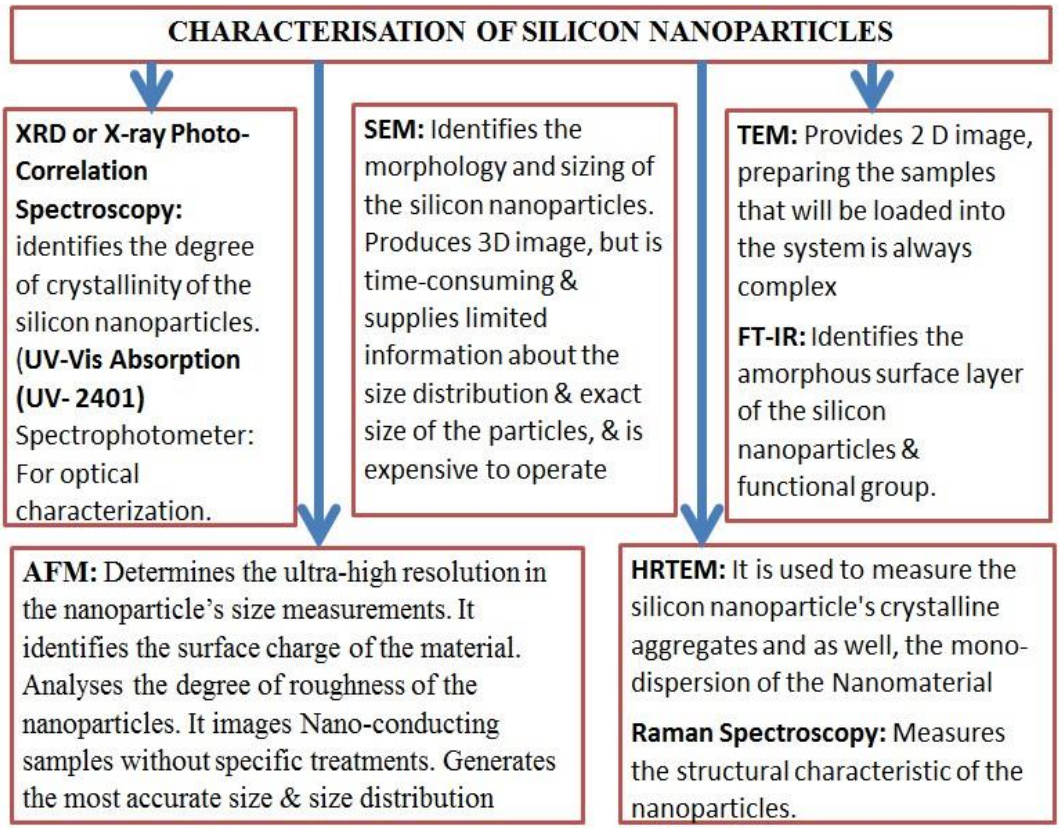


Figure 2-5 Silicon nanoparticles characterization techniques

2.7 Characterization of Si NPs

In this study, the work of Venkateswaram et al (2012) is used as a case study to describe the characterization of silicon nano particles (SiNPs) produced using magnesiothermic reduction method (MRM) for solar cells fabrication. The MRM according to the authors is a cost-effective method used for SiNPs production. The work was chosen because it was a comprehensive characterization, and the techniques employed include XRD, particle size analyzer (PSA), FT-IR, TEM, UV-Vis absorption. Figure 2-6 through Figure 2-10 show the XRD, PSA, FT-IR, TEM, UV-Vis absorption results of the characterization, respectively, while the XRF result is presented in Table 2-6.

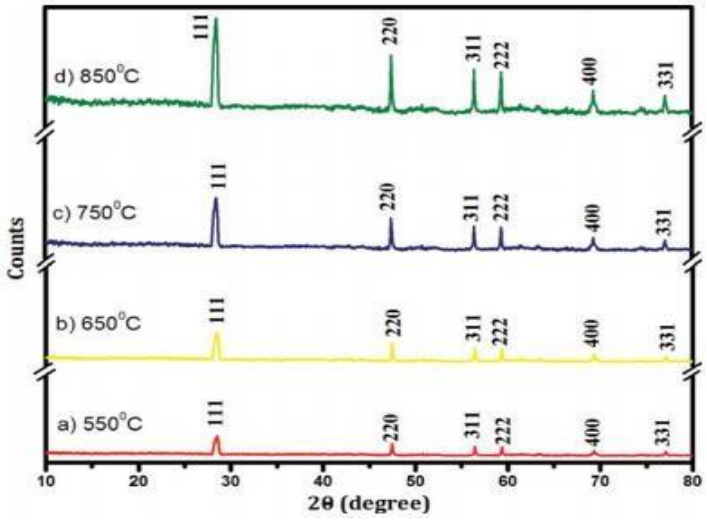


Figure 2-6 XRD patterns of nanosilicon at different sintering temperatures. Adapted from Venkateswaran et al. (2013)

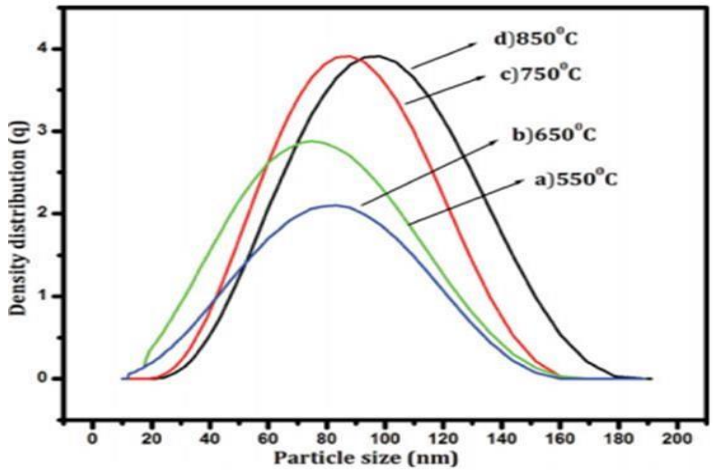


Figure 2-7 Particle size distribution of nano silicon at different sintering temperatures Venkateswaran et al. (2013)

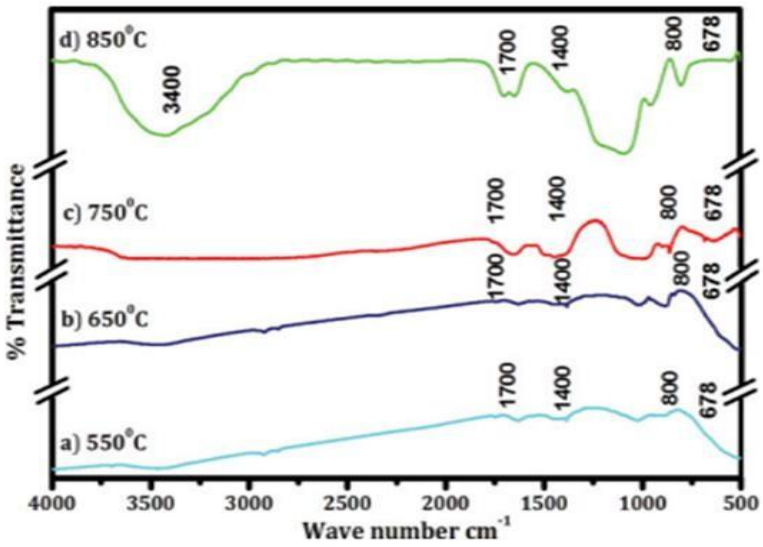


Figure 2-8 FTIR spectrum of nano silicon at different sintering temperatures. Adapted from Venkateswaran et al. (2013)

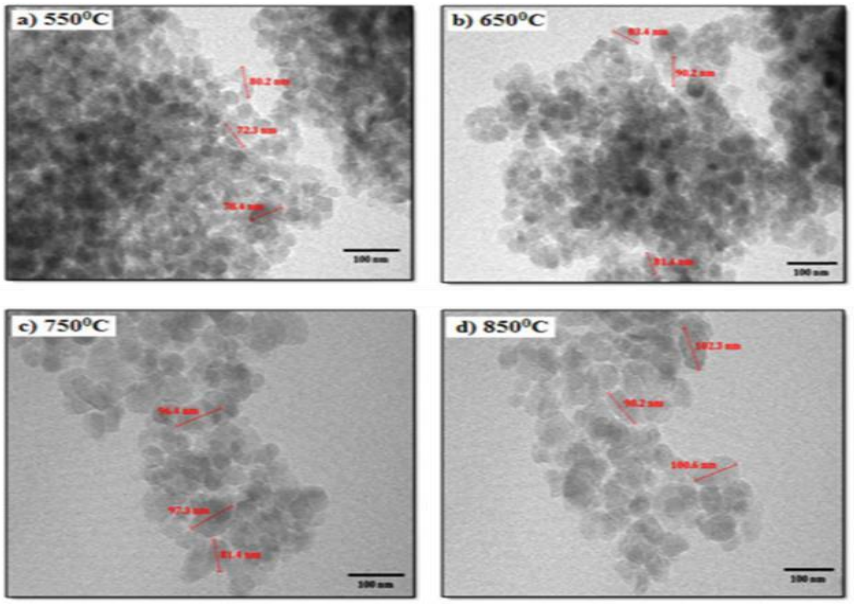


Figure 2-9 TEM images of nano silicon at different sintering temperatures Venkateswaran et al. (2013)

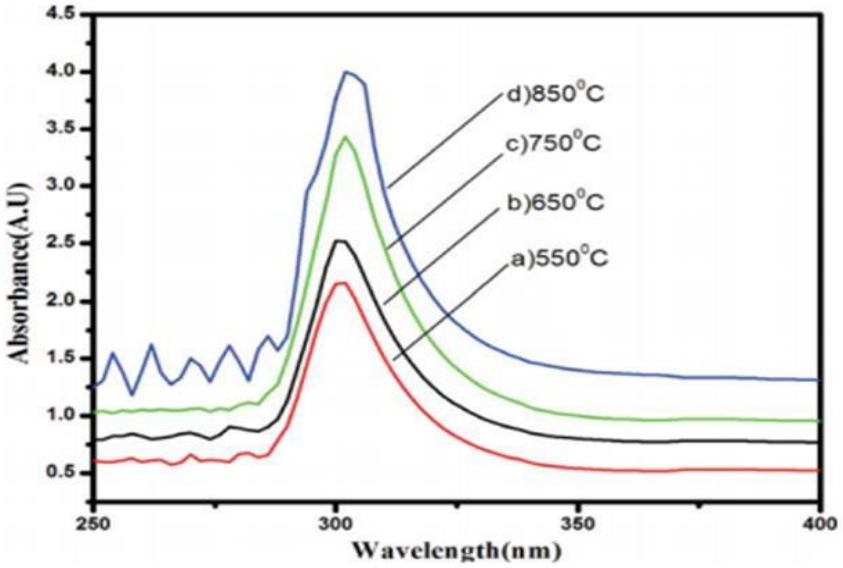


Figure 2-10 UV–Vis Absorption Spectra of Nano Silicon at Different Sintering Temperatures . Adapted from Venkateswaran et al. (2013)

Table 2-6 XRF results for SiNPs produced by Venkateswaran et al. (2013)

Temperature (°C)	Analyte	Results (%)
550	Si	90.17
	Mg	6.63
	Ca	2.42
	Fe	0.78
650	Si	93.43
	Mg	4.77
	Ca	1.32
	Fe	0.48
750	Si	96.30
	Mg	1.80
	Ca	0.98
	Fe	0.92
850	Si	98.20
	Mg	0.714
	Ca	0.584
	Fe	0.584

From Figure 2-6, sharp well-oriented crystalline peaks (111, 220, 311, 222, 400 & 331) were obtained for 550, 650, 750, & 850 ℃ and it was an indication of crystalline silicon formation.

The average crystallite sizes were 42.60, 47.24, 54.38, 56.21, 59.47, & 63.18 nm and the sharp peaks were a revelation of face-centered cubic structures formation and the reduction in the Si NPs size was achieved by lowering the sintering temperature. According to Venkateswaram et al. (2013), SiNPs obtained at temperature of 850 ^{o}C is suitable for solar cell fabrication. PSA was done for SiNPs synthesized at similar temperature values as those used in XRD analysis. Figure 2-7, the PSA of the Si NPs were in the range of 40-125, 48-104, 55-119 and 60-134 nm for 550, 650, 750, & 850 ^{o}C, respectively. The maximum distribution particle size was 72 ±3, 80 ± 3, 84 ± 3, and 94 ± 3 nm for the above-mentioned temperature conditions, respectively and the size of the SiNPs increased with an increase in temperature.

Venkateswaram et al. (2013) in Figure 2-8 obtained strong absorption bands was obtained at 800 cm^{-1} which corresponded to the Si-H_2 bending mode. Absorption bands were also found at 1400 cm^{-1} and 1700 cm^{-1} and peaks at 678 cm^{-1} which were an indication of Si-Si stretching mode. The presence of -OH stretching band was found at 3400 cm^{-1}. In Figure 2-9, also obtained from Venkateswaram et al. (2013), all the temperatures studied had an agglomeration spherical morphology at a particle size of between 70 - 100 nm, but the agglomeration morphology obtained at 850 ^{o}C was higher than the morphology obtained from every other temperature studied. The UV-Vis analysis displayed in Figure 2-10, based on the work of Venkateswaram et al. (2013), confirmed that the absorption peaks and wavelength of around 300 – 310 nm was present at 850 ^{o}C. The SiNPs thus produced had pure phase formation, high purity, and good absorption peaks and were usable in solar cells fabrication. The XRF result shown in Table 2.6, based on Venkateswaram et al. (2013), equally affirms the potentials of SiNPs for solar cells fabrication. However, Venkateswaram et al. (2013) concluded that MRM was still more attractive for SiNPs

production due to its cost effectiveness. Contrary to that deduction, Ahire et al. (2012) submit that chemical synthesis is more attractive because of the possibility of surface modification and control of Si particle size distribution although the possibility of contamination of residual side products may be a setback.

2.8 Solar Cell Technologies

Photovoltaic technology involves harnessing of incident optical energy from the sun. The most widely used semiconductor material in conventional solar cells is silicon (Si) (Ghahremanirad et al., 2016). This material is widely used in photovoltaic industry and more than 90 % of the PV market is dominated by silicon solar cells (Mutlugun et al., 2008; Sampaio and González, 2017). However, the solar conversion efficiency and photovoltaic device parameters are very low due to the intrinsic properties of silicon. Thus, there is limited capability to collect the photo-generated carriers across silicon solar cell and the electrical energy generated under UV illumination is very low. Silicon has a high refractive index (> 30%), and some of the incident radiation is reflected hence the low conversion efficiency (Prevo et al., 2007).

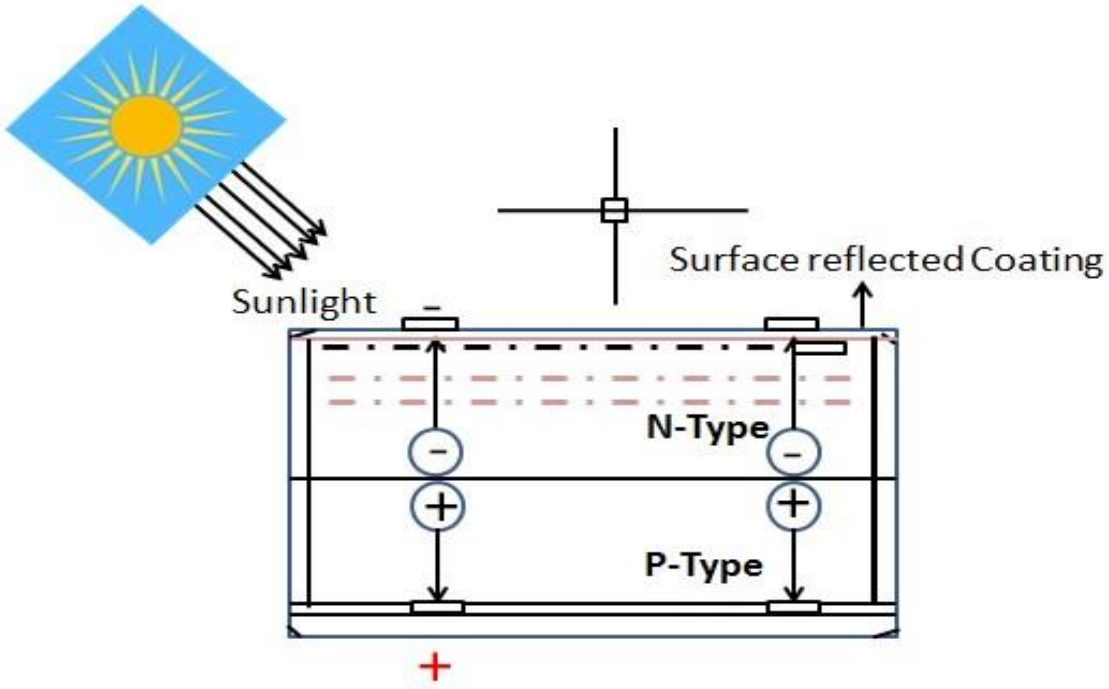


Figure 2-11 Solar cell working mechanism. Adapted from Kumar et al. (2016)

Figure 2-11 shows the working mechanism of a Si-based solar cell. The flow of charge carrier e^- and $H^+$is governed by the fermi level that drives each charge to its respective electrode. Basically, a photovoltaic solar cell is a thin wafer which consists of a very thin layer of phosphorous doped (n-type) silicon on top of a thicker layer of boron-doped (p-type) silicon. An electrical field is created near the top surface of the cell where the two materials meet (the P-N junction). The photovoltaic effect is created when sunlight hits the semiconductor surface, thus exciting an electron which is attracted towards the n-type semiconductor material and resulting in generation of current. Current generated by a photovoltaic (PV) solar cell is dependent on its efficiency, size (surface area) and intensity of sunlight hitting the surface (Kumar Moluguri et al., 2016). Figure 2-12, obtained from the National Renewable Energy Laboratory (NREL) website, illustrates the progress in solar cell efficiency for thin film-based technologies from 1975-2020.

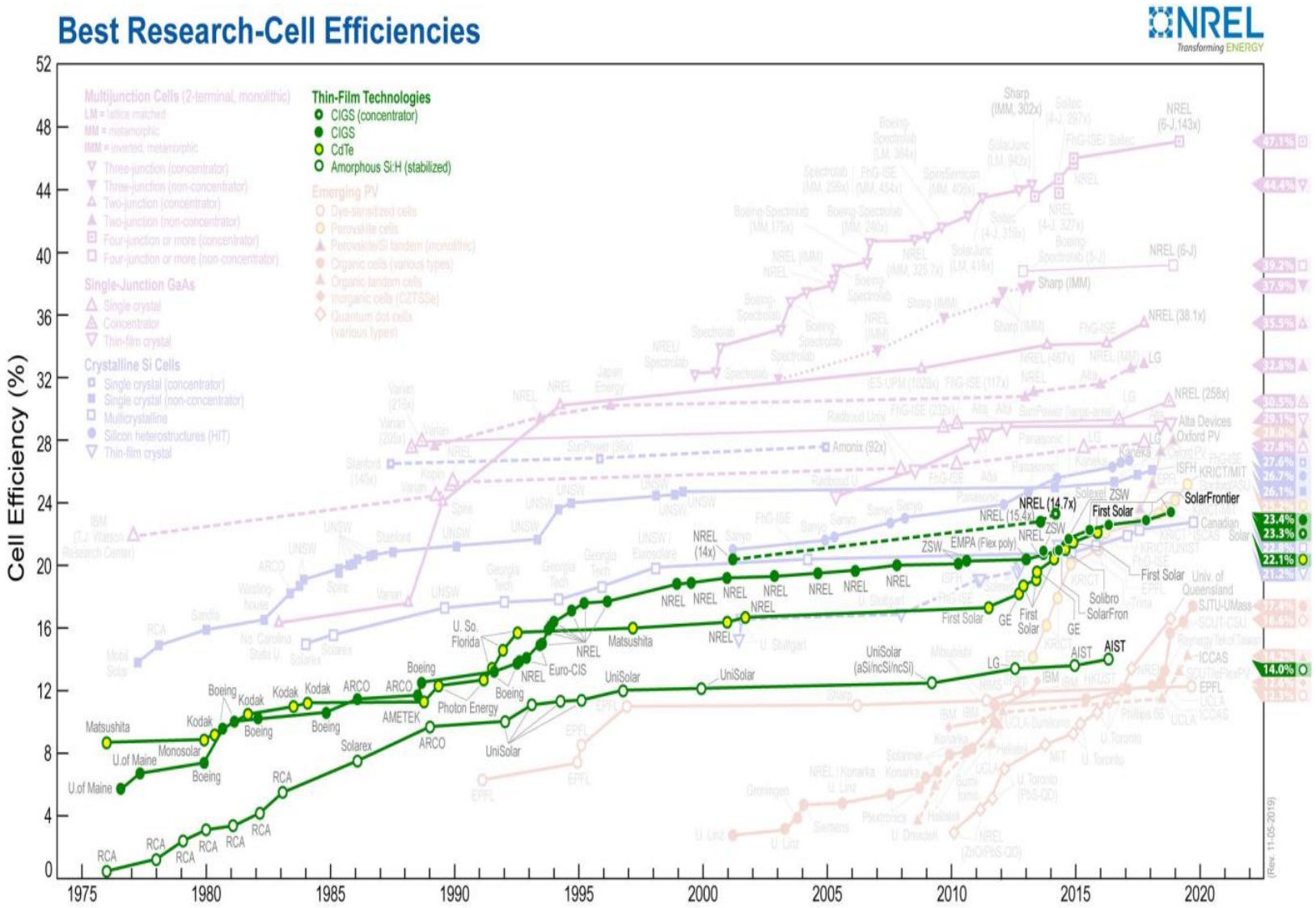


Figure 2-12 NREL data on the progress in efficiency of thin film based solar cells from 1975-2020 (National Renewable Energy Laboratory, 2020)

The recent researches on thin film based photovoltaic technologies have demonstrated a high potential for developing low-cost thin film-based silicon PV technologies (Martin et al., 2004). The major advantage of these technologies is that there is a material reduction as compared to silicon wafers (Sopori, 2007). With evolving technology and research, solar cells which make use of a thin layer of active materials are proposed. However, they have a challenge of absorbing long-wavelength light as it passes through the thin layer of active material without being absorbed hence the use of light-trapping structures (LTS) is applied to improve absorption in the active layer (Ghahremanirad et al., 2016). The cost reduction, adaptability and high efficiency of thin-film solar cells lead to their use in power generation mobile devices and building integrated photovoltaics. The fabrication of these cells is however complex and challenging since there is a contradictory interchange between their optical and electrical properties (van Dijk et al., 2016). For excellent optical performance, the photovoltaic solar cell should be thicker while for best electrical performance and reduction in cost, a thin photovoltaic solar cell is considered the best. This can be efficiently achieved by the improvement of the diffusion length of charge carriers (van Dijk et al., 2016). For commercialization purposes, thin film silicon solar cell technology requires its energy conversion efficiency values to be increased with a technique commensurate with low cost of fabrication.

2.8.1 Current trends in solar cell technology

Razykov et al. (2011) reported that solar photovoltaic market was growing annually at a rate of 35-40%, while photovoltaic production was at 10.66 GW in 2009. The crystalline silicon and polycrystalline silicon wafer technologies dominate more than 80% of the global PV industries. Gallium Arsenide and single junction crystalline solar cells are almost reaching their maximum

theoretical maximum efficiency, whereas; thin film solar cells have promising efficiency results (Razykov et al., 2011) and the efficiencies are highlighted in the Table 2-7.

Table 2-7 Conversion efficiencies of selected thin film solar cells

Thin Film Solar Cells	Conversion Efficiency
CIGS	19-20 %
CdTe	16-17 %
Tandem or Multi-Junction 7	40%
TiO_2-Dye Family	<10%

Razykov et al. (2011), concluded that continuous research and development (R&D) is biased towards increasing the efficiency of thin film solar cells and nano-PV devices. They also highlighted that emphasis should be on the development of cost-effective manufacturing technologies that will lower the solar module production cost.

Solar photovoltaics are proving to be a promising opportunity for power generation and business (Devabhaktuni et al., 2013). There is a remarkable improvement by international, governmental and non-governmental organizations in supporting solar technology uptake in different nations. The progress has improved the quality of living to those who were once lacking modern energy. Developing societies will benefit from a rise in solar PV system installation. These authors concluded that due to intervention by more organizations volunteering their financial, technical and professional services, solar photovoltaic technology is becoming cost-effective. The current efforts by industry leaders and researchers have also reduced the costs and improved the

efficiencies, hence; increasing the demand of solar PV technologies. There is a speculation that in the next decade solar power will be the primary, integrated and cost-effective power source that reduces environmental impact and increase energy security (Devabhaktuni et al., 2013).

Photovoltaic cell technologies can be divided into three generations which are 1st, 2nd and 3rd generation PVs. The overall efficiency and performance of these PV generations vary due to types of semiconductor materials used. The more commercially mature generations are the 1st and 2nd Generations while 3rd Generation is in R&D phase and premature (Gangopadhyay et al., 2013; Khan and Arsalan, 2016)

2.8.2 Methods of silicon solar cell fabrication

The most common solar cell technologies are monocrystalline, polycrystalline and amorphous. Monocrystalline silicon cells are produced from pure silicon (single crystal) wafers. The wafer substrates are cut from column ingots grown by Czochralski (CZ) process (Goetzberger et al., 2003; Miles, 2006). Single-crystal solar cells are cut from pieces of unbroken silicon crystals. The crystals are shaped as cylinders and sliced into circular disks. These slices can be cut into other shapes such as rectangular or square to optimize the space to be occupied by cells on the module. Polycrystalline solar cells are made from silicon substrates cut from polycrystalline ingots formed by melting and pouring silicon into a mould. The mould forms a squared cross-section. Thin slices are cut from the block. There is no material loss on the fact that the discs are square shaped in nature. As the material cools down it crystallizes in an imperfect manner causing the polycrystalline cells to have a somewhat lower energy conversion efficiency compared to the single crystalline cells. The polycrystalline cells are slightly larger in size per gained watt than the

monocrystalline cells (Nordtröm, 2012). The methods used to make polycrystalline cells include the heat exchange method (HEM), electromagnetic casting (EMC) and directional solidification system (DSS) with DSS being the most common method (Miles, 2006) .Basically, the chemical route is used to produce polycrystalline cells while the metallurgical route is used to produce monocrystalline cells (Xakalashe and Tangstad, 2012) as shown in Figure 2-13. The production of monocrystalline solar cells is more complex compared to the production of polycrystalline solar cells. Both cell types are then polished and treated to repair potential damages that could have occurred during slicing.

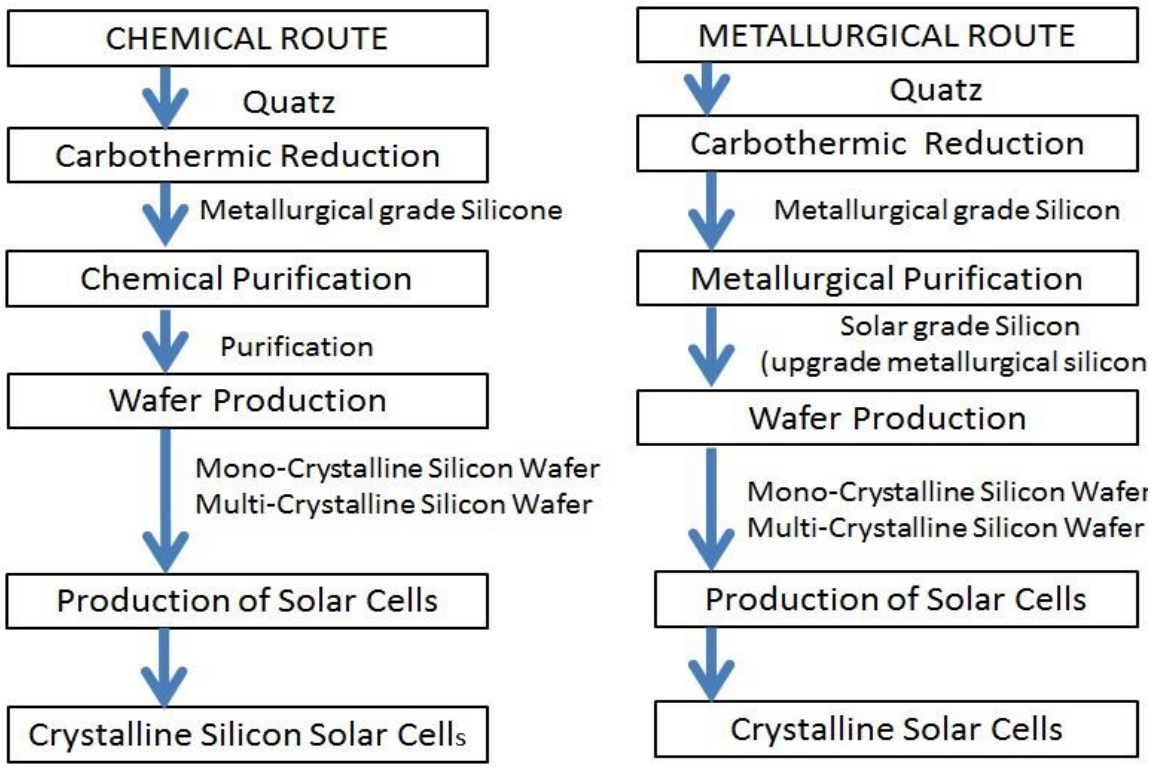


Figure 2-13 Stages to produce crystalline silicon solar cells from quartz. Adapted from Goetzberger et al. (2003)

Meanwhile, the amorphous silicon cells (a-Si) are produced by use of hydrogen to passivate the dangling bonds in Si. A common practice is the deposition of the produced silicon film on a glass substrate. The deposition methods include plasma enhanced chemical vapour deposition, hot-wire catalytic deposition, very high frequency (VHF) glow discharge deposition, indirect microwave deposition and hot-wire glow discharge deposition (Deng and Schiff, 2003)

2.8.3 Nano Photovoltaics (Silicon Nanoparticles in Solar Cells)

According to PV Magazine USA: 2017, European researchers have become the first to record Success in the effort to integrate a nano-photonic structure into a crystalline silicon solar cell, boosting its light absorption and greatly reducing silicon use. This breakthrough, the researchers say, sets a pathway for scaling down the texture of crystalline solar cells from the micro to the nanoscale.

The use of silicon nanoparticles in solar cell production not only saves material but also improves the efficiency of the solar cell device (Barcaro et al., 2017). Recently, the use of selforganized plasmonic nanoparticle layers within the device window layer or back reflector using the deposition and subsequent annealing of thin metal films has been explored (Chen et al., 2013). The accurate tailoring of periodic nanoparticle arrays to the absorption characteristics of the amorphous silicon material is expected to yield an increase in performance compared to randomized particles (Crudgington et al., 2017).

In photovoltaic cells, it is regarded that the purity of silicon needs to be above 99.9999 wt% (Six nines) to enable long carrier diffusion length. Silicon (Si) nanowires and nanoparticles can provide the following advantages: absorption enhancement, efficient carrier extraction and reduced

requirements for material quality in solar photovoltaics (Zong et al., 2015). Figure 2-14 shows silicon nanoparticles incorporated in a solar cell to enhance solar cell performance. Nanosized crystalline silicon is a viable material for use in photovoltaics. The growth process for traditional nanocrystalline silicon involves hydrogen dilution, which hinders the amorphous material's performance, or post-process annealing, which adds another step to the growth process. Decoupling the growth of a-Si and Si-NPs solves this problem (Klafehn, 2016).

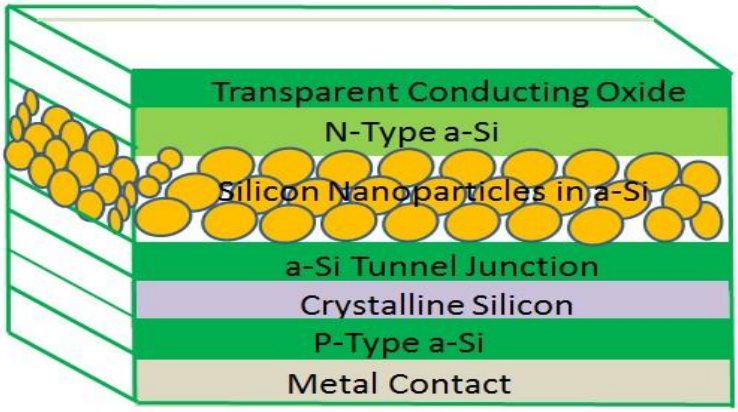


Figure 2-14 Quantum-confined Si-NPs Can Be Used as a High Bandgap Layer in Lieu of Other Materials, Allowing for a Multi-Bandgap Solar Cell Composed Entirely of Silicon (Adapted from Klafehn, 2016).

2.8.4 Bulk heterojunction organics solar cells (OSCs)

Organic solar cells have made fast progress in the last decades and are close to a broad commercialization (Tress et al., 2011). Organic solar cells (OSC) cells are a potential alternative to conventional Si solar cells, which includes (i) dye-sensitized (Kuang et al., 2007), (ii) polymer (Li et al., 2011a), and (iii) small-molecule (Mutolo et al., 2006) cells. Of all the OSCs, polymer based solar cells offer the following benefits light weight, low cost, mechanical flexibility, high

throughput during manufacturing and large surface area reel-to-reel coating processes. It is also anticipated that organic solar cells could be produced commercially if the power conversion efficiency (PCE) of approximately 10% is achieved (Würfel et al., 2015). The highest power conversion efficiency polymer solar cells have been fabricated from an active layer composed of a blend of regioregular poly(3-hexylthiophene) (P3HT) and the fullerene derivative [6,6]-phenyl-C61 butyric acid methyl ester (PCBM) (Chen and Rieke, (1992) ; Hummelen et al., (1995). The P3HT and PCBM blend forms a phase-separated ‘‘bulk-heterojunction’’ (BHJ) nanostructure that provides a large interfacial area for exciton dissociation. When photo-excited, the P3HT network acts as an electron donor and transporter of holes to the cell anode, while the PCBM network acts as an electron acceptor and transporter of electrons to the cell cathode (Kim et al., 2007; Li et al., 2005, 2011a; Reyes-Reyes et al., 2005; Salinas et al., 2011). The structure and operation of a polymer based organic solar cell is presented in Figure 2-15**.**

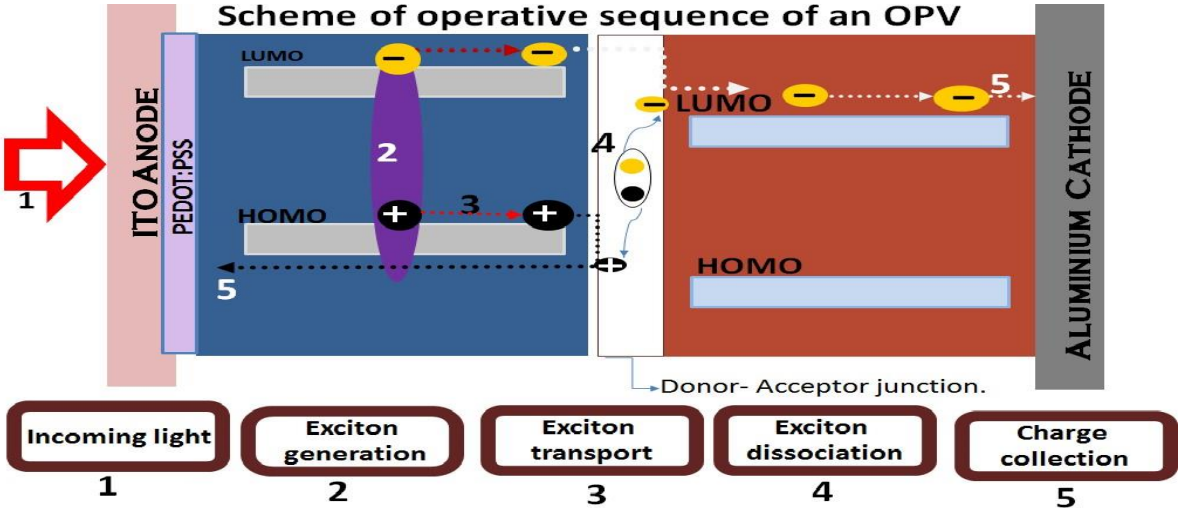


Figure 2-15 Operational sequence of an organic solar cell (Adapted from Otieno et al. (2018*)*

The operational principle of bulk heterojunction organic solar cells is based on photovoltaic effect. This is both a physical and chemical phenomenon resulting from the generation of a potential difference at the polymer/fullerene interface as a result of a photo/light response (Jovanov et al., 2017). The photovoltaic effect in an organic solar cell can be described as shown in Figure 2-15. In summary, it follows the following sequence;

1. Light-absorption to generate strongly bound electron-hole pair (exciton).
2. Exciton diffusion to the donor acceptor interface.
3. Exciton dissociation leading to the separation of charge carriers.
4. Charge transport within the device layers to the respective electrodes (Otieno, 2015) 5. Charge collection at the electrodes

2.8.5 Silicon nanoparticles enhancing properties of OSCs

The main thrust on the commercialization of the organic solar cells is the improvement of the power conversion efficiency (PCE). Several studies conducted to improve PCE focused on change of parameters such as: optical properties of the (P3HT: PCBM) blend (Zhu et al., 2015); donor material absorbance by the mixing of energy-band engineered polymers to increase the bandwidth for adsorption (Yang et al., 2015); optimization of domain and size (Ding et al., 2018; Morgenstern et al., 2016) and interface engineering (Pfadler et al., 2014). Another approach which has gained attention among researchers is the development of hybrid solar cells with active material into which inorganic semiconductor particles are incorporated (Zhou et al., 2011). Inorganic particles that have been utilized in organic solar cells include CdS (Lee et al., 2008); CdTe (Gur et al., 2006); CdSe (Yang et al., 2011); $CuInS_2$ (Arici et al., 2003); PbSe (Tan et al., 2009); PbS (Tsang et al.,

2009); SnO_2 (Kudo et al., 2007), TiO_2 (Kuo et al., 2008); and ZnO (Bhat et al., 2011; Hames et al., 2010; Takanezawa et al., 2008).

According to Zhao et al. (2016), PCE can be improved when SiNPs was incorporated into P3HT:PCBM solar cells which resulted in a cascade band structure. Size reduction and doping are effective ways used in the fine-tuning of energy levels in semiconducting nanoparticles. To understand the use of doped NPs in hybrid solar cells, SiNPs with n and p-type dopants have been synthesized and utilized with active material. The P3HT:PCBM blend serves as a reference material blend because of its continued approval in fundamental hybrid solar cells research (Chi et al., 2014). Hemaprabha et al. (2018) investigated the effect of using n and p-type nano silicon in P3HT: PCBM at different weight percentages. A PCE of 3.46 % was attained using doped p-type silicon nanoparticle. The team concluded that together with size reduction, the fine-tuning of energy levels in NPs, can be achieved through doping and mixing at appropriate weight ratios.

2.8.6 Challenges of producing nano silicon from agro waste

Genuine progress in the valorization of agricultural waste require a close partnership between chemists and engineers to enable new ideas from chemists to be rapidly transformed to meet the needs of global increasing population. An initial challenge faced is the difference in the effect of human exposure to engineered nanoparticles compared naturally occurring nanoparticles. Engineered nanoparticles may be better equipped to evade immuno response against foreign bodies because of their size or protective coatings. The actual extent of health and environmental risks raised due to the exposure to engineered nanoparticles need further study (Prasad et al., 2014).

Nanoparticles are generally synthesized using a bottom-top or top-bottom approach based on whether a chemical process was used to produce the materials or the material is produced through size reduction from its bulk state through chemical attrition or physical milling processes (Adebisi et al., 2017). In the bottom-top approach, nanoparticles can be synthesized using chemical and biological methods by self-assembly of atoms to new nuclei which grow into a particle of nanoscale size while in the top-bottom approach, suitable bulk material is broken down into fine particles by size reduction using various lithographic techniques e.g. grinding, milling, sputtering and thermal/laser ablation. Most of these methods for the synthesis of nanoparticles are very expensive (Kharissova et al., 2013). The challenges in the field are outweighed by benefits of nanotechnology to research.

2.9 Concluding Remark

The literature review demonstrated that production of nano silicon particles from bio-waste ashes has attracted the interest of researchers in recent decades as an economical and environmentally effective waste management approach. The various routes for which SiNPs had been produced such as pyrolysis, leaching, sol-gel, acid pretreatment, combustion, precipitation, supercritical CO_2-drying, biotransformation, calcination, and magnesiothermic reduction demonstrate the growth of knowledge on the obtainment of SiNPs from agro-wastes and inorganic sources. MRM, it was submitted, is the best method in SiNPs production in respect of cost effectiveness. Other researchers, however, submit that the chemical synthesis technique is more attractive because of the possibility of surface modification and control of Si particle size distribution, but contamination of residual side products may be a setback. The current study, however, outlined different characterization methods to update on the current and effective techniques for an understanding of

the nature of the nanomaterials produced. This will project the material for the suitable application. To date, major characterization techniques include XRD, UV-Vis Absorption, SEM, TEM, FTIR, AFM, HRTEM and Raman Spectroscopy. For the past 20 years, researchers have focused on different feedstock mainly silane, silica, SiO_2, $SiCl_4$, bamboo, sugar cane bagasse, rice husk, groundnut shell, coffee husk and had applied ultrasonification, microwave-induced decomposition, PLA, low-temperature solution route, plasma-enhanced chemical vapor deposition (PECVD), spark discharge process, metallothermic process and hydrometallurgical.

More so, the production of SiNPs using combustion, vacuum directional solidification, halidothermic reduction, pyro-chemical process and vermicomposting with annelids technologies proved attractive because, the processes enhance the SiNPs high active surface state, physical characteristics, outstanding photoluminescence and biocompatibility in solar cell fabrication. The review, however, indicated that the conversion efficiency in existing solar cell applications remains very low (ranging from 17 to 25%). The efficiency of photovoltaic solar cells depends on the size (surface area) and the intensity of sunlight hitting the surface. For over 20 years, latest research efforts had recorded photovoltaic efficiency of over 45% in 2016, using multijunction solar cells whereas in 2004 below 5% conversion efficiency was achieved on the application of organic solar cells technology. Thus, the review shows that there is still more research work required in production of silicon nano particles to fully support solar cell technology and to reduce environmental challenges posed by bio waste.

Chapter 3 : Methodology

3.1 Introduction

Relevant literature has been explored and reviewed hence the birth of this chapter to lay down the methodology for this work. In this chapter, the methods for the extraction of nano silica and preparation of nano silicon from sugarcane bagasse ash are reported. Fabrication and testing methods for the solar cell material are detailed. Based on the identification of the area of contribution of this study to the field, this study has been divided into the following steps as shown in Figure 3-1.

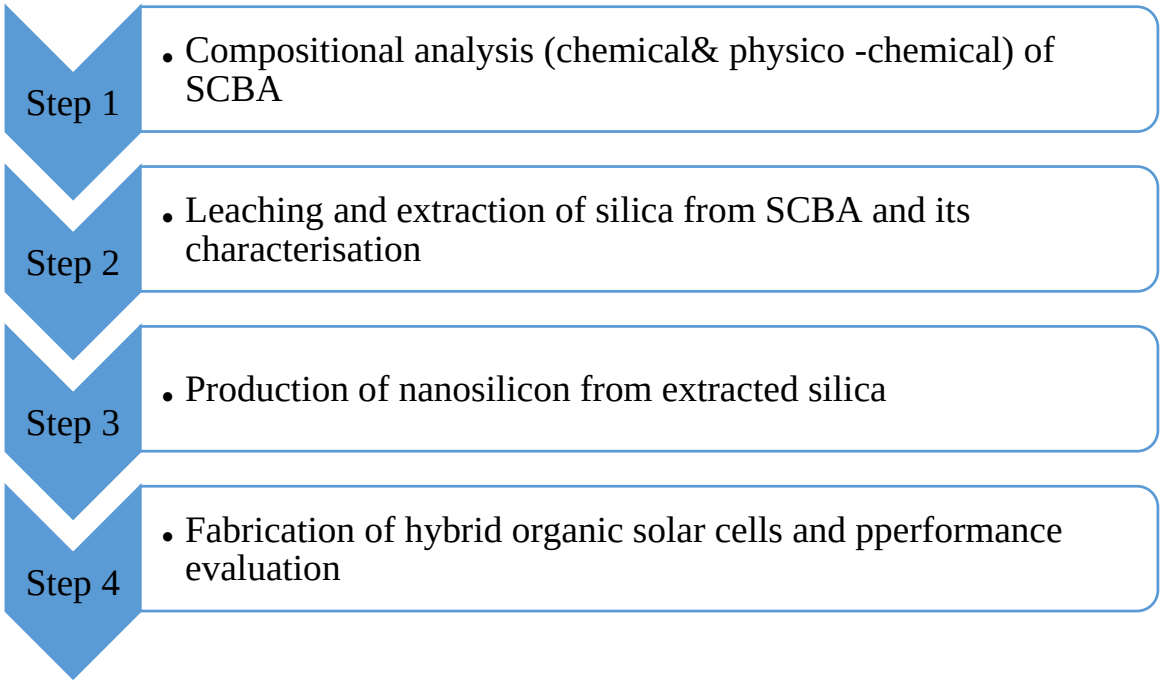


Figure 3-1 Overview of the methodology employed in this study

3.2 Chemicals and Chemical Reagents

Chemicals and chemical reagents used for the various experiments were of analytical reagent grade and were used without further purification. Sodium hydroxide, citric acid, hydrochloric acid,

activated carbon, hydrofluoric acid, nitric acid and magnesium powder (99%), were purchased from Sigma-Aldrich (Pvt) Ltd, Republic of South Africa. Chemicals used for fabrication of solar cell by spin coating namely acetone, ethanol, poly(3,4-ethylene doxythiophene, polystyrene, P3HT and PCBM were also purchased from Sigma-Aldrich.

Deionized water was used for all experiments that were performed in aqueous media.

3.3 Sugarcane Bagasse Ash Availability and Sampling Procedure

Sugarcane bagasse ash used in this study was obtained from Green Fuels, Chisumbanje a bioethanol company in south-eastern Zimbabwe. The production of ethanol is estimated at 43 weeks/year. For any research which involves synthesis to get a product, there is need to explore the availability of the feedstock/raw material for the research (Dixit et al., 2019). Figure 3-2 gives images of the sugarcane bagasse ash and the production plant.



Figure 3-2 Sugarcane bagasse ash (a) and the source plant at Green Fuels, Chisumbanje (b)

3.3.1 Assumptions

The following assumptions were made in the estimation of the quantity of sugarcane bagasse ash availability:

- For every tone of cane, 26% of bagasse is produced (Martines-Filho et al., 2006)
- For every 260 kg of bagasse, approximately 5.2% ash is obtained (Farirai et al., 2019).

Table 3-1 Annual estimated quantity of sugarcane bagasse ash produced

Description	**Quantity in Tons**
Bagasse used by boiler per hour	58.60
Surplus bagasse	28.60
Bagasse produce per day	1404
Bagasse ash produced per day	33.70
Total bagasse produced per season	422604
Total bagasse ash produced per season	21975

As shown in Table 3-1, a large quantities, 21 975 tons, of sugarcane bagasse ash is produced per season. The challenge then lies in the disposal of the ash, hence currently it is used for landfilling and as fertilizer in the sugarcane plantations, but these applications are far from enough to consume the entire waste resource.

3.4 Sampling Method

The samples of sugarcane bagasse and ash collected are shown in images in Figure 3-3.



Figure 3-3 As received (a) sugarcane bagasse bottom ash (b) sugarcane bagasse fly ash (c) sugarcane bagasse

3.4.1 Sugarcane bagasse ash (SCBA)

The different forms of sugarcane bagasse ash produced at the facility were sampled of the following points: the bottom ash outlet of the boiler and the ash sluice water holding tank to collect sugarcane bagasse bottom ash (SCBBA), the wet fly ash outlet to collect sugarcane bagasse fly ash (SCBFA) and the ash heap for both types. The samples were air dried and classified using sieving equipment.

3.4.2 Comprehensive characterization of sugarcane bagasse ash

The sugarcane bagasse was rinsed with deionized water to remove dust and sand particles. The as-received ashes of SCBBA and SCBFA and dried SCB were further ground using a pulverizer. The three samples were sieved through a 40-μm sieve in preparation for analysis. The ash content of raw sugarcane bagasse was determined according to ASTM D2974-8 standard (Standard Test Methods for Moisture, Ash, and Organic Matter of Peat and other Organic soils) (ASTM, 2000). Thermal behavior of samples was investigated by using a thermogravimetric analyzer (TGA) (Q600 SDT Thermal Analyzer TA Instrument, USA). The samples were heated in the absence of oxygen at a rate of 10 ^{o}C/min to a temperature of 800 ^{o}C. Chemical analysis of SCB, SCBBA and SCBFA was carried out via X-Ray Fluorescence Spectrophotometer (Panalytical PW2404 X-ray

Fluorescence Spectrophotometer). For the determination of surface chemistry, Fourier Transform Infrared Spectrophotometer, FTIR (Perkin Elmer 100 FTIR Spectrophotometer), was used. An X-Ray Diffractometer (German Diffractometer D2 PHASER Bruker X-Ray with Cu Kα radiation) was used to determine the degree of crystallinity of the samples. A Field Emission Scanning Electron Microscope (Carl Zeiss Sigma FESEM Oxford XACT EDX detector) equipped with Energy-dispersive X-ray was used to check morphology and elemental composition. The results and findings are discussed in Chapter 4. Based on the preliminary results on comprehensive characterization of sugarcane bagasse and its ashes, sugarcane bagasse bottom ash (SCBBA) was found to be rich in silica than other samples and was hence used further experimental work.

3.4.3 Leaching and thermal treatment of sugarcane bagasse ash (SCBA)

The method by Pa et al. (2016) was adopted with minor modifications. 50 g of pulverized sugarcane bagasse ash were suspended in 500 ml of 5% citric acid solution in a beaker. The suspension was refluxed for 3 hours at 90 ℃ to remove metallic impurities. The sugarcane bagasse ash was separated by centrifugation, and the residue was washed repeatedly with deionized water to neutrality. The citric acid-leached ash sample was subsequently dried in an oven at 110 ^{o}C. After drying the ash samples were placed in a muffle furnace at 700 ^{o}C for three hours to eliminate unburnt hydrocarbons.

3.4.4 Extraction of nano silica from sugarcane bagasse ash

The extraction method was adapted from Nazriati et al. (2014) with minor modifications. Citric acid leached sugarcane bagasse ash (20 g) was dispersed in 60 ml of 2 M NaOH in a 500 ml round bottomed flask. The suspended SCBA was refluxed for 1 hour with constant stirring using a

magnetic stirrer to dissolve the silica resulting in the production of a sodium silicate rich solution. The reaction of the alkaline leaching experiment is given in Equation (3.1):

$$SiO_2(SCBA) + 2NaOH\ (\text{aq}) \rightarrow Na_2SiO_3(\text{aq}) + H_2O\ (\text{l}) \qquad \textit{Equation 3.1}$$

The suspension was cooled to room temperature and filtered to remove impurities using a Whatman No. 41 ashless filter paper. One portion of sodium silicate rich solution was passed through a column packed with activated carbon. The two portions of sodium silicate rich solutions were then titrated separately with 1M HCl with constant stirring until pH 5. The reaction is given in Equation (3.2):

$$Na_2SiO_3 + 2HCl \rightarrow SiO_2 + 2NaCl + H_2O \qquad \textit{Equation 3.2}$$

The gel obtained was aged for 10 hours, separated by centrifugation and washed with deionized water, dried in an oven at 110 ^{o}C for 24 hours to obtain white silica powder. The nano silica produced was characterized using XRF, FTIR, XRD, BET, SEM and TEM. Experimental procedures up to isolation of nanosilica are illustrated in Figure 3-4.

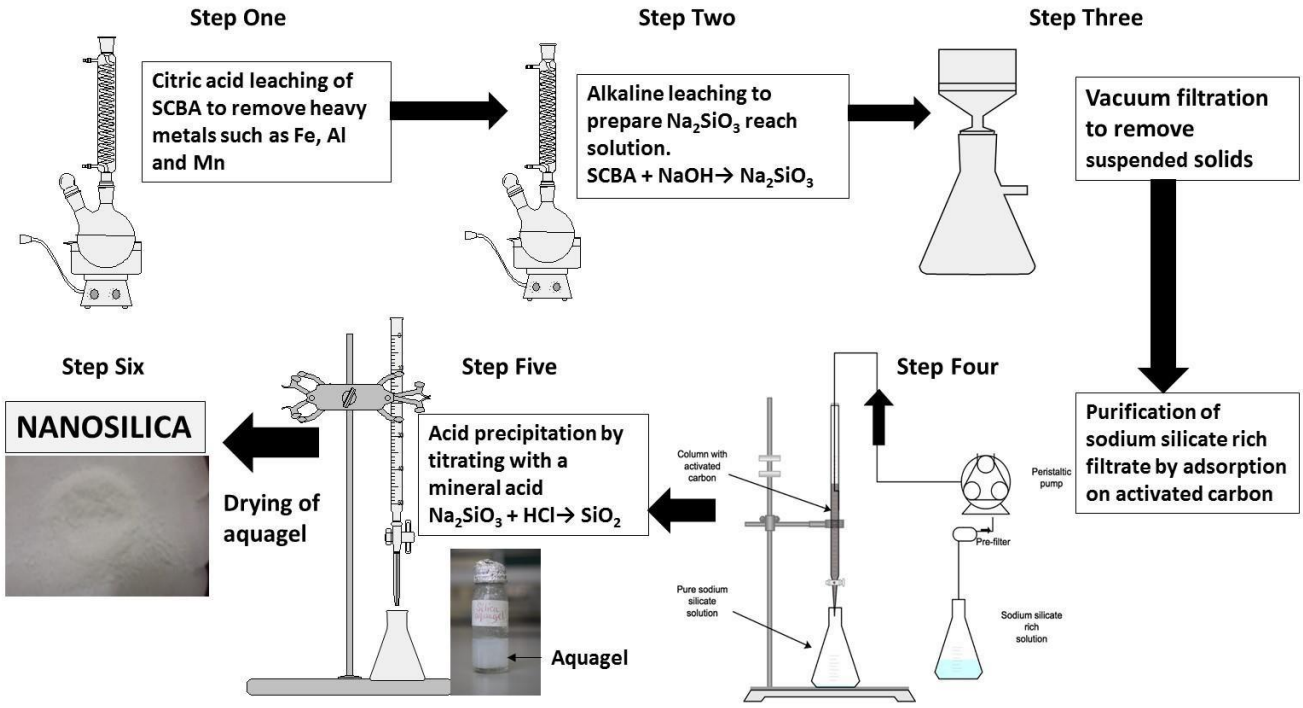


Figure 3-4 Experimental flow diagram for the extraction of nano silica from sugarcane bagasse ash

3.5 Magnesiothermic Reduction of Nano Silica into Nano Silicon

Nano silica extracted from sugarcane bagasse ash via sol gel adsorption method described in Section 3.4.4, was used as the precursor for the production of nano silicon using magnesiothermic reduction with minor modification as described elsewhere (Bao et al., 2007; Onojah et al., 2012; Venkateswaran et al., 2013). Nano silica and magnesium powder were mixed in a molar ratio of 1:2.1, and then powders were homogeneously ground with a mortar and pestle. The homogeneously ground mixture was subjected to a pyrolysis temperature of 700°C for 4 hours in a muffle furnace. The chemical reaction is presented in Equation 3.3:

$$SiO_2\,(s) + 2Mg(s) \quad \rightarrow \quad 2MgO(s) \; + \; Si(s) \qquad \textit{Equation 3.3}$$

A portion of the obtained brownish powder (as -produced silicon) was washed with aquaregia (1HNO_3:3HCl) to remove MgO while the other portion was washed with 2% HF. Figure 3-5 shows the flow diagram of magnesiothermic reduction method (MRM) for nano silica into nano silicon.

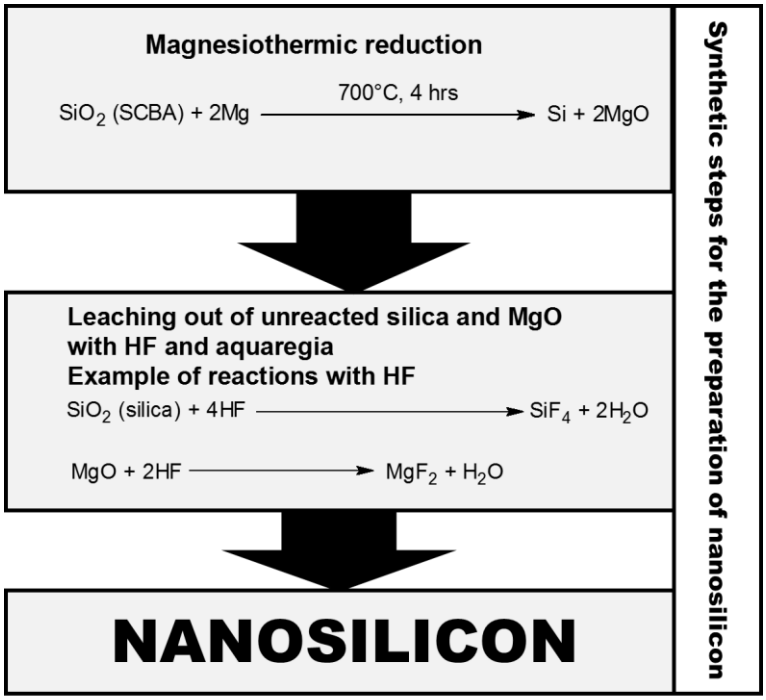


Figure 3-5 Synthetic steps in the magnesiothermic reduction of SCBA nano silica into nano silicon

Physicochemical properties of the as-produced nano silicon were characterized using XRF, XRD, TEM, and SEM, Fourier Infrared spectrophotometer and N_2 physisorption at 77 ℃. The results obtained were compared to commercial grade silicon.

3.6 Instrumental Characterization of Nano Silica and Nano Silicon

The following characterization methods were used for studying the properties of nano silica and nano silicon; (i) X-ray Fluorescence Spectrophotometry (XRF), (ii) X-ray Diffractometry (XRD) (iii) Fourier Transform Infrared Spectrophotometry (FTIR), (iv) N_2 physisorption, (v) Scanning

Electron Microscopy (SEM) coupled with energy dispersive x-ray (EDX) microanalysis and (vi) Transmission Electron Microscopy (TEM).

3.6.1 X-ray fluorescence spectrophotometry

Major elements in the form of oxides were determined using the Panalytical PW2404 X-ray fluorescence spectrophotometer. Samples were fused using Johnson Matthey Spectrolflux 105 at 1100°C. Standard calibrations were done with the use of synthetic oxide mixtures.

3.6.2 X-ray diffractometry

This technique allows the determination of the nature of the crystallized phases by viewing the sample at selected diffraction/scattering angles and measuring peak intensity. These angles of diffraction are related to the characteristics of the crystal lattice and to the incident radiation (wavelength L) by the law of Bragg:

$$2d_{(\mathrm{hkl})}\, sin\, \theta = \mathrm{n}\, \lambda \qquad \textit{Equation 3.4}$$

Where dhkl is the distance between 2 index planes or diffraction planes of Miller hkl in Å; θ is the Bragg angle; λ is the wavelength of radiation in Å.

3.6.3 Fourier transform infrared spectrophotometry

The surface functionalities and the type of functional groups on the surfaces of the samples were determined using a Perkin Elmer 100 FTIR Spectrophotometer at wavelength range 500-4000 cm^{-1} while in absorbance mode. About 2 mg of sample was placed on the instrument diamond attenuated total reflectance (ATR) accessory. The sample was positioned on the sample holder and using the turning knob to exert on the sample before the spectrum would be produced.

3.6.4 Nitrogen physisorption

The complete isotherms of N_2 adsorption-desorption allows the characterization of the porous texture of a material: the specific surface, porous volume and the shape of the pores. Complete isotherms of adsorption-desorption of N_2 at 77 K on entirely automatic equipment, ASAP Micromeritics.

3.6.5 Scanning electron microscopy

Scanning electron microscopy makes it possible to observe the morphology of the samples. The samples were double coated with 60% palladium and 40% gold (Pd/Au) prior to SEM analysis to prevent charge build-up. CARL ZEISS sigma field electronic scanning electron microscope (FESEM) was used to observe the surface morphology of the samples.

3.6.6 Transmission electron microscopy

Transmission electron microscopy was used to determine the morphology and the particle size of the samples. In this work, a FEI Tec T12 TEM was used.

3.7 Fabrication of Organic Solar Cell

The fabrication of the organic solar cell follows three stages:

a. Doping of a portion of nano silicon with Boron to obtain p-type nano silicon.

b. Spin coating of PEDOT: PSS reference hole transport layer and PEDOT:PSS with blends of nanoparticles

c. Aluminum cathode metallization through thermal evaporation

3.7.1 Doping of nano silicon particles

A method reported by Goval and Soni. (2017) was adopted for the doping of a portion of nano silicon particles to get p-type nano silicon particles with the intention to fine tune energy levels in the semiconducting particles. Boric acid (H_3BO_3) acid was used as a source of boron to synthesize p-type nano silicon powder. Aqueous solution of boric acid in requisite amount (50 ppm) was added to the SiNPs powder, and the solution was dried. The dopant mixture was crushed in an attrition mill for 4 h to allow homogeneous distribution of boron in the nano silicon (Goyal and Soni, 2017). The efficiency of the doping process was verified through a process which started with parallel experiments, the first in which nanoparticles are added to the hole transport layer during organic solar cell fabrication and the second where doped nanoparticles were added into the hole transport layer. Further detail is given in the section that follows.

3.7.2 Organic solar cell fabrication

3.7.2.1 Substrate cleaning

Substrate cleaning is a crucial step in the preparation of high-quality thin films as well as for high adherence to the substrate. In this present study, ITO coated glass and quartz substrates for all the analysis were used. The quartz and ITO substrates were first cut in small pieces measuring 125 mm^2. For ITO each piece had a portion wet etched through a reaction between the HCl and Zn paste embossed on the film. The etched ITO and cut quartz were then ultra-sonicated in a soap solution then rinsed thoroughly in deionized water bath. After rinsing they were cleaned in acetone bath for 15 minutes, rinsed in deionized water followed cleaning in ethanol solution for 15 minutes. Finally, they were rinsed in deionized water bath for 15 minutes and then allowed to dry with nitrogen flush. The main aim of cleaning the substrates by acetone is to remove the

inorganic/organic impurities respectively and finally acetone is removed by ethanol cleaning. Ultrasonic cleaning in deionized water bath was done to remove any other foreign particles that stay on the surface of the substrates.

Nano silica, nano silicon, p-type nano silicon (Boron doped) were added in PEDOT: PSS (Poly (3,4-ethylene dioxythiophene:poly (styrene sulfonate)) a hole transport layer to make four different solution F1(reference), F2(SiO_2NPs), F3(SiNPs) and F4(p-type SiNPs). The solutions were made by adding 0.5 mg nano particles in 1 ml of PEDOT: PSS (1.3 wt. % dispersion in H_2O). The resulting solutions were ultra-sonicated for 30 minutes before being spin-coated onto ITO-coated glass substrates. PEDOT: PSS and a blend of nano particles and PEDOT: PSS without nanoparticles (reference) were then spin-coated on top of the ITO layer at a speed of 2000 rpm for 60 seconds and then annealed over a hot plate at 100 ˚C for 10 min to remove any residual water. The active layer comprising poly(3-hexylthiophene):[6,6]-phenyl-61-butyric acid (P3HT: PCBM) polymer blend solution (Sigma-Aldrich) was prepared by mixing P3HT and PCBM at 1:1 ratio in chlorobenzene, with a total concentration of 20 mg/ml as described elsewhere (Otieno et al., 2016). The mixed solution was spin-coated at 2000 rpm for 60 seconds to form a homogenous film of thickness of approximately 215 nm. The purpose of blending was to improve the PCE of the devices. Electrical data to show changes in conductance and optical absorbance were collected as described in section 3.8.3.

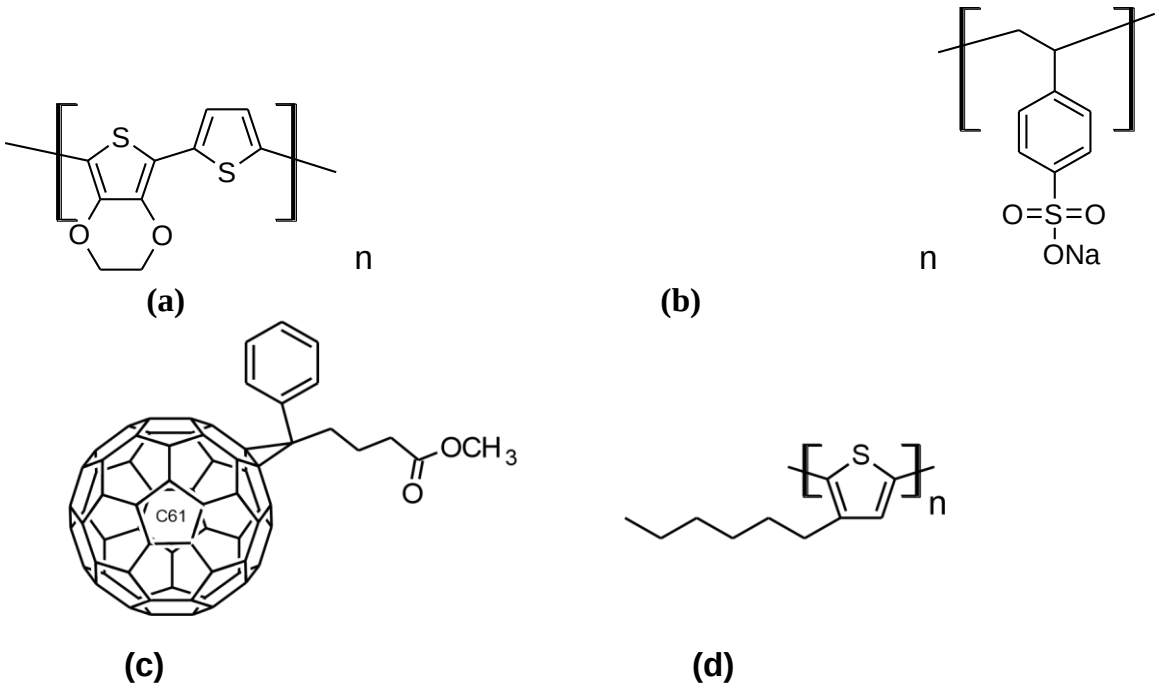


Figure 3-6 Chemical structures of (a) poly (3, 4-ethylene dioxythiophene (PEDOT), (b) poly(styrene sulfonate) (PSS), (c) [6,6]-phenyl-C61-butyric acid methyl ester (PCBM), and (d) poly(3-hexlythiophene) P3HT) (Otieno et al., 2016).

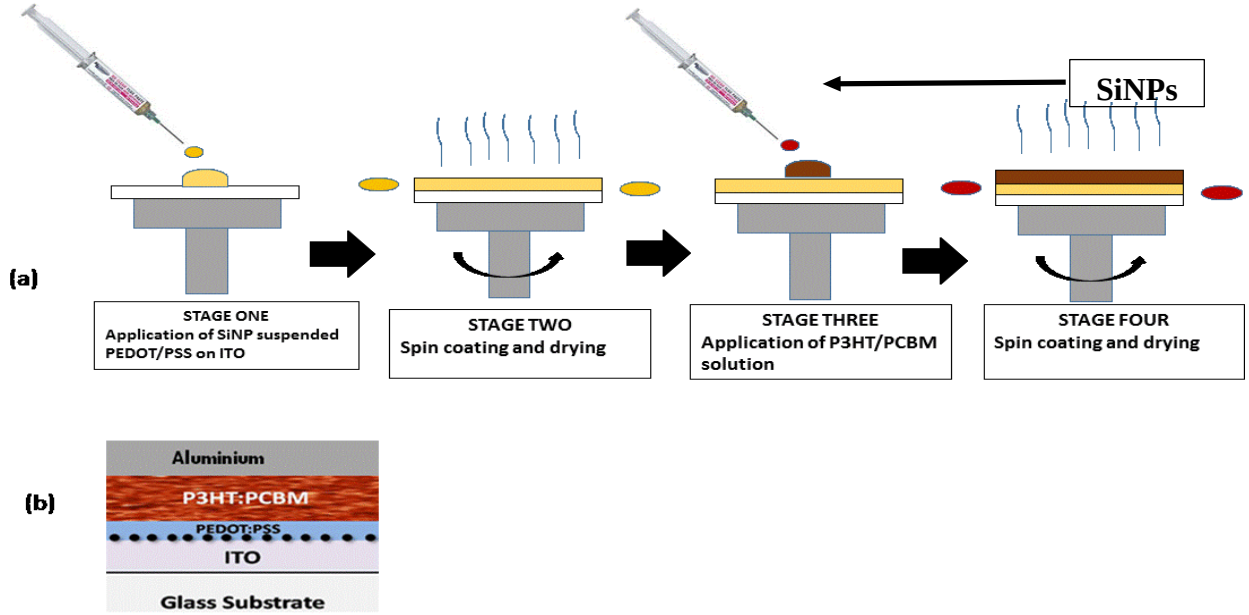


Figure 3-7 (a) Illustration of spin coating procedure (b) Cross-sectional area of an organic solar cell incorporated with SiNPs (b) (adapted from Otieno (2015) with minor modifications)

3.7.3 Thermal evaporation

Aluminum cathode was metalized through thermal evaporation as shown in Figure 3-8. The device was then annealed in argon ambient at 100 ˚C for 15 minutes at a base pressure of 1 atm to remove organic polymer solvent. The thickness of the active layer was approximately 220 nm.

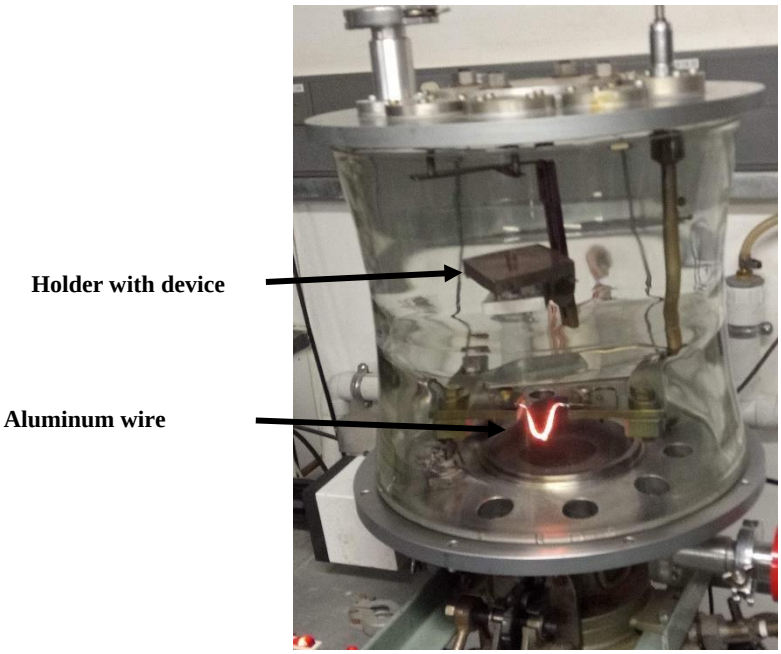


Figure 3-8 Thermal evaporation set-up for application of aluminum cathode to the device

3.8 Solar Cell Characterization Techniques

3.8.1 Raman spectroscopy

Raman spectroscopy is a technique used for studying molecular vibrational modes. Plasmonic nanostructures can be used in enhancing the signal up to 1012 Hz at plasmonic resonance. Moreover, plasmon enhanced Raman scattering enable for detection of a single molecule due to its high sensitivity (Otieno, 2015). Raman data was collected under room conditions.

3.8.2 Atomic force microscopy

The atomic force microscope is designed to measure local properties such as height, and degree of roughness, using a sharp probe which is adjusted into proximity with the sample surface (Liu et al., 2016). In this study a Veeco Dimension 3100 Atomic Force Microscope (AFM).

3.8.3 Optical properties and J –V characteristics

The absorption of the device was measured using UV-Vis NIR-500 Carry Spectrometer while the current density–voltage (J–V) characteristics were obtained using HP 4141B source measure unit (SMU) under 100 mW/cm^2 illumination (AM 1.5G). All the measurements were carried out at room temperature under standard conditions

3.9 Concluding Remark

The chapter submitted methods and procedures employed in the synthesis of nano silica and nano silicon. Also presented was the methodology for the fabrication of an organic solar cell and characterization techniques applied. Procedures for the analytical experiments conducted in this study are described. Results obtained from the experimental protocols are described in subsequent chapters.

Chapter 4 : Chemical and Physicochemical Analysis of SCB, SCBBA and SCBFA

In this chapter, results of the compositional analysis of the raw sugarcane bagasse (SCB), sugarcane bagasse bottom ash (SCBBA) and sugarcane bagasse fly ash (SCBFA) are reported.

4.1 Introduction

Sugarcane processing to produce ethanol and sugar generates by-products such as molasses and bagasse (Alves et al., 2017). Sugarcane bagasse is burned in boilers to produce steam, which is utilized in the factory processes and also to power turbines for the production of electrical energy, which supplies the factory's energy needs, with the excess being sold in the region (Souza et al., 2011). The burning of sugarcane bagasse produces sugarcane bagasse ash (SCBA), which is of negligible cost and is used for landfilling (Huabcharoen et al., 2017). Handling and improper disposal in soils, water and air lead to pollution, which results in environmental challenges and human health problems (Rovani et al., 2018). For every ton of burnt bagasse, 25 to 40 kg of bagasse ash is generated (Sales and Lima, 2010), and subsequently a considerable amount of ash is produced annually. SCBA cannot be used as a fertilizer since it does not have enough mineral nutrients required for agriculture rather it can increase heavy metals to the soil (Xu et al., 2019). Most scientists have worked tirelessly to find other alternative uses of sugarcane bagasse ash. These uses include but not limited to feedstock for ceramics (Teixeira et al., 2008), glass – ceramic material production (Teixeira et al., 2014), synthesis of zeolites (Patcharin et al., 2012) , geo polymers (Faisal and Muhammad, 2016), sodium silicate (Tchakouté et al., 2017), silica aerogels (Nazriati et al., 2014), mesoporous silica (Rahman et al., 2015). However, most focus on SCBA utilization was mainly in production of cementious materials due to good pozollanic properties

(Chusilp et al., 2009; Ganesan et al., 2007; Hernández et al., 1998). SCBA is rich in silica (Rovani et al., 2018; Sales and Lima, 2010). The concentration of silica in sugarcane ranges from 0.3 to 8.4%, about 70-800 kg/ha of plant available silicon is harvested with the sugarcane crop from arable soils annually. Crop uptake of silicon by sugarcane exceeds those of the macronutrients such as nitrogen, phosphorous and potassium (Matichenkov and Calvert, 2002).

Sugarcane is grown commercially in the Lowveld of Zimbabwe which includes Chisumbanje, Nyanyadzi and Chiredzi (Nhiwatiwa et al., 2017). Sugarcane is known to absorb more silicon in the form of silicic acid (H_4SiO_4) than any other mineral nutrient from the soil, accumulating approximately 380 kg/ha of Silicon (Si), in a 12-month-old crop (Savant et al., 1999). However, the silica content in sugarcane bagasse ash is highly dependent on the geographical location and the environment where the sugarcane is grown as well as the farming practices (Martines-Filho et al., 2006). Ethanol and sugar production create by-products such as sugarcane bagasse that can still be tapped for added profitability (Torres-Agredo et al., 2014). Souza et al., (2011) submits that for every ton of harvested sugarcane, 250 kg of sugarcane bagasse are produced, and 6 kg of ash generated giving a 42: 1 bagasse to ash ratio. This ratio closely relates to a 40:1 ratio for the same materials which is reported by (Sales and Lima, 2010b) who submitted that each ton of bagasse generates 25 kg of ash. In this chapter, results of investigation of compositional analysis of Zimbabwean sugarcane bagasse ash to explore its suitability for the production of nano silicon for solar cell application are presented.

4.2 Experimental

The comprehensive characterization methods applied to SCB, SCBBA and SCBFA are described in detail in Chapter 3 (Section 3.4.2) of this thesis.

4.3 Results and Discussion

4.3.1 XRF analysis

The results for chemical composition of samples determined by XRF are shown in Table 4-1. Silica (SiO_2) is a major component in all the three samples. This is also supported by XRD analysis (Figure 4-5), which shows the presence of silica in the form of quartz, cristabolite and tridymite as the major components in the samples. The results are also supported by the work reported by Payá et al. (2002). XRF analysis indicated to the presence of oxides of magnesium, calcium, phosphorous, iron, potassium, sodium, titanium, manganese and aluminum. The silica composition of the sugarcane bagasse ash used in this study concurs with earlier studies conducted in the same country, Zimbabwe (Table 1-2) and strongly correlates with results obtained in other geographical locations as reported by Abdulkadir et al. (2014) in Nigeria and in (Table 1-2) for Columbia. This is probably indicative of the composition of the constituent at the different locations without implication that the soil profiles are similar.

Table 4-1 Chemical composition of SCB, SCBBA and SCBFA

Compound	SCB	SCBBA	SCBFA
SiO_2	60.75	71.49	69.67
Al_2O_3	6.66	6.2	4.69
Fe_2O_3	4.84	3	2.67
CaO	7.54	3.3	3.06
MgO	3.63	1.79	1.37
K_2O	7.04	4.79	8.03
Na_2O	4.34	4.61	4.2
SO_3	0.28	0.11	0.82
TiO_2	1.41	0.80	0.44
MnO	0.17	0.14	0.17
P_2O_5	0.97	0.61	1.02
LOI	1.26	0.31	0.48

The sugarcane bagasse bottom ash (SCBBA) sample exhibited high silica content of 71.49 wt.% compared to the sugar cane bagasse fly ash (SCBFA), 69.67 wt.% and sugar cane bagasse (SCB), 60.75 wt%. Literature suggests that the silica content in sugarcane bagasse ashes ranges from as low as 31.41 wt% (Castaldelli et al., 2013) to as high as 96.2 wt % (Sales and Lima, 2010). Thus, the values obtained falls within the range. However, the percentage oxide impurities is on the higher side indicating the need to conduct acid leaching prior to the extraction of silica to eliminate these oxide impurities (Pa et al., 2016).

4.3.2 Ash content, calorific value and elemental composition

In Table 4.2 the results for moisture, ash, calorific value, carbon, nitrogen, hydrogen, sulphur content, volatile matter are shown. It is observed that the lowest moisture content was found in SCBFA with 1.90% compared to SCBBA and SCB with 2.97% and 6.40% respectively. SCB retains moisture after the extraction of juice for ethanol produced while SCBBA and SCBFA are by-products from the boiler therefore moisture content is expectedly lower. The percentage ash content for the sugarcane bagasse, (SCB) obtained from ASTM method and TGA is 6.92 and 5.2% respectively. Both values fall in the range between 5 -7% as reported by Ferreira-Leitao et al. (2010). Norsuraya et al. (2016) reported that the percentage ash content of sugarcane bagasse differs with the source of the bagasse. The variation in the ash content of sugarcane bagasse is due to farming practices during growing of sugarcane and harvesting techniques (Anwar, 2010; Fang et al., 2019). SCB showed higher content in volatile matter of 58.54 % compared to SCBBA and SCBFA with 5.46 and 4.89% respectively as these two are by-products from burning of bagasse in the boiler. High volatile matter and fixed carbon for SCB, positively influence the biomass calorific value (CV) (Machado et al., 2018; dos Reis et al., 2012). The CV for SCB, SCBBA and SCBFA were 17. 36 MJ/kg, 1.79 MJ/kg and 0.31 MJ/kg, respectively. The CV obtained in this study is supported by other previous studies. Vieira (2012) reported calorific value of 18.25 MJ/kg for sugarcane bagasse from Minais Gerais in Brazil and Machado et al. (2018) reported a CV of 15.55 MJ/kg and 17.15 MJ/kg for bagasse from Parana and Mato Grosso do Sui in Brazil, respectively.

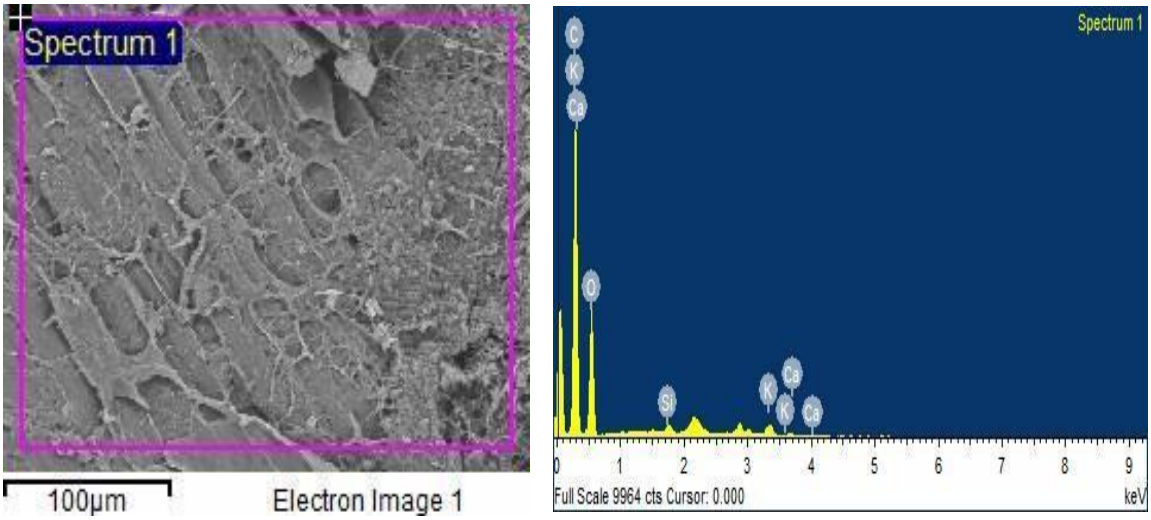
Table 4-2 Physicochemical characterization of sugarcane bagasse samples

Parameter	Sample		
	SCB	**SCBBA**	**SCBFA**
Ash content (%)	6.92 (ASTM) 5.20 (TGA)	-	-
Moisture Content (%)	6.40	2.97	1.90
Volatile mater (%)	58.54	5.46	4.89
Fixed carbon (%)	29.86	-	-
Calorific Value (MJ/kg)	17.36	1.79	0.31
Elemental Analysis			
Carbon (%)	42.42	11.35	4.06
Hydrogen (%)	5.23	-	-
Nitrogen (%)	0.55	0.10	0.09
Sulphur (%)	-	-	-

The higher the moisture and ash content the lower the calorific value. If volatiles and fixed carbon are present in large quantities it results in increased calorific value (Quirino, 2005). SCB exhibits high carbon, hydrogen and nitrogen content of 42.42%, 5.23% and 0.5% respectively. SCBBA and SCBFA lost carbon, hydrogen and nitrogen during combustion of SCB in the boiler. For all the three samples, Sulphur content is negligible. The source of bagasse influences its elemental composition (Das et al., 2004).

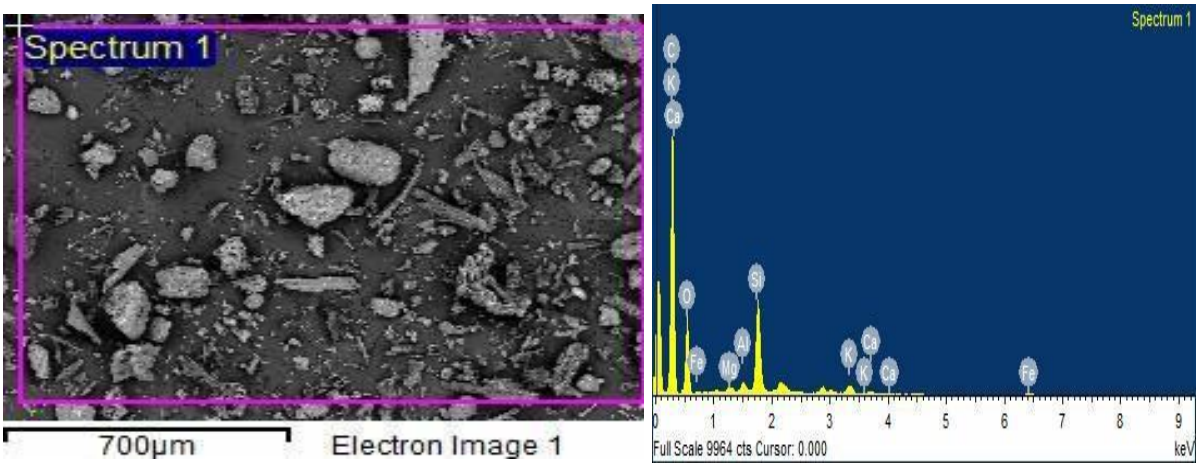
4.3.3 FESEM-EDX analysis

Microscopic observation shows particle shape and structure variation in all the three samples. The SEM images and EDX spectra of the three samples SCBBA, SCBFA and SCB observed by Field Emission Scanning Electron Microscope and Energy Dispersive X-ray analysis are shown in Figure 4-1**,** Figure 4-2 and Figure 4-3**,** respectively. The fibrous nature of the SEM for SCB is typical of plant material. The samples are rich mainly in carbon and silicon and, to a lesser extent, in elements such as aluminum, calcium, magnesium, oxygen and iron. The spectra are comparable to those reported in the literature confirming that the samples contains silicon and unburnt carbon (Jagadesh et al., 2015; Payá et al., 2002)



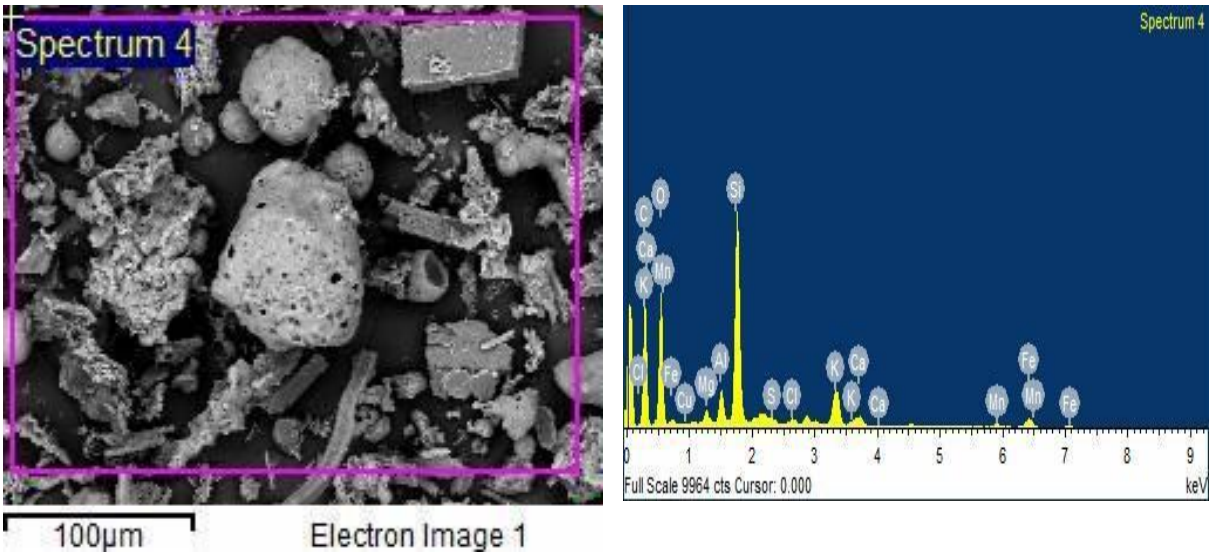
a b

Figure 4-1 a) Morphology b) Spectrum of SCB



a b

Figure 4-2 Morphology b) Spectrum for SCBBA



a b

Figure 4-3 a) Morphology b) Spectrum of SCBFA

Table 4-3 EDX elemental composition of SCB, SCBBA and SCBFA

Element	Weight composition (%)			Atomic composition (%)		
	SCB	**SCBBA**	**SCBFA**	**SCB**	**SCBBA**	**SCBFA**
C	56.96	63.26	40.63	64.41	72.25	53.92
O	41.01	27.63	33.96	34.82	23.69	33.83
Mg	-	0.29	0.67	-	0.16	0.44
Al	-	0.50	1.69	-	0.25	1.00
Si	0.49	6.04	12.32	0.24	2.95	6.99
S	-	-	0.20	-	-	0.10
Cl	-	-	0.64	-	-	0.29
K	1.30	0.98	3.93	0.45	0.34	1.60
Ca	0.24	0.36	1.07	0.08	0.12	0.43
Mn	-	-	0.99	-	-	0.29
Fe	-	0.94	3.88	-	0.23	1.11
Cu	-	-	0.02	-	-	0.00
Total	**100**	**100**	**100**	**100**	**100**	**100**

Table 4-3 shows the elemental composition of the three samples SCB, SCBBA, SCBFA from EDX analysis. The carbon content is higher in SCBBA compared to SCB and SCBFA. This could have been attributed to the presence of carbon tape used for sample preparation for SEM analysis. However, the carbon content for SCB (42.42%) as shown in Table 4-2 is higher than that of SCBBA and SCBFA but comparable to 43. 35% reported by Machado et al. (2018), thus more acceptable of the two analyses. The silicon content in the three samples SCB, SCBBA and SCBFA is 0.49, 6.04 and 12.32 wt % respectively. Both ashes exhibited

higher silicon content than raw SCB because of the accumulation of silicon during combustion of sugarcane bagasse. Xu et al. (2019), Moraes et al. (2016) and Embong et al. (2016) reported that reactive amorphous silica in sugarcane comes from ground water. Sugarcane absorbs silicic acid from groundwater and polymerize into amorphous silica in sugarcane cells. When sugarcane bagasse is burnt in a thermal power plant as fuel, reactive amorphous silica is produced and accumulates in sugarcane bagasse ash (Embong et al., 2016a; Moraes et al., 2016; Xu et al., 2019). Thus, we cannot rule out the thermal history of the feedstock as abundance may not necessarily be due to Si uptake but rather due to accumulation after decomposition.

4.3.4 FTIR analysis

The FTIR spectra of SCB, SCBBA and SCBFA samples are shown in Figure 4-4. The strong absorption bands at 1011 - 1080 cm^{-1} was observed in all the three samples. It depicted the presence of Si-O-Si (siloxane) functional groups affirming the presence of silica although the absorption band in SCB may be overlapped by C-O-C stretching vibrations.

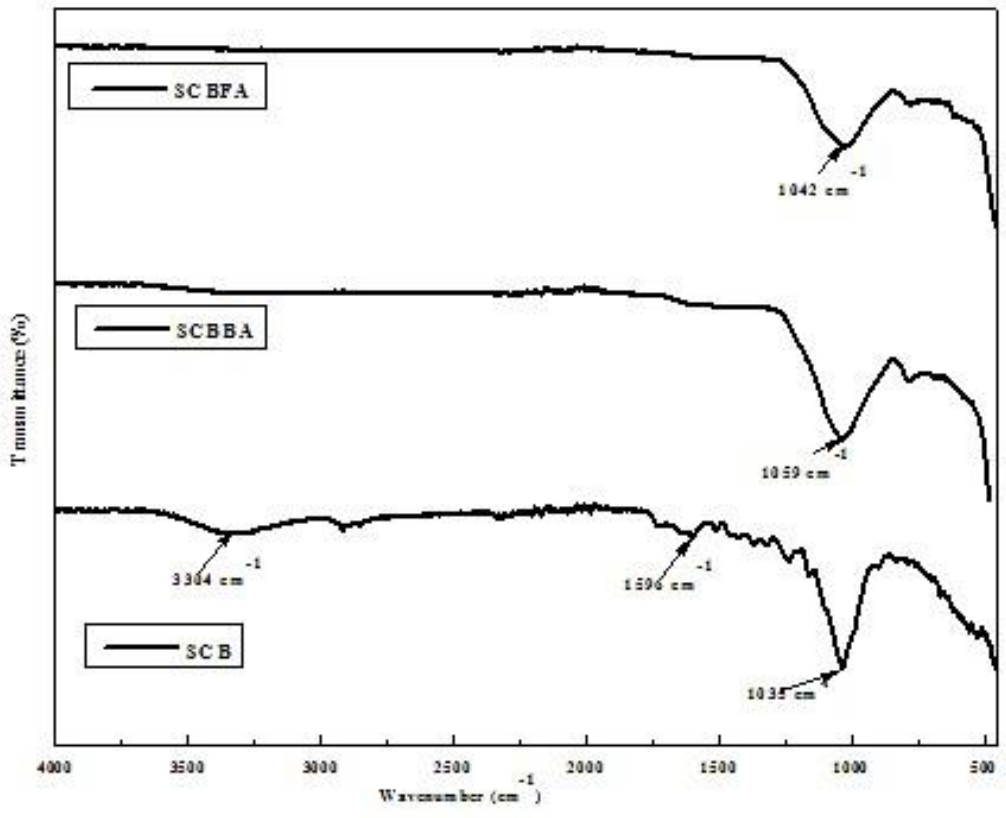


Figure 4-4 FTIR spectra for the (SCB), (SCBBA) and (SCBFA)

At 3304 cm^{-1}, the vibration is due to symmetric and asymmetric vibration of (O-H) water bounded in sugarcane bagasse due to adsorbed moisture and –OH groups on organic matter such as lignin and cellulosic material and the surface energy of H_2O on sugarcane bagasse. The vibration at 1596 cm^{-1} ,due to carboxyl groups, indicates that the sample is rich in carbon. Arif et al. (2017) and Jagadesh et al. (2015) reported different absorption bands in sugarcane samples, one strong vibration between 500 cm^{-1} and 1100 cm^{-1}, this indicated the presence of symmetric stretching vibration of silicon bonds. The second stretch at 3400 cm^{-1} affirmed the presence of hydroxyl group confirming availability of water molecules in the samples (Arif et al., 2017; Jagadesh et al., 2015; Payá et al., 2002)

4.3.5 XRD analysis

The XRD patterns for SCB, SCBBA and SCBFA are presented in Figure 4-5. The peaks observed are characteristics of the following mineral phase's quartz, cristabolite and tridymite with predominance of quartz. It is known that quartz transforms to tridymite and then to cristabolite with increasing temperature. Since SCBBA and SCBFA are by products from the boiler cristabolite and tridymite form of silica is predominant compared to SCB with silica which is highly amorphous as seen by the broad peak between 10^{o} to 30^{o} (Umamaheswaran and Batra, 2008). The unidentified peak on the SCB profile could be an organic compound based on form factors of the compounds.

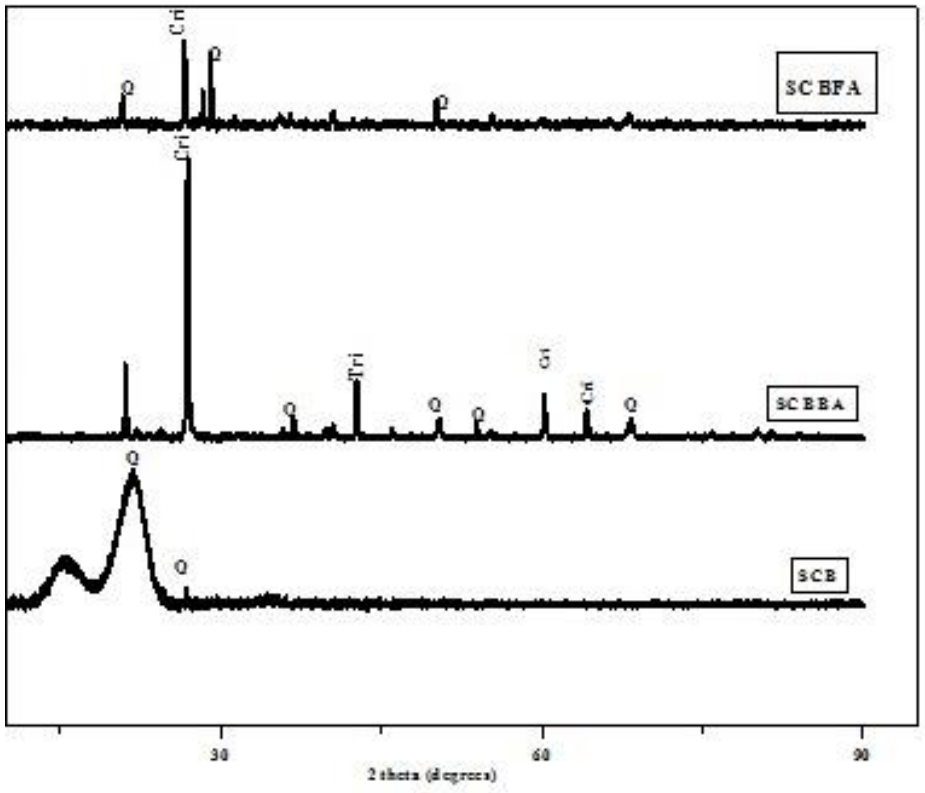


Figure 4-5 XRD pattern for SCB, SCBBA and SCBFA (Q-quartz, Cri-cristabolite & Tri-Tridymite)

4.3.6 Thermogravimetric analysis

The results for thermogravimetric analysis for sugarcane bagasse, sugarcane bagasse bottom ash and sugarcane bagasse fly ash are shown in Figure 4-6**.** Thermogravimetric analysis makes it possible to follow the weight loss of samples as function of temperature. Through the TGA curve, it is possible to relate different regions of weight losses as function of temperature with different biomass components. Sugarcane bagasse exhibits maximum weight loss of up to 80 wt.% between 300 ^{o}C and 700 ^{o}C and subsequently a sharp exothermic peak in the TGA curve. This could be due to volatilization of unburnt carbon and other organic matter present.

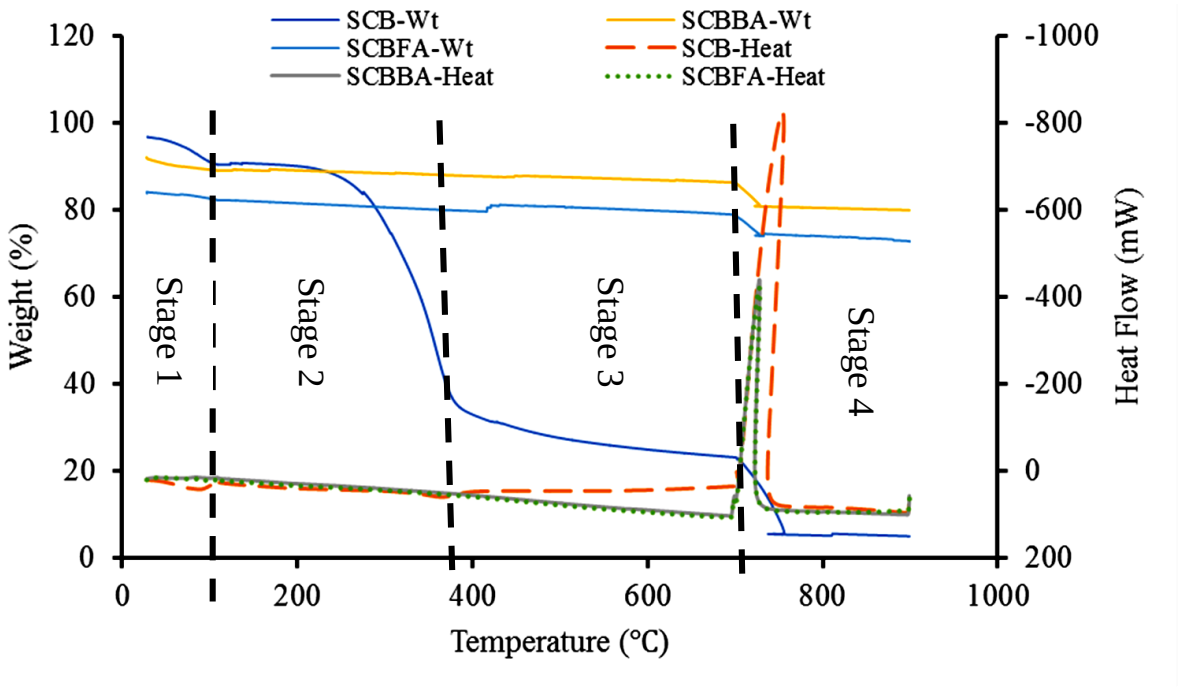


Figure 4-6 Thermogravimetric curve of SCB, SCBBA and SCBFA samples

The weight loss at various temperatures corresponds to decomposition of components. The weight loss at 100 ^{o}C (Stage 1) is a result of water loss while the weight loss around 380 ^{o}C (Stage 2) is as a result of decomposition of volatile matter. The formation of ash between 500 and 700 ^{o}C (Stage 3) resulted in negative heat flow showing that energy is consumed for ash formation. Continued weight loss beyond 700 ℃ (Stage 4) is indicative of higher temperature ashing. Speight (2015) describes high temperature ashing as mainly the oxidation of pyrite and marcasite (FeS_2) to ferric sulfate, $Fe_2(SO_4)_3$ and sulfur dioxide (SO_2). Some of the SO_2 may remain in the ash in combination with calcium, but much is lost. Of the major mineral groups, only quartz (silica) is not significantly altered during high temperature ashing but silica phase transitions are possible during this stage. Mohomane et al. (2017) studied thermal degradation of sugarcane bagasse and observed three zones of weight loss. They attributed the first zone at 100 ^{o}C to moisture content loss, the second region between 350 - 500 ^{o}C to organic matter decomposition and the third zone observed between 550 – 700 ^{o}C due to ash formation (Mohomane et al., 2017).

For SCBBA and SCBFA powders, the total weight loss was 9 wt.% and 7 wt.%, respectively. The weight loss was due to loss in moisture content and unburnt organic matter since incomplete combustion also occurs in the boilers. The lower weight loss of the ashes is evidence of lower loss on ignition (LOI) as seen in the physicochemical composition shown in Table 4.2. From the DTA curves of SCBBA and SCBFA, an endothermic peak around 60 ^{o}C corresponds to moisture content loss. Some researchers including Torres Agredo et al. (2014) and Frias et al. (2007, 2011), reported endothermic peaks attributed with decomposition of carbonates between 500 – 600 ^{o}C. In this work, the observed peaks for the SCBBA and SCBFA occurred at around 700 ℃ against the

reported 600 ℃ indicating to a difference in the ash constituents (Frias et al., 2007; Frías et al., 2011; Torres-Agredo et al., 2014).

4.4 Concluding Remark

The compositional analysis study of sugarcane bagasse and its ashes confirms that silica is the predominant compound in the samples. It is evident from both XRF and EDX analyses that the samples contain iron, aluminum, calcium, magnesium, phosphorous, potassium oxides. The strong vibrations observed by FTIR analysis confirm the presence of silicon bonds in the samples. The scientific and technical study on SCB, SCBBA and SCBFA using XRF, XRD, SEM- EDX, FTIR and TGA enabled the following conclusions:

1. The crystalline nature of the silica in SCBBA and SCBFA can not be affirmed except if the temperature of the boilers exceeds 700 ℃. However, the presence of crystalline peaks in XRD spectrum usually suppresses the presence of shallow and broad amorphous silica bands. Transformation of amorphous silica to crystalline silica has been reported to occur only above 700 ℃.
2. The extraction of silicon from sugarcane bagasse ash is worth pursuing as the ashes are rich in silica.

Chapter 5 : Extraction of Silica from SCBA

5.1 Introduction

After the extraction of sugar juice, a fibrous waste (sugarcane bagasse) is produced which is mainly used for cogeneration of electricity in the same industry (Embong et al., 2016). Environmental issues related to the disposal of sugarcane bagasse ash is a major factor that is encouraging many researchers to further explore the potential utilization of this waste (Ren et al., 2014). Bagasse ash has negligible cost and is easily overlooked in landfills (Bezerra and Ragauskas, 2016). Sugarcane bagasse ash has adequate silica content with a wide industrial application which ranges from pharmaceutical products, chromatograph column packing, detergents, adhesives, electronics, dental material, cosmetics and ceramics (Grau et al., 2015; Imran and Khan, 2018). However, many industrial processes in the conversion of sugarcane into sugar and ethanol and later the burning process of the sugarcane bagasse for electricity production result in ashes with high impurity content. These impurities include iron and aluminum oxides which complicate the process silica purification (Affandi et al., 2009; Lee et al., 2017).

Research on the pretreatment sugarcane bagasse ash residue for the removal of naturally occurring alkali and alkaline earth metals has been done and reported by Rodríguez-Machín et al. (2018). A study done by Embog et al. (2016) indicated that the amount of SiO_2 present in the raw sugarcane bagasse ash was less than 60 wt.% after incineration of bagasse while after pretreatment with high concentrated acid it increased up to 80 wt.% SiO_2 (Embong et al., 2016). Despite the positive result from this pre-treatment process with strong concentrated inorganic acid, secondary issues such as safety, handling and acid waste disposal emerged.

This chapter reports on pretreatment of SCBA for the extraction of SiO_2 using an environmentally friendly organic acid (citric acid). The leaching behavior was dependent on leaching time, acid concentration and temperature. An important part of the research was to find the parametric leaching conditions that give the highest increase in the percentage of extracted SiO_2. The design of experiment followed by parametric effects was carried out using a response surface methodology. Response Surface Methodology (RSM) is widely used for statistical analysis. It is used for the design of experiments, models development and analyzing the effect of multiple variables (Bezerra et al., 2008).

Several alternative methods for the extraction of silica from sugarcane bagasse ash have been reported by different researchers. Silica was extracted from SCBA using a dissolution and precipitation process (Vaibhav et al., 2015). Another team of researchers, Affandi et al. (2009), reported three different methods for the extraction of silica from SCBA, pretreatment of the ash with HCl which produced 91.38% pure silica, cation exchange resin to enhance purity to 99.37% and washing of the precipitate with deionized water which resulted in 99.16% purity. San et al. (2014) also reports of two other methods for the extraction of silica; laser ablation and calcination with alkali treatment.

In this Chapter, a report is given on sol-gel synthesis of silica from sugarcane bagasse ash coupled with an adsorption column of activated carbon to enhance the purity of silica produced. The sugarcane bagasse ash used in this study contained a high percentage of inorganic impurities thus modification of the conventional method is reported. The chemical and physical properties of silica produced from sodium silicate derived from sugarcane bagasse ash have been extensively studied.

However, as far as we could be certain, there is a relatively little study on using activated carbon in enhancing the purity of sodium silicate before the precipitation of silica. The findings reported in this chapter could be beneficial in enhancing the purity of silica for use in different applications.

5.2 Experimental

5.2.1 Investigation of the effect of leaching condition on the pre-treatment of SCBA with citric acid

To develop a model that explains the effect (main and interactive) of leaching conditions on the silica extracted during leaching of SCBA, Response Surface Methodology (RSM) approach was used. RSM evaluates interactive effects of operating variables when compared with the use of one-factor-a-time (OFAT) approach (Carley et al., 2004). Consequently, a full two factorial design, obtained with the use of Design Expert software (version 11, 2018 from Stat-Ease Inc.), was used to investigate effect of leaching variables such as leaching time, leaching temperature and acid concentration of the leaching solution on the percentage of silica extracted from SCBA. A total of 9 experimental runs were carried out and the percentage of SiO_2 extracted was obtained from each run using Equation (5.1):

$$X\ (\%) = \frac{w_2 - w_1}{w_1} \times 100 \qquad \textit{Equation 5.1}$$

Where X is the percentage of silica extracted, w_1 the percentage of silica before extraction and w_2 the percentage of silica after extraction. The models of each response were expressed in terms of coded variables and analysis of variance (ANOVA) was performed to evaluate the statistical significance of each model. A p-value of less than 5% indicates that model terms are significant, while less than 1% indicates that model terms are highly significant. The fit of the model was also

checked by the coefficient of determination (R^2), which is a measure of how well the sample data fits to the regression equation. The significance of the regression and statistical coefficient was checked using F-test.

Table 5-1 Levels and coded factors of parameters for 2-3 design

Parameters	**Levels**		
Code	-1	0	+1
Temperature (℃)	50	70	90
Time (minute)	60	90	120
Concentration (M)	1	1.5	2

5.2.2 Enhancement of silica purity using sol-gel coupling adsorption method

The detailed method for the extraction of silica and enhancement of its purity is described in Chapter 3 of this thesis (section 3.4.4). In this section, the sol-gel coupling adsorption method was used to enhance the purity of the silica obtained from section 5.2.1. For in-depth understanding of the effect of coupling sol-gel method with adsorption, 2 different strategies were adopted; the sol gel without adsorption method and sol gel with adsorption method. Consequently, the obtained silica from these methods was referred to as Silica-A (for sol gel without adsorption method) and Silica-B (for sol gel with adsorption method).

In the current study activated carbon was used to enhance the purification of silica. The flow diagram forms part of the direction for future work given in Chapter 7 which is outside the scope of the current

research but can find use in high capacity cation exchangers. Figure 5-1 summarizes the routes for the purification of sodium silicate prior to silica extraction.

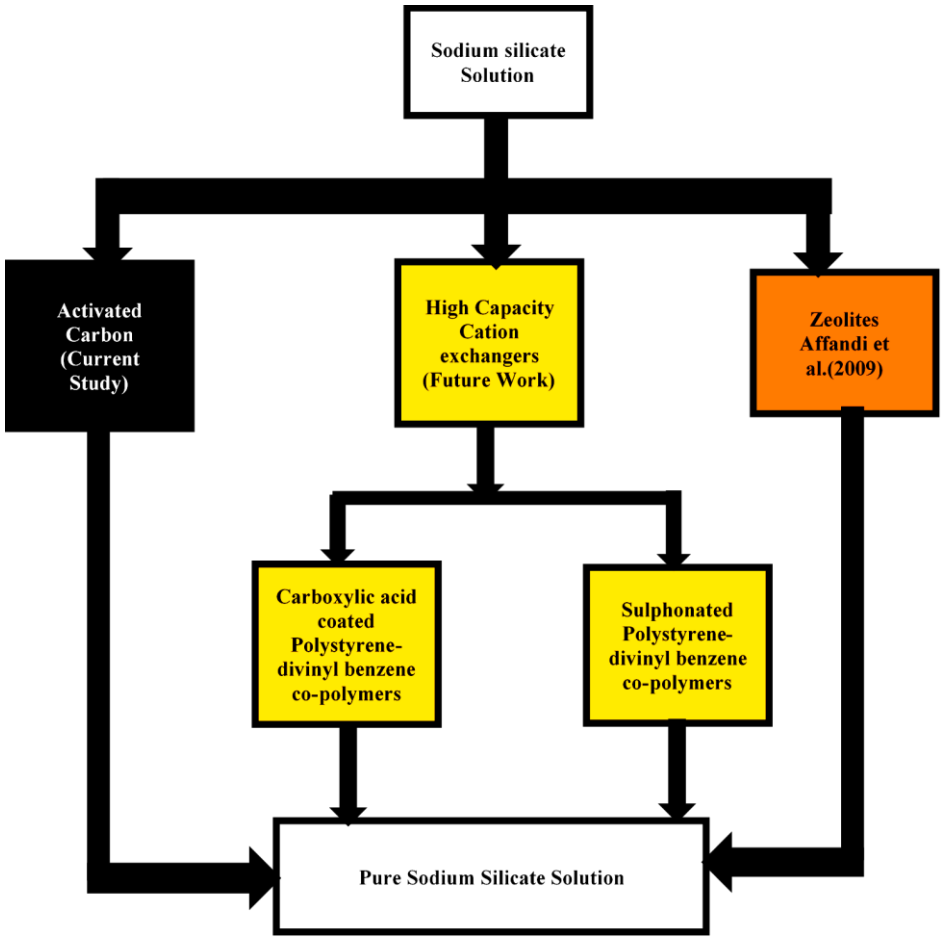


Figure 5-1 Summary of the enhancement of the purity of sodium silicate before precipitation of silica.

5.3 Results and Discussion

5.3.1 Characterization of SCBA

Table 5-2 shows the results of experimental runs of the model-predicted % silica extraction and the experimental % silica extraction obtained using Equation (5.1). XRF was used to determine the chemical composition of the leached SCBA. The results depict a significant 10 % increase in

SiO_2 wt. % after leaching the raw sugarcane bagasse ash for each experimental run. The experimental data was analyzed using the Design-Expert software and a second-order regression equation was obtained. The model included linear and interactive terms for the variables tested. The equation describes the silica extracted (Y) with respect to temperature (A) , time (B) and concentration (C).

The regression equation is shown in Equation (5.2):

$$Y = 12.29 + 1.55A + 0.49B + 2.59C - 0.29AC \qquad \textit{Equation 5.2}$$

Equation 5.2 implies that the three variables (A,B,C) had effect on the leaching behaviour of SCBA. The interactive effect of temperature and concentration (AC) also has a significant effect on the regression equation. The values with positive coefficients represent an additive effect on the responses, these factors (A, B, C) increase the percentage of extracted silica while the negative coefficients show negative effects on the responses, such as AC which decreases the silica extracted. The results from the ANOVA, shown in Table 5-3 also show that the model of SiO_2 extraction is significant. The significance of each coefficient was determined by their corresponding p-values calculated statistically. Smaller p-values indicate higher significance of the corresponding coefficient. Models terms with p values less than 0.05 including the independent variables and the interacting variables were considered as significant variables. The influence of concentration and temperature are significant. Also, the interaction between acid concentration and leaching temperature is significant. Time was not very significant in this model. It can be observed that the predicted values were quite close to the actual values. This further justifies the significance

of the model justified by R^2, the coefficient of determination which signifies the proportion of the variance in the response that is predicted from the three independent variables.

Table 5-2 The designed experiment and responses

Run	Temperature (^oC)	Time (min)	Concentration (M)	Actual Response (Y)	Predicted Response (Y)
1	50	60	1	6.67	6.75
2	90	120	2	15.13	16.00
3	90	60	2	15.89	15.02
4	50	60	2	14.18	13.76
5	70	90	1.5	8.32	8.32
6	50	120	2	14.32	14.74
7	90	60	1	10.46	11.68
8	90	120	1	13.89	12.67
9	50	120	1	7.81	7.73

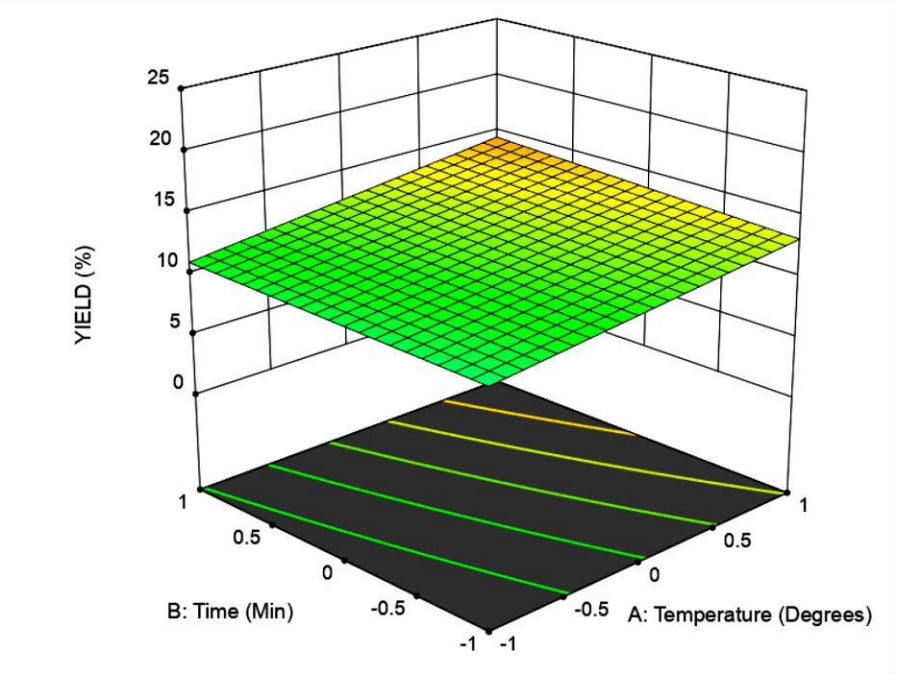
Table 5-3 Analysis of variance (ANOVA)

Parameter	Degree of Freedom	Sum of Squares	Mean Squares	Test Statistics, F	P – Value
Model	**4**	**81.4**	**20.35**	**12.51**	**0.033**
A- Temperature	1	60	19.19	11.80	0.04
B- Time	1	120	1.95	1.2	0.35
C- Concentration	1	60	53.51	32.89	0.01
AC	1	6.75	6.75	4.15	0.0105
Curvature	1	14.04	14.04	8.63	0.0606
Residual	3	4.88	1.63		
Cor- Total	8	100.32			

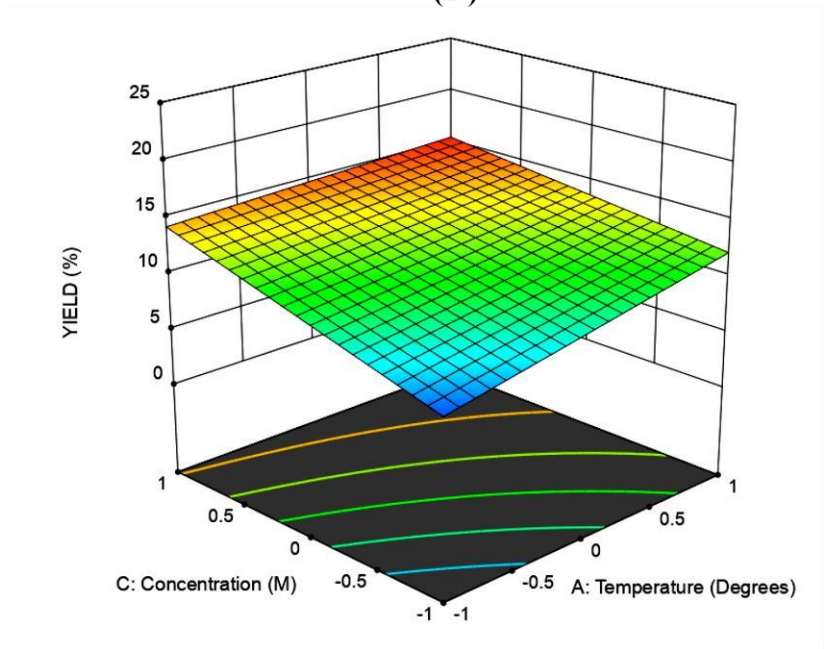
Statistical Output	SiO_2
Model F-value	0.033
Model prob > F	<0.05
R^2	0.94 (0.95 from scatter plot)
CV %	10.76
Adjusted R^2	0.87
Adequate Precision	8.89
Standard Deviation	1.28
Mean	11.85

The three-dimensional response surface plots give a better understanding of the interactive effects of variables on the silica recovery. The plot is based on the model equation 5.2.

(A)


YIELD (%)
25
20
15
10
5
0
1
0.5
0
-0.5
-1
B: Time (Min)
A: Temperature (Degrees)

(B)


YIELD (%)
25
20
15
10
5
0
1
0.5
0
-0.5
-1
C: Concentration (M)
A: Temperature (Degrees)

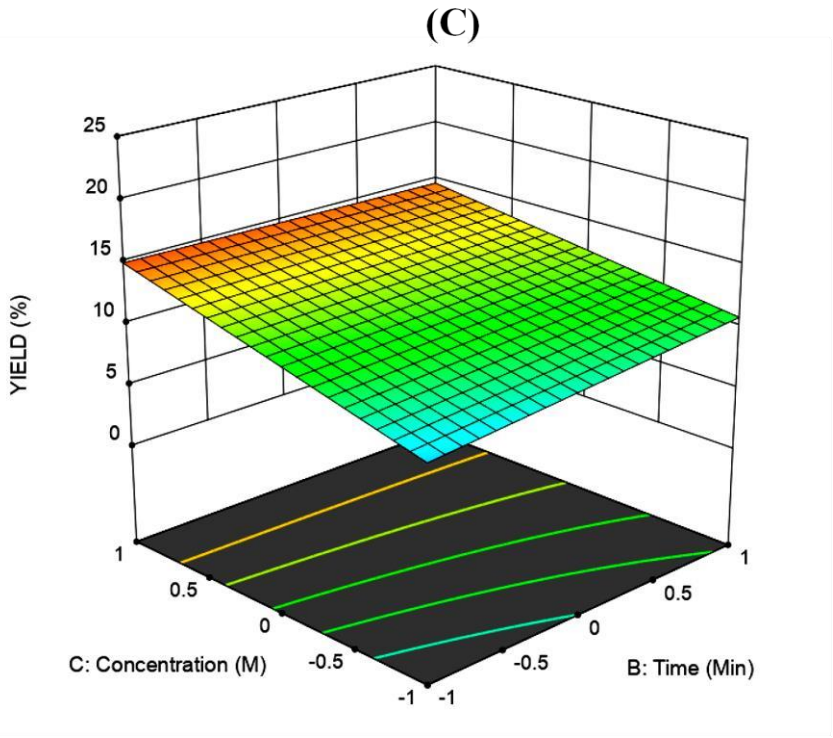


Figure 5-2 3D response surface plot for the effects of temperature (A), time (B) and acid concentration (C) on the extraction of SiO_2

Figure 5.2A shows the interactive effect of time and temperature on silica extracted. The increase in silica extracted is higher when the temperature is increased at shorter times; at higher temperature, time has less effect on the yield of silica. Figure 5.2B shows the interaction between temperature and concentration. The silica extracted is highest at higher temperatures and concentration. This is expected and thus implies to higher yields in a short time. The increase in extracted silica is reduced at lower concentrations even with increasing temperatures. Figure 5.2C shows the interaction between concentration and time. At shorter times, the silica extracted increases with increasing concentration. The change in extracted silica is not significant with increasing time, however, there is significant increase in the extraction with increasing concentrations even at shorter time. This is

expected since the amount of SiO_2 is finite and saturation happens due to completion of reaction. The highest silica extracted is found at shorter times and higher concentrations. The ANOVA table (Table 5-3), explains the effects better using p-values. Among the 3 parameters, concentration has the highest influence on silica yield (p-value=0.01) followed by temperature (p-value=0.04). Time is not a significant factor.

5.3.2 Enhancing purity of extracted silica using sol-gel coupling adsorption method

5.3.2.1 Chemical composition of silica-A and silica-B

The results in Table 5-4 suggest that the purity of silica increased from 48.27-98.92% for the sugarcane bagasse ash derived silica. Since concentration is a relative amount, the reduction of impurities therefore increases the amount of SiO_2 but this does not infer that the absolute amount of SiO_2 has changed. The aluminum oxide content was 0.49 % in silica-A and in 0.03% silica-B. As evidenced by XRF results, most metal impurities which include iron, manganese, magnesium, calcium, potassium, titanium, and chromium were adsorbed by the activated carbon due to its large specific surface area of 1308 m^2/g which enhances the physical adsorption of dissolved or dispersed substances from liquids (Goher et al., 2015). Activated carbon facilitates the removal of heavy metals by complexation or by electrostatic attraction of metal ions to various surface oxygen-containing functional groups (Yin et al., 2007). The citric acid pre-treatment was also vital in the reduction of percentage metal impurities from sugarcane bagasse ash before extraction of silica. It is evident in Silica-A and this can be attributed to the effect of citric acid pre-treatment. The major impurities reduced also due to pretreatment were Al_2O_3 from 6.2 to 0.49 %, Fe_2O_3 from 3 to 0.03%, MnO from 3.3 to 0 % and CaO from 4.79 to 0.44%.

Table 5-4 Chemical composition of raw ash, silica-A and silica-B

Constituents	**Raw SCBA (%)**	**Silica-A (%)**	**Silica-B (%)**
SiO_2	71.49	48.27	98.92
Al_2O_3	6.2	0.49	0.03
Fe_2O_3	3	0.03	0.01
MnO	3.3	0.00	0.00
MgO	1.79	0.02	0.00
CaO	4.79	0.44	0.02
Na_2O	4.61	16.50	0.25
K_2O	0.11	0.31	0.05
TiO_2	0.80	0.02	0.00
P_2O_5	0.14	0.10	0.01
Cr_2O_3	-	0.02	0.00
NiO	0.61	0.00	0.00
LOI	0.31	21.64	0.71

5.3.2.2 Degree of crystallinity of silica-A and silica-B

This technique allows for the determination of the nature of the crystallized phases by measuring the angles of diffraction of X-rays by the crystalline plane of the solid. These angles of diffraction are related to the characteristics of the amorphous and crystal lattice. The XRD patterns are illustrated in Figure 5-3.

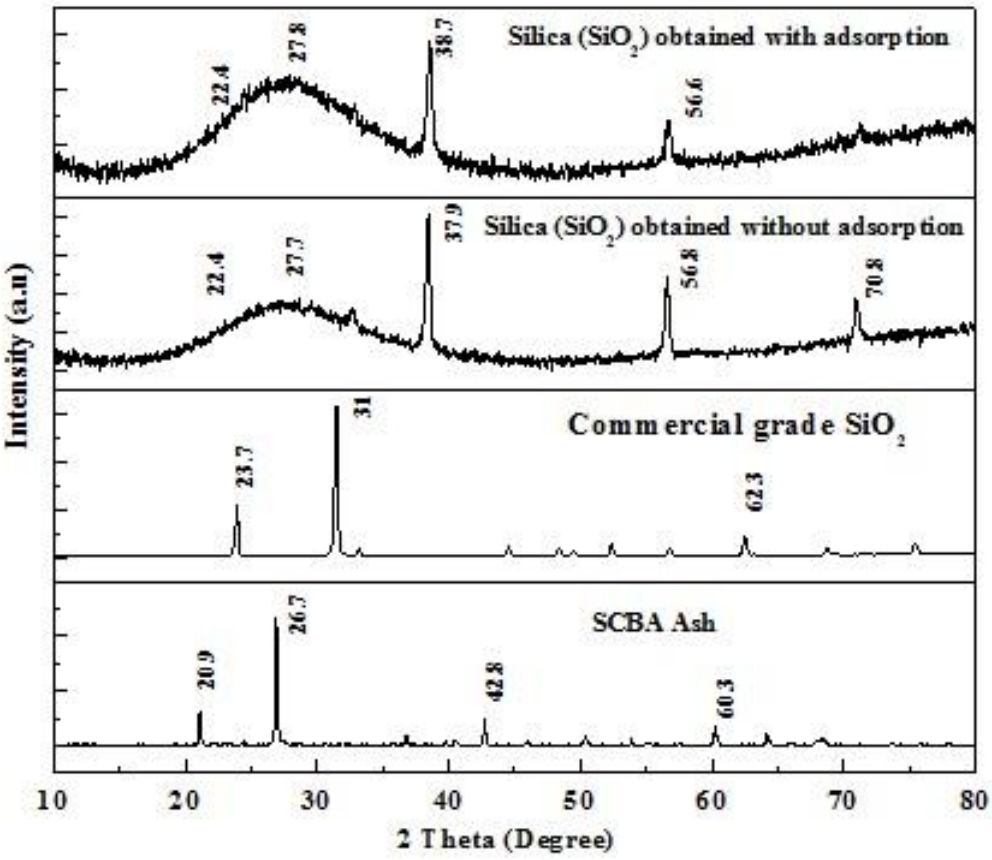


Figure 5-3 XRD pattern for SCBA, commercial grade silica, silica (A) and silica (B)

The commercial grade SiO_2 used is crystalline while the produced silica are amorphous. A similar comparison has been reported by Rovani et al. (2018). The peaks observed in the amorphous material may be due to other impurities as they are not in tandem with those of quartz peaks.

5.3.2.3 Surface nature of silica-A and silica-B

The FTIR spectra for SCBA, commercial grade SiO_2, silica-A and silica-B are shown in Figure 5-4. For all the four samples, the bands observed between1011-1068 cm-1 are attributed to Si-O-Si asymmetric stretching. The presence of a band at about 770-797 cm^{-1} is due $Si = O$ bending (Espindola-Gonzalez et.al., 2010). The absence of $O - H$ and $H - O - H$ bands in silica, which are normally present in amorphous silica due to its hydrophilic nature, is because the drying temperature of the sample was about 110 ℃ which was enough to remove free water and the water of crystallization. Thereafter the sample was preserved to ensure no contact with moisture in the air.

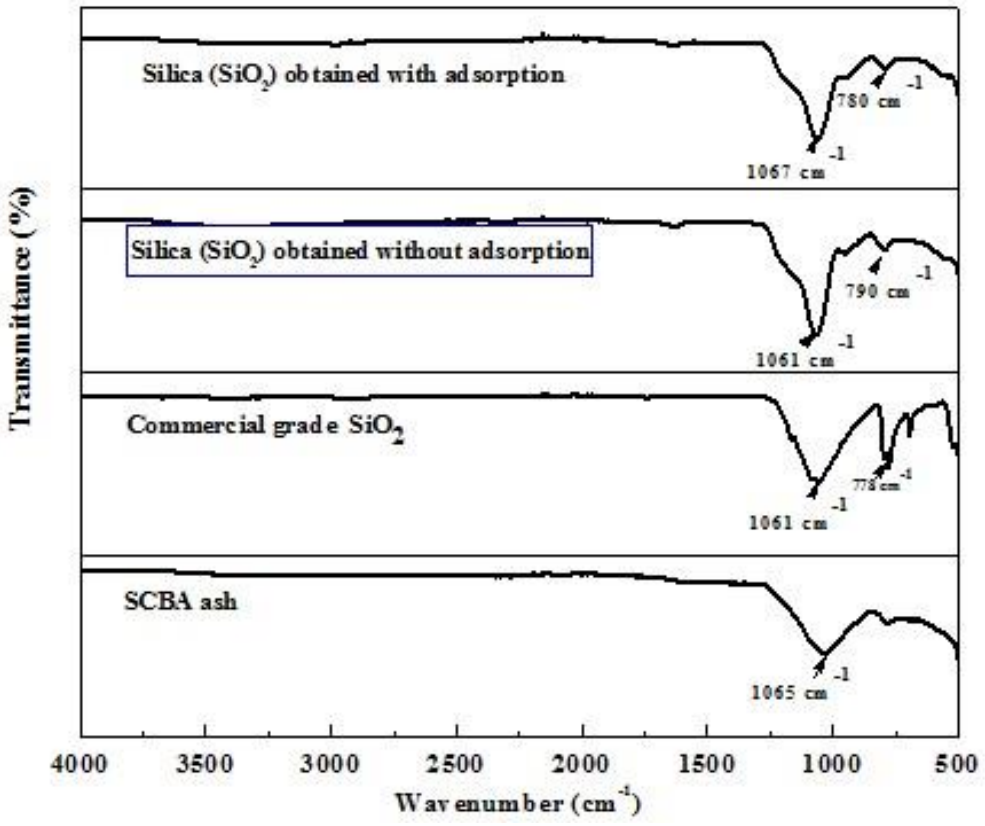


Figure 5-4 Surface chemistry of SCBA, commercial grade silica, silica (A) and silica (B)

5.3.2.4 Textural properties of silica-A and silica-B

The complete isotherms of N_2 adsorption-desorption allow the characterization of the textural properties of a material, the specific surface area, porous volume and the shape of the pores. Nitrogen adsorption and desorption isotherms were measured at 77.2 K using ASAP 2460-Micromeritics equipment as shown in Figure 5-5.

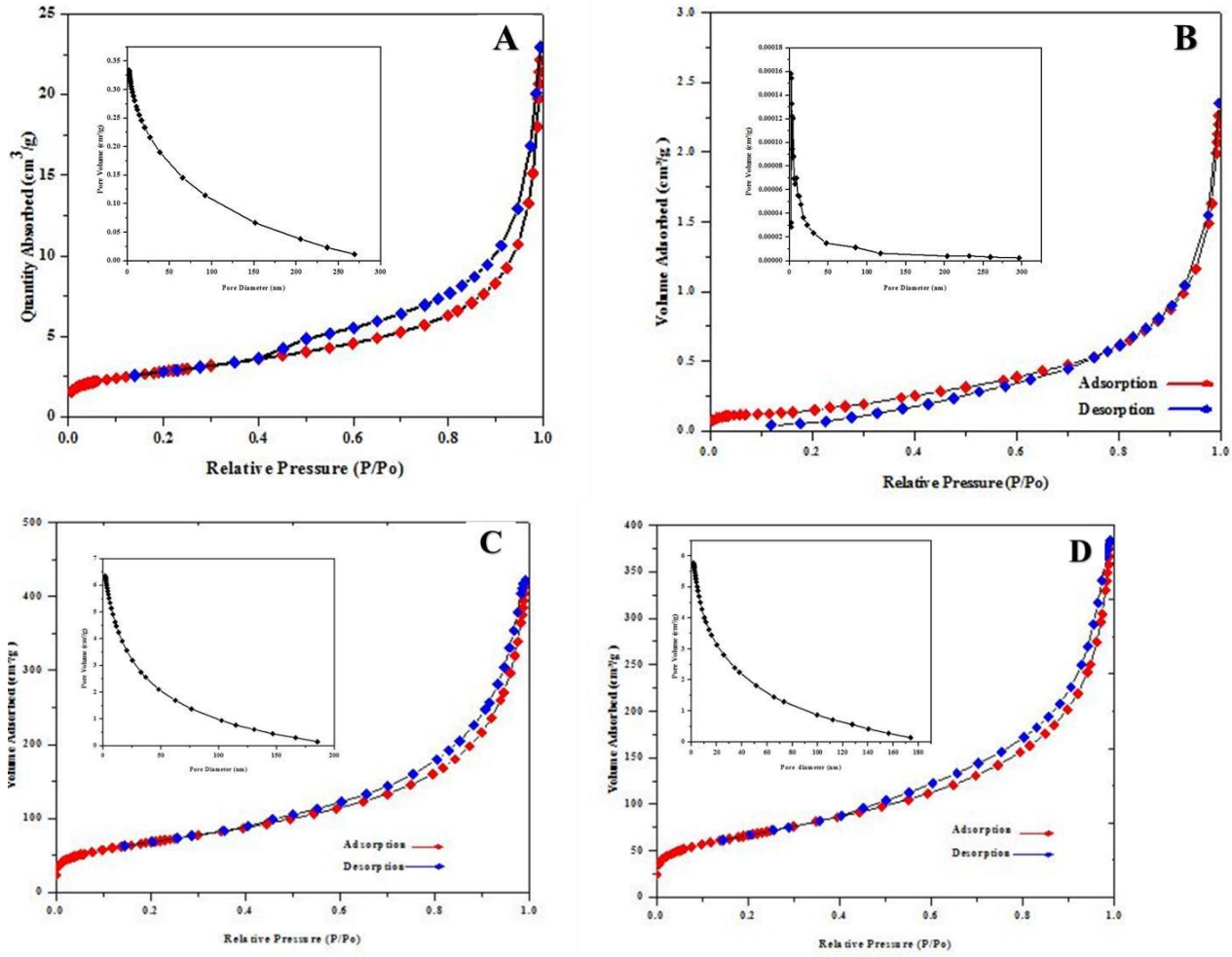


Figure 5-5 Nitrogen adsorption-desorption isotherm for A-SCBA, B-commercial grade silica, C-silica (A) and D-silica (B)

In the N_2 adsorption-desorption measurements, Type II isotherms are observed for all the four samples with a Hysteresis of H3 type. This is associated with slit-shaped pores formed from aggregates of plate-like particles, thus resulting in large pore size distribution (Groen et al., 2003; dos Santos et al., 2017).

The pore size distribution curves for SCBA, commercial grade SiO_2, silica-A and silica-B exhibit a wide pore distribution between 2 nm and 50 nm, indicating that these materials are mesoporous. A small distribution of pores above 50 nm also depicts the presence of macropores in the structure. These results suggest the coexistence of mesopores and macropores in the four samples. The average pore diameter for SCBA, commercial grade SiO_2, silica-A and silica-B are 16 nm, 15 nm, 12 nm and 10 nm, respectively. The surface area of all the materials was evaluated using the BET Method and the pore size by BJH method (isotherms with hysteresis) and their textural properties are summarized in Table 5-5.

Table 5-5 Textural properties of the samples

Sample ID	**S_{BET} (m^2/g)**	**V_p (cm^3/g)**	**D_p (nm)**
SCBA	9.98	0.0033	16
Commercial grade SiO_2	0.563	0.0035	15
Silica-A	228	0.637	12
Silica-B	240	0.577	10
Commercial grade activated carbon	1308	0.5138	0.8216

S_{BET}- specific surface area; **V_p**- pore volume; **D_p**- pore diameter.

It is seen that the silica-B exhibits high specific surface area compared to commercial SiO_2, silica-A and SCBA. However, the specific surface area is comparable to the 265 m^2/g for bio-silica which was synthesized from sugarcane waste ash (Alves et al., 2017).

5.3.2.5 Morphology of silica-A and silica-B

The SEM image of the SCBA shown in (A) reveals heterogeneous material with irregular shapes. High roughness of sample which was observed is associated with the release of organic matter during the burning process of bagasse for the generation of electricity in the bioethanol plant. The morphology of SCBA is similar to those observed by other authors (Alves et al., 2017; Batra et al., 2008; Faria et al.,2012).

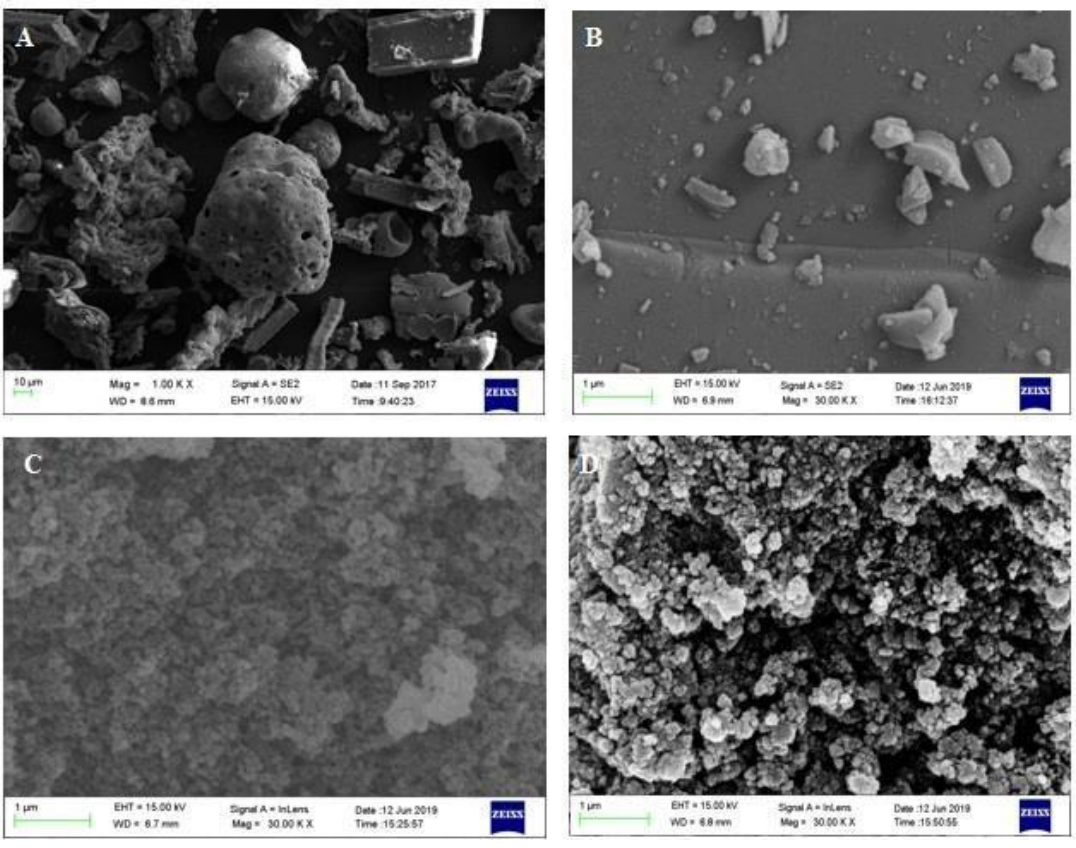


Figure 5-6 SEM images for (A) SCBA (B) commercial SiO_2 (C) silica-A (D) silica-B

The agglomeration of particles which results in clusters is due to alkaline treatment during synthesis stage and is more pronounced for the silica-A in Figure 5-6. The SEM image shown in (D) for the silica- B is clearer and this supports that activated carbon also reduced the degree of alkalinity for silica thus the reduction in agglomeration.

TEM determines the particle size as well as the morphology of the samples. For commercial grade silica, it is evident that there is an intensive agglomeration of particles as shown in Figure 5-7(A). The particle size is not uniform, and they range from 20 –140 nm. Silica-B exhibits uniformly distributed particle size ranging from 6- 24 nm as shown in Figure 5-7(C). For the silica- A, the particle sizes are randomly distributed and size ranges from 10 -46nm as shown in Figure 5-7(B).

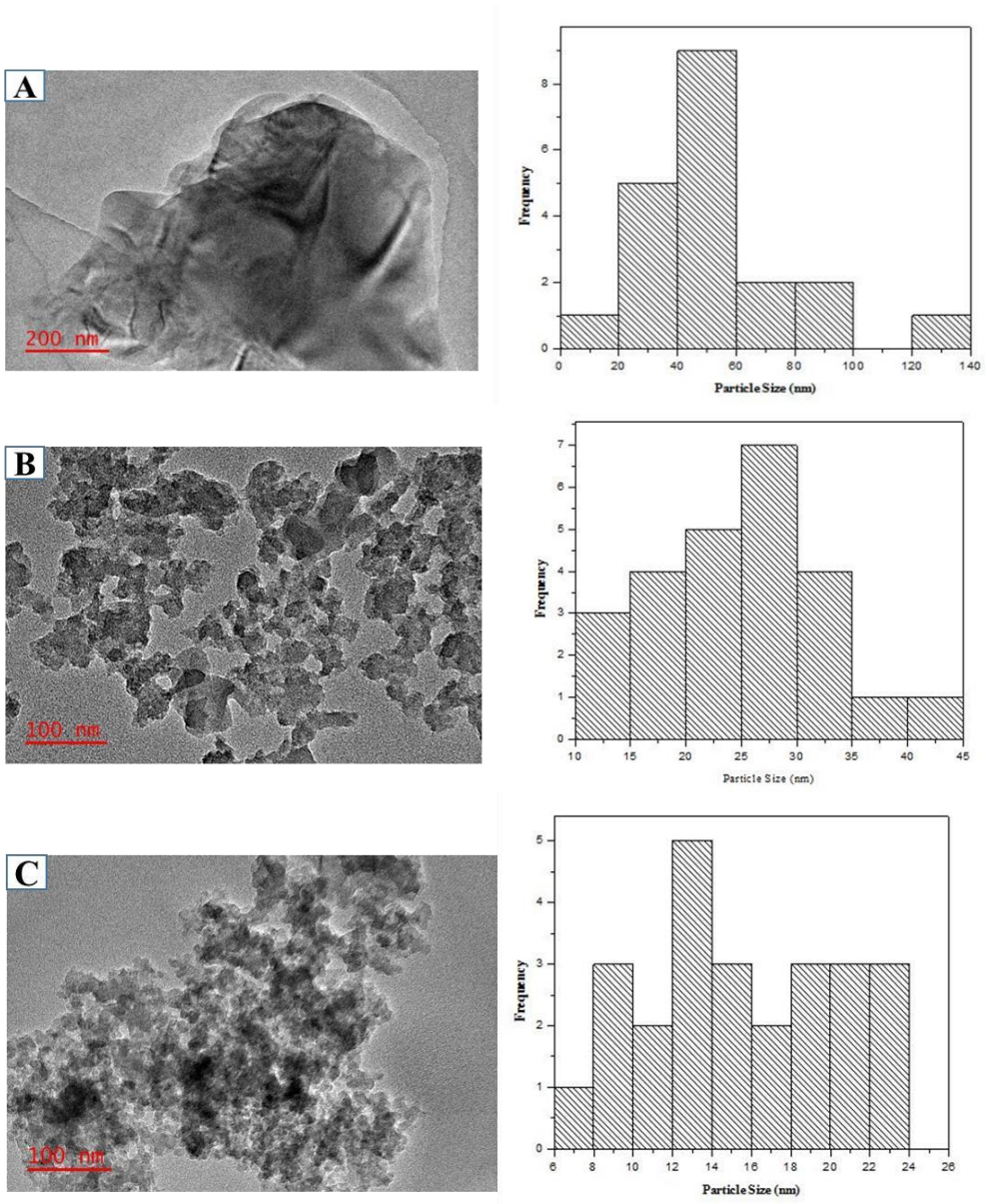


Figure 5-7 TEM images and corresponding particle size distribution for A) commercial grade SiO_2, B) silica-A and C) silica-B

The morphology of the nano-silica obtained from the sugarcane bagasse ash is like those obtained and reported elsewhere (Bahrami et al., 2017; Hassan et al., 2014; Rafiee et al., 2012; Rovani et al., 2018; To et al., 2017). This method of incorporating an adsorption column in the process of

the synthesis of nano silica particles is promising in controlling the size; however, nonuniform silica nanoparticles were also obtained.

5.4 Concluding Remark

The results for the parametric effect gave an appropriate predictive model for silica extraction from sugarcane bagasse ash using citric acid. The effects of the individual variables leaching time , acid concentration and temperature were investigated, and the concentration-temperature interactive effect was identified to be of statistical significance. Concentration was the variable of greatest significance on silica extraction followed by temperature and lastly time which had no significant impact on the model. The optimum leaching conditions were determined to be a bath temperature of 90 ℃, acid concentration of 2 M and leaching time of 60 min with a response of 15.89 wt.%. Recommended is further investigation of shorter leaching times. This study strongly suggests that an organic acid can effectively leach SCBA for improved silica yield.

The use of sol-gel method coupled with adsorption column containing activated carbon for the first time to enhance the purity of the sodium silicate hence more pure silica was obtained from sugarcane bagasse ash. The process successfully produced high purity silica of 98.92%. The silica obtained is nano silica as evidenced by the TEM images and the particle size for the highly pure silica ranged from 6 -24 nm. The textural property indicates high specific surface area of 240 m^2/g for the SiO_2 obtained for adsorption and specific surface area of 228 m^2/g for SiO_2 obtained without adsorption. The mass of feedstock used was kept constant for all samples to simplify yield comparisons. This shows that the adsorption stage also improved the surface area of the synthesized nano-silica. It can be deduced that the surface area of the synthesized nano silica is

excellent compared to the commercial silica (0.56 m^2/g) used for comparison in this work. The nano-silica obtained can be used for various applications due to the good textural properties.

Chapter 6 : Production of Nano Silicon and Hybrid Organic Solar Cell

6.1 Introduction

Nano silicon can find use in hybrid organic solar cells. This research therefore sought to fabricate and test the performance of a hybrid organic solar cell which uses silicon nanoparticles obtained from sugarcane bagasse ash. A power conversion efficiency (PCE) of 10 % is considered acceptable for the commercial production of organic solar cells (Würfel et al., 2015). The highest power conversion efficiency reported is in polymer solar cells fabricated from a blended active layer consisting of regioregular poly(3-hexylthiophene) (P3HT) and [6,6]-phenyl-C61 butyric acid methyl ester (PCBM), a fullerene derivative (Chen and Rieke, 1992; Hummelen et al., 1995).

The major drawback to the commercialization of OSCs is the power conversion efficiency (PCE). Several studies conducted to improve PCE through focused on change of parameters such as; optical properties of the (P3HT: PCBM) blend (Zhu et al., 2015); donor material absorbance by the mixing of energy-band engineered polymers to increase the bandwidth for adsorption (Yang et al., 2015); optimization of formation of domain and size (Ding et al., 2018; Morgenstern et al., 2016) and interface area engineering (Pfadler et al., 2014). Another approach which has gained attention among researchers is the development of hybrid solar cells with active material into which inorganic semiconductor particles are incorporated (Zhou et al., 2011). Inorganic particles that have been utilized in organic solar cells include CdS (Lee et al., 2008); CdTe (Gur et al., 2006); CdSe (Yang et al., 2011); $CuInS_2$ (Arici et al., 2003); PbSe (Tan et al., 2009); PbS (Tsang et al., 2009); SnO_2 (Kudo et al., 2007), TiO_2 (Kuo et al., 2008); and ZnO (Bhat et al., 2011; Hames et al., 2010; Takanezawa et al., 2008).

Liu et al. (2008) were the first to explore the utilization of elemental silicon nanoparticles in hybrid bulk heterojunction solar cells. The SiNPs showed a maximum PCE of 1.15% when incorporated in P3HT. An increase in PCE for the hybrid to 1.47% was obtained upon additional optimization of the process parameters, electrode selection and active material (Liu et al., 2010). According to Zhao et al. (2016), PCE improved when SiNPs was incorporated into P3HT:PCBM solar cells which resulted in a cascade band structure. Size reduction and doping are effective ways used in the fine-tuning of energy levels in semiconducting nanoparticles. To understand the use of doped NPs in hybrid solar cells, SiNPs with n and p-type dopants have been synthesized and utilized with active material. The P3HT:PCBM blend serves as a reference material blend because of its continued approval in fundamental hybrid solar cells research (Chi et al., 2014).

Hemaprabha et al. (2018) investigated the effect of using n and p-type nano silicon in P3HT: PCBM at different weight percentages. A PCE of 3.46 % was attained using doped p-type silicon nanoparticle. The team concluded that together with size reduction, the fine-tuning of energy levels in NPs, can be achieved through doping and mixing at appropriate weight ratios.

Elemental SiNPs have been used in inorganic-organic hybrid solar cells, and improvement in PCE has been reported. However, the SiNPs used were derived from pure silicon wafers, therefore in this work sugarcane bagasse ash waste-derived SiNPs was used in the fabrication of hybrid inorganic-organic solar cell material.

6.2 Experimental

6.2.1 Production and characterization of nanosilicon from SCBA-derived silica using magnesiothermic reduction

The materials and procedure used for the extraction of nano silicon from sugarcane bagasse ash derived silica and characterization techniques employed in this chapter are provided in detail in Chapter 3 (Section 3.5).

6.2.2 Production of hybrid organic solar cell and performance evaluation

The materials for the fabrication of the organic solar cell as a proof of concept and the testing techniques with the detailed description of experimental procedure employed in this chapter are provided in Chapter 3 (Section 3.6 and 3.7) of this thesis. The full names for the devices fabricated are summarized in Table 6-1.

Table 6-1 Device structures

Sample ID	Device structure
F1	ITO/PEDOT:PSS/P3HT:PCBM/Al
F2	ITO/PEDOT:PSS+ SCBA SiO_2 NPs/ P3HT:PCBM/Al
F3	ITO/PEDOT:PSS+ SCBA SiNPs/P3HT:PCBM/Al
F4	ITO/PEDOT:PSS+ SCBA p-type SiNPs/P3HT:PCBM/Al

The resulting device structure using the procedure described is shown in Figure 6-1.

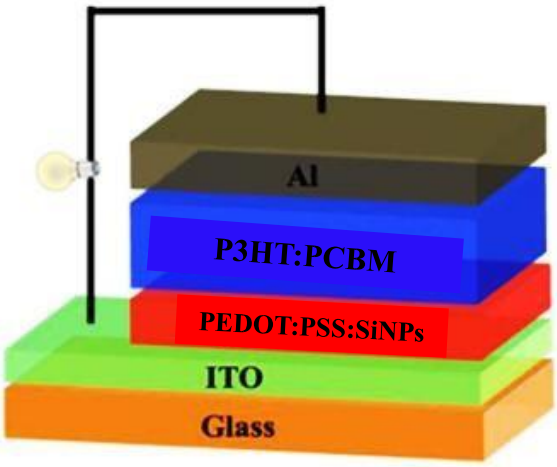


Figure 6-1 Schematic diagram of the hybrid organic solar cell

The current density–voltage (*J–V*) characteristics were obtained using HP 4141B source measure unit (SMU) under 100 mW/cm^2 illumination (AM 1.5G). All the measurements were carried out at room temperature under standard conditions. In evaluating the device performance, it was assumed that the solar cell behaves as an ideal diode shown in the equivalent circuit diagram in Figure 6-2. An equivalent circuit is a way of understanding the operation and behaviour of an electrical circuit or apparatus. It requires the deconstruction of the circuit into ideal simple circuit elements – e.g. diodes, resistors, inductor, capacitors, rectifiers, voltage and current sources. The device characteristics can be expressed as follows:

Short circuit current density:

$$J = J_{SC} - J_O\left(^{qV}/_{K_B T} - 1\right) \qquad \textit{Equation 6.1}$$

Where *Jo* is a constant, q is electron charge while V is voltage across the terminals

Open circuit current density:

$$V_{OC} = \frac{K_B T}{q} \ln\left(\frac{J_{SC}}{J_O} + 1\right) \qquad \textit{Equation 6.2}$$

Fill factor:

$$FF = \frac{J_{max} V_{max}}{J_{SC} V_{OC}} \qquad \textit{Equation 6.3}$$

Power conversion efficiency:

$$\eta = \frac{P_{maz}}{P_{in}} = \frac{J_{max} V_{max}}{J_{SC} V_{OC}} = \frac{J_{SC} V_{OC} FF}{P_{in}} \qquad \textit{Equation 6.4}$$

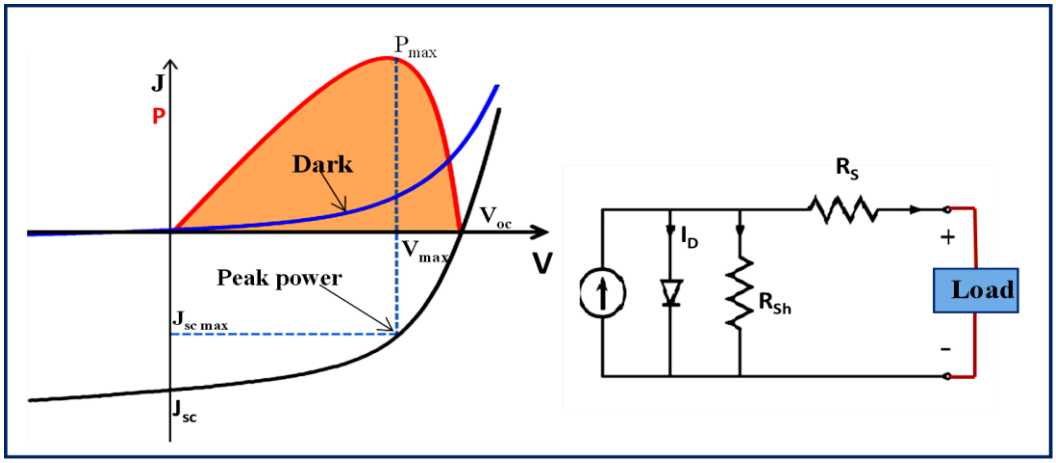


Figure 6-2 The J-V characteristics of a solar cell in the dark and under illumination; The equivalent circuit diagram.

6.3 Results and Discussion

6.3.1 Production of nanosilicon

Figure 6-3 depicts the extracted nano silica (Silica-B), the produced nano silicon from Silica B and the fabricated hybrid inorganic-organic solar cell devices. The elemental composition of synthesized nano silicon from XRF analysis is presented in Table 6-2. The percentage silicon in commercial grade silicon, nano Si washed with aquaregia (nano-Si_{AQ}) and nano Si washed with 2% HF (nano-Si_{HF}) was obtained to be 43.45%, 39.06% and 42.67%, respectively. For every 100% SiO_2, 46 % is elemental silicon (Kang et al., 2017; Zhang et al., 2016).



A **B** **C**

Figure 6-3 Nano silica (A), nano silicon (B) and fabricated solar cell devices (C)

Table 6-2 Elemental composition of commercial grade silicon and synthesized nano silicon

Element	**Commercial grade Si (%)**	**Nano-Si_{AQ} (%)**	**Nano-Si_{HF} (%)**
Si	43.45±0.03	39.06±0.04	42.67±0.03
Al	not detected	0.71±0.02	0.10±0.01
Fe	not detected	1.24±0.01	0.07±0.002
Mn	not detected	0.04±0.003	0.007±0.001
Cu	not detected	0.02±0.0009	not detected
Zn	not detected	0.07±0.001	not detected
Mg	not detected	0.45±0.13	0.34±0.08
Ca	0.17±0.0009	1.14±0.003	0.28±0.001
K	not detected	1.18±0.004	0.28±0.002
Ti	not detected	0.44±0.003	not detected
P	0.24±0.003	0.69±0.009	0.35±0.005
Cr	not detected	0.11±0.0057	not detected

The commercial grade silicon is 1.8% purer than nano Si washed with 2% HF. This confirms that despite HF being harmful it is an effective etching acid to improve the purity for silicon. It should be noted that Si reacts violently with HF to generate a gaseous product. Whereas the nano silicon washed with 2% HF is 8% purer than nano Si washed with aquaregia. Therefore, HF is a better reagent in etching nano silicon where purity is of priority like in solar cell fabrication. The purity of the synthesized nano silicon is comparable to the theoretical of 46%, therefore sugarcane bagasse ash can be a source of nano silicon for this current application.

6.3.1.1 Degree of crystallinity of produced nanosilicon

The X-ray diffractometer pattern for commercial grade silicon, nano silicon washed with Aquaregia (Nano-Si_{AQ}) and nano silicon washed with Hydrofluoric Acid (Nano-Si_{HF}) is presented in Figure 6-4. The synthesized Nano-Si_{AQ} and Nano-Si_{HF} are crystalline with sharp intensity at 2θ of 34º and 32º respectively, compared to the commercial grade which is showing to be both amorphous and crystalline.

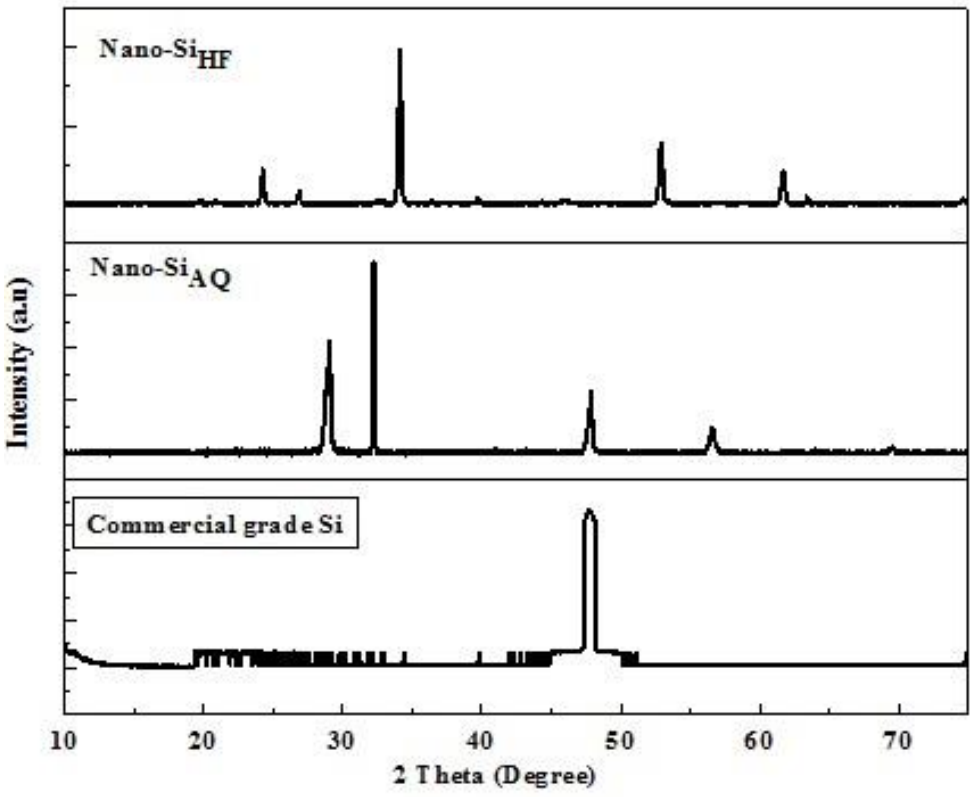


Figure 6-4 XRD pattern for commercial grade silicon, nano silicon washed with aquaregia and nano silicon washed with 2 % HF.

The crystallite size estimated by Scherrer Equation based on 2θ of 34º (Nano-Si_{AQ}), 32º (NanoSi_{HF}) and 47º (commercial grade silicon) are 0.24 nm, 0.26 nm and 0.18 nm respectively. This work is

supported by Falk et al. (2019) who synthesized nano silicon particles from sugarcane bagasse ash using magnesiothermic reduction and the crystallite size estimated by the Scherrer equation based on 2θ of 28º was 28 nm (Falk et al., 2019).

6.3.1.2 Determination of level of impurity in waste water produced after washing of nano silicon

The impurity level of water used to wash the nano silicon using aquaregia and 2% HF is presented. Fig 6-5 presents data of atomic absorption spectroscopy (AAS) analysis of wastewater obtained by washing of the nano silicon when using aquaregia and 2% HF. AAS was used to determine the metal impurity levels in the waste water after washing the nano silicon obtained from magnesiothermic reduction. The major metal ion impurity was Mg with 32.37 and 39 mg/L respectively. HF is very efficient in etching silicon compared to other acids.

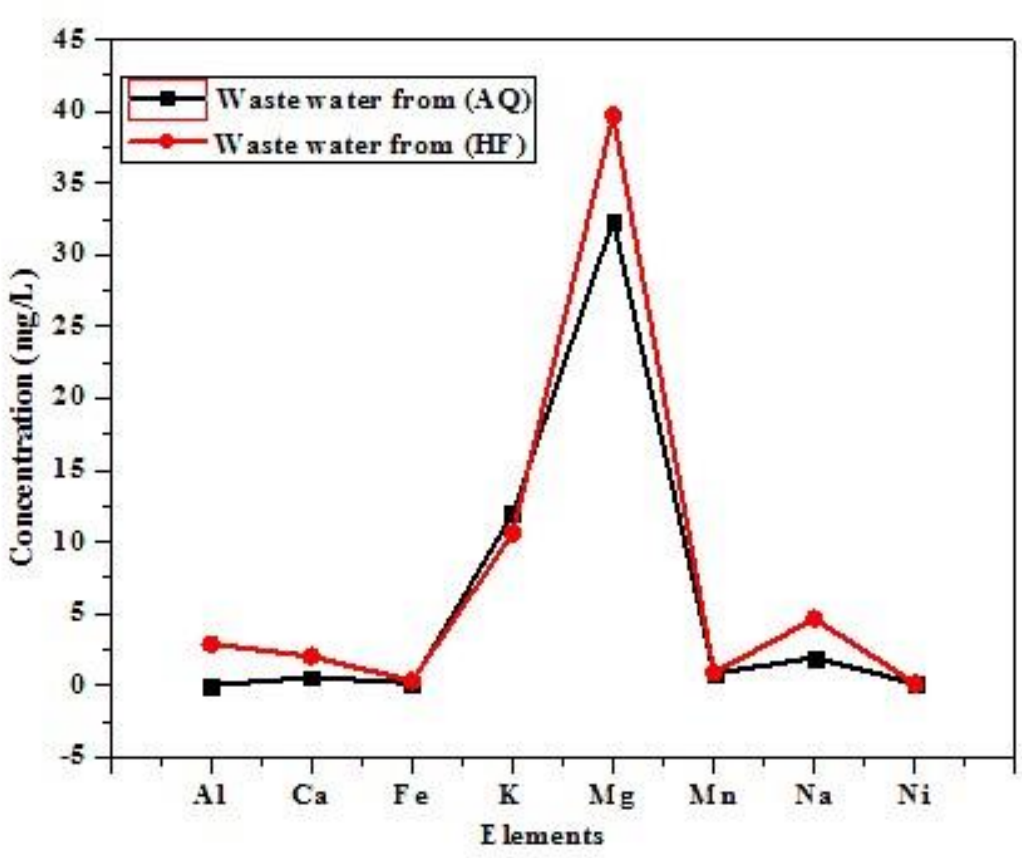


Figure 6-5 Trace elements in wastewater after washing nano silicon with aquaregia and 2% HF

Santos et al. (1990), reported the purification of metallurgical silicon where particle size, time, temperature and concentration of etching agents (HNO_3, H_2SO_4, HC1 and HF) were of importance. It was found that using only Hydrochloric acid (16%, 5 h, 80°C) and a relatively coarse fraction it is possible to remove approximately 85% of the impurities and to obtain 99.9% pure Si after further etching/washing with hydrofluoric acid (2.5%, 2 h, 80 °C). All the other acids and their mixtures, including aqua regia, gave results poorer than those for hydrochloric acid. The finer fractions were more difficult to purify (Santos et al., 1990). Xi et al. (2018) reported a novel metal assisted chemical leaching/etching method to remove impurities from metallurgical grade silicon**.** HF, silver nitrate ($AgNO_3$) and hydrogen peroxide (H_2O_2) were employed to purify MG-Si. The

impurities (Fe, Al, Ca, Ti, Mn, Ni, Cu, V, Cr, Ag, B and P) concentration were reduced from 4550.40 mg/L to 106.09 mg/L and the purity of MG-Si increased from 99.55 to 99.99% (Xi et al., 2018). Lei et al. (2017), investigated the use of various leaching approaches. Compared with aqua regia and HF, HCl + HF was determined to be the optimal for the elimination of impurities from MG-Si. The use of a combination of HCl + HF and aqua regia reduced the quantity of impurities from 6126 mg/L to 94 mg/L. (Lei et al., 2017). Lu et al. (2017), investigated the effect of acetic acid on the leaching behavior. The focus was on impurities affected by the addition of acetic acid to a conventional acid mixture composed of hydrochloric acid and hydrofluoric acid. The etching results revealed that the HCl–HF– CH_3COOH mixture is a better lixiviant for dissolving impurities in MG-Si. The extraction yield of impurities in HCl–HF–CH_3COOH leaching was found to increase by 7% compared to conventional HCl–HF leaching. (Lu et al., 2017).In this current study 2 % HF showed to be effective in removal of metal impurities compared to aquaregia.

6.3.1.3 Surface chemistry of produced nanosilicon

The evolution of the FTIR spectra of commercial grade Si, Nano-Si_{AQ} and Nano-Si_{HF} is presented in Figure 6-6. The typical band peak that appeared in nano silicon is Si-O stretching mode (1011 cm^{-1}). A similar observation was made by earlier studies (Kale and Solanki, 2010).

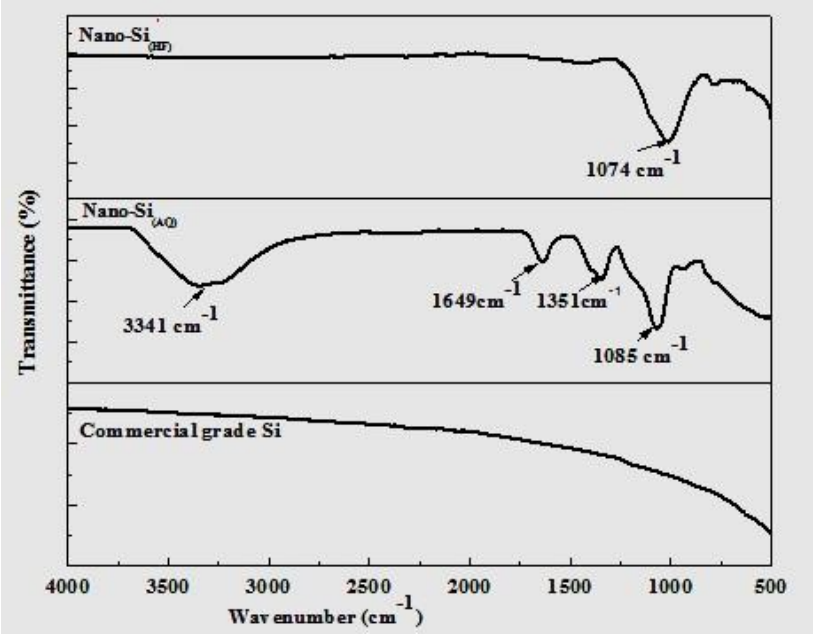


Figure 6-6 Surface chemistry for commercial grade silicon, Nano-Si$_{AQ}$ and Nano-Si$_{HF}$

For commercial-grade silicon, there is no observed peak, and this confirms the absence of traces of silica and affirms that the sample is pure silicon metalloid. The other spectra suggest that further purification is needed to attain purity of commercial grade silicon.

6.3.1.4 Raman spectroscopy for nano silicon

The Raman spectra for the synthesized nano silicon particles (Nano-Si$_{HF}$) is presented in Figure 6-7. A Raman peak at 520 cm^{-1} with the full width at half maximum (FWHM) of 2.9 cm^{-1} was observed. This was due to the scattering of the first order optical phonon of nano silicon. The outcome is supported by the work reported by Li et al. and co- workers (Li et al., 1999). In their work for the Raman spectra for crystalline silicon, they observed a peak at 520 cm^{-1} and a FWHM of 2.8 cm^{-1}.

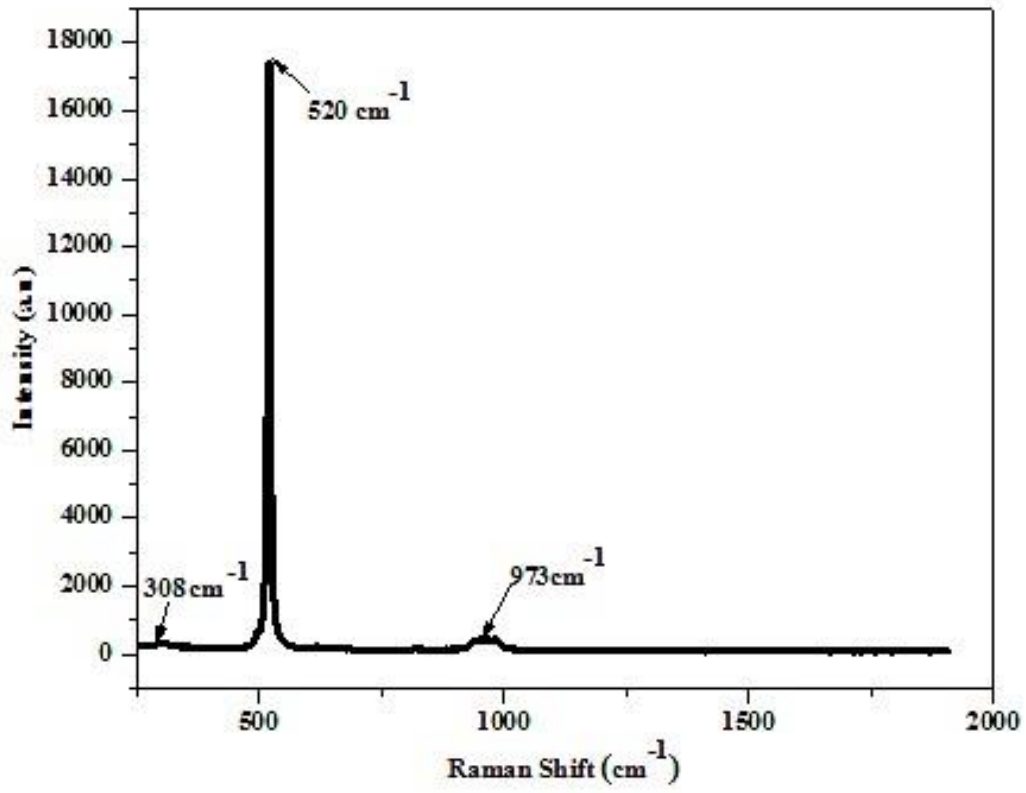


Figure 6-7 Raman spectrum for the synthesized nano silicon (Nano-Si_{HF})

Also, there are two broad peaks at 308 cm^{-1} and 973 cm^{-1}, respectively, which are due to the scattering of two transverse acoustic (2TA) phonons and two transverse optical (2TO) phonons respectively. Li et al.(1999), reported 300 and 970 cm^{-1} for 2TA and 2TO, respectively (Li et al., 1999). Holzapfel et al. (2006), reported a prominent silicon signal with the most notable Raman feature seen at 518 cm^{-1}, with a full width at half maximum (FWHM) of 6 cm^{-1}. This can be assigned to the scattering of the first order optical phonon mode (TO). Two peaks at 300 and 950 cm^{-1} were observed and these were assigned to the scattering of the second-order transverse acoustic phonon mode (2TA) and the second-order optical phonon mode (2TO), respectively (Holzapfel et al., 2006). Falk et al. (2019), reported the Raman spectra of the synthesized nanoSi. The intense band of Si

located at 513.7 cm^{-1} was associated with the Si–Si stretching mode and the small peak centered at 960.3 cm^{-1} was owing to the stretching mode amorphous Si-Si (Falk et al., 2019).

6.3.1.5 Textural properties of nanosilicon

Nitrogen physisorption of commercial grade silicon, Nano-Si_{AQ} and Nano-Si_{HF} are presented in Figure 6-8. The textural properties of the commercial-grade silicon and the synthesized NanoSi_{AQ} and Nano-Si_{HF} were determined using N_2 adsorption-desorption method and results are summarised in Table 6-3.

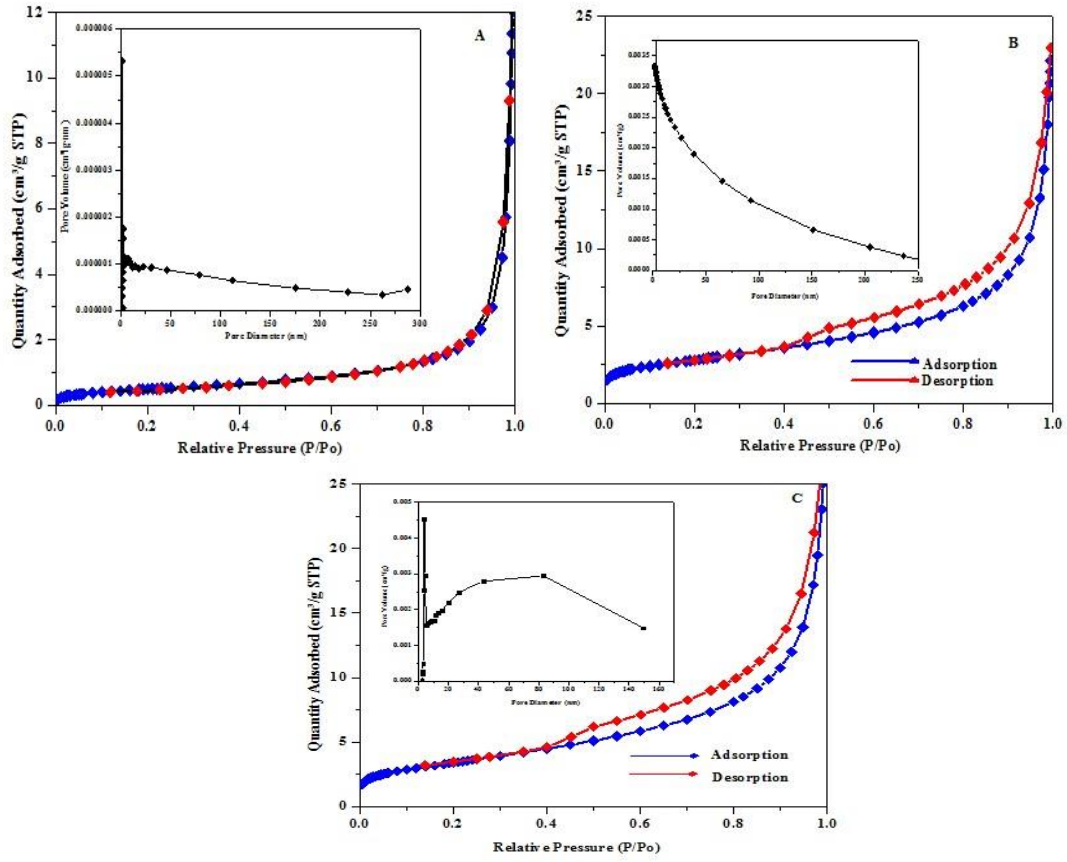


Figure 6-8 BET isotherms and pore size distribution curves for A) commercial grade silicon B) Nano-Si_{AQ} and C) Nano-Si_{HF}.

Table 6-3 Textural properties of commercial grade silicon, Nano-Si_{AQ} and Nano-Si_{HF}

Sample ID	S_{BET} (m^2/g)	V_p (cm^3/g)	D_p (nm)
Commercial grade Si	1.84	0.0186	38
Nano-Si_{AQ}	20.39	0.186	30
Nano-Si_{HF}	30.14	0.194	25

The BET specific surface area (BET_{SSA}) pore volume and pore diameter for Nano-Si_{HF} were 30.14 m^2/g, 0.194 cm^3/g and 25 nm, respectively and for Nano-Si_{HF} were 20.39 m^2/g, 0.186 cm^3/g and 30 nm while BET_{SSA}, pore volume and pore diameter for commercial grade silicon is 1.8398 m^2/g, 0.0186 cm^3/g and 38 nm. The nano silicon etched with HF showed high surface area than silicon washed with aquaregia and that of commercial grade silicon. The amount of adsorbed gas increases steadily with increasing of P/P_0 at the lower P/P_0 regions. This is attributed to monolayer and multilayer adsorption. For both synthesized Nano-Si_{AQ} and Nano-Si_{HF} isotherms, the hysteresis loop is observed at a range of $0.4 < P/P_0 < 1.0$, which is associated with capillary condensation taking place in the mesopores (Wang et al., 2006). The loop at high P/P_0 side (close to 1.0) is related to large pores. The nitrogen adsorption isotherms of SCBA nano silicon and commercial grade silicon are similar to Type II proposed by the International Union of Pure and Applied Chemistry (IUPAC) (Ahn et al., 2016).

6.3.1.6 Morphology of the nanosilicon

The morphology of the nano silicon powders after the magnesiothermic reduction process and etching/leaching with HF and aquaregia were evaluated by SEM as shown in Figure 6-9. It is observed that both Nano-Si_{HF} and Nano-Si_{AQ} have the similar morphology to the nano silica

(characteristic of materials in the nanometric scale) synthesized and reported in Chapter 5. The SEM shows that particles from all the three samples are agglomerated.

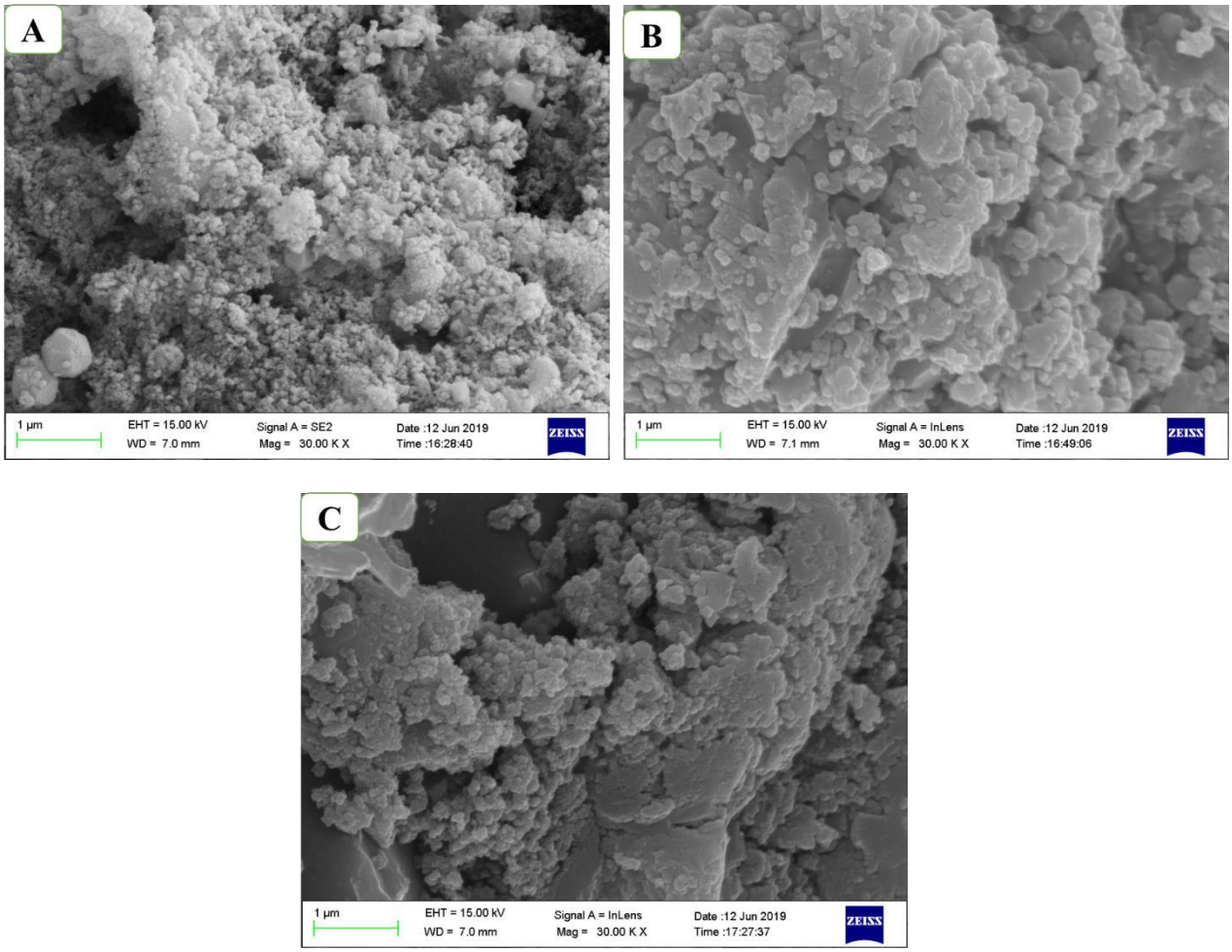


Figure 6-9 SEM micrographs for A) commercial grade silicon B)nano-Si_{AQ} and C) Nano-Si_{HF}.

The particle size distribution as shown in Figure 6-10 and Figure 6-11 is not representative of single particles but agglomerates which are also in the nano range. Falk et al. (2019), reported magnesiothermic reduction of nano silica from sugarcane bagasse ash and concluded that the agglomeration state was favored by the magnesiothermic reduction process through TEM analysis (Falk et al., 2019).

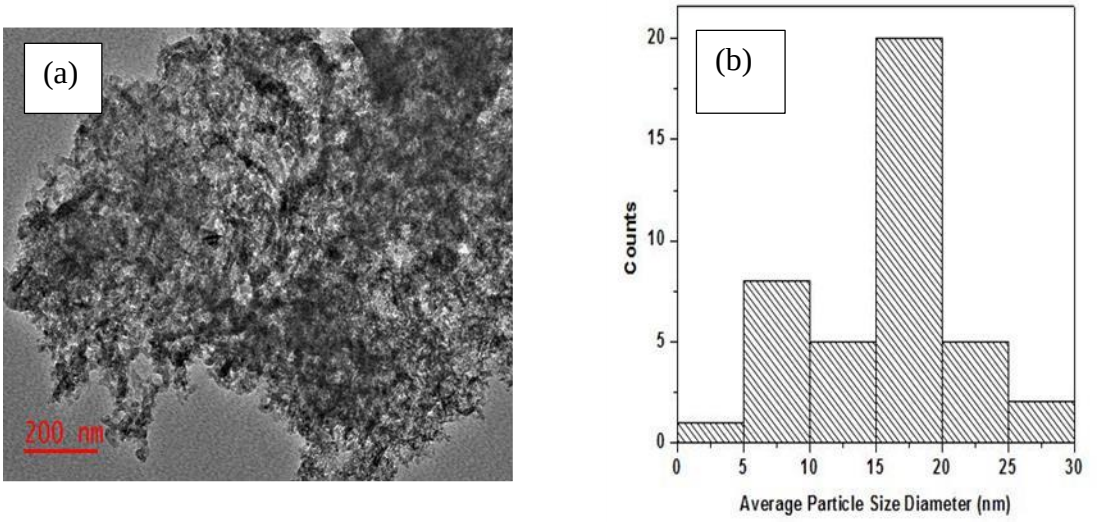


Figure 6-10 (a) TEM micrograph of nano-Si_{AQ} and (b) corresponding particle size distribution

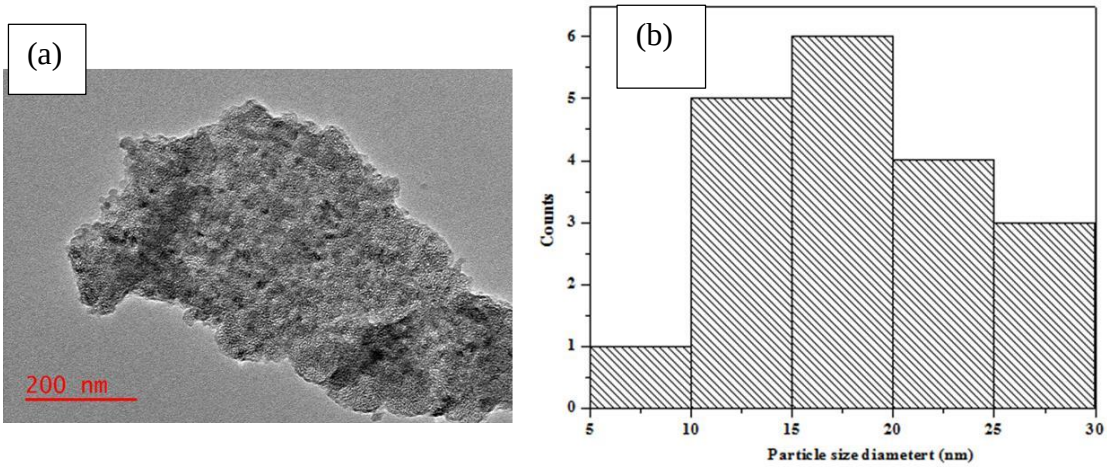


Figure 6-11 (a) TEM micrograph of nano-Si_{HF} and (b) corresponding particle size distribution

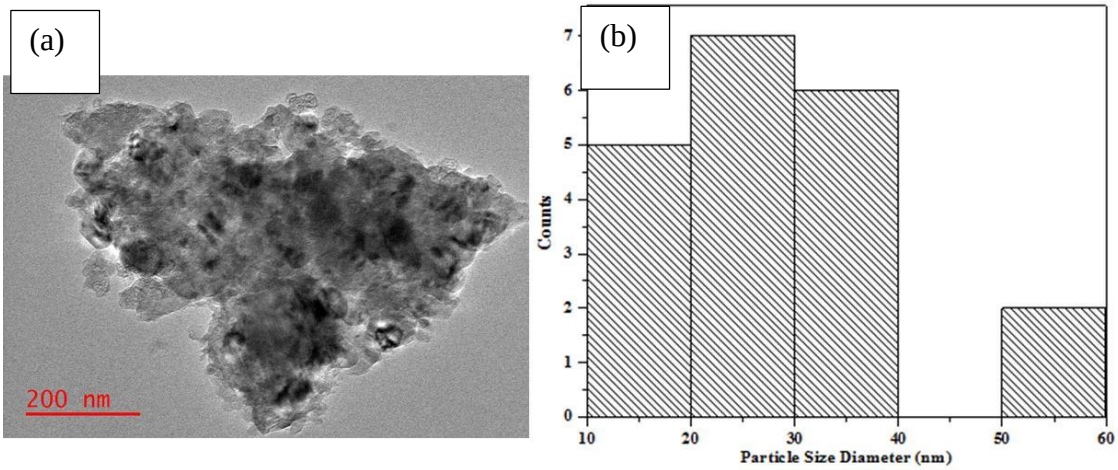


Figure 6-12 (a)TEM micrograph of commercial-grade silicon and (b) particle size distribution

6.3.2 Fabrication and performance evaluation of hybrid organic solar cell

6.3.2.1 Scanning electron microscopy (SEM)

The SEM images presented in Figure 6-13 were taken from a PEDOT: PSS film with and without sugarcane bagasse ash derived SiNPs. The reference film in Figure 6-13 (A) shows a smooth, homogeneous morphology. This is supported by smoother films seen on the AFM in Figure 6-14 (A). Nomenclature of the device architectures F1, F2, F3 and F4 and the reference device is as given in Table 6-1.

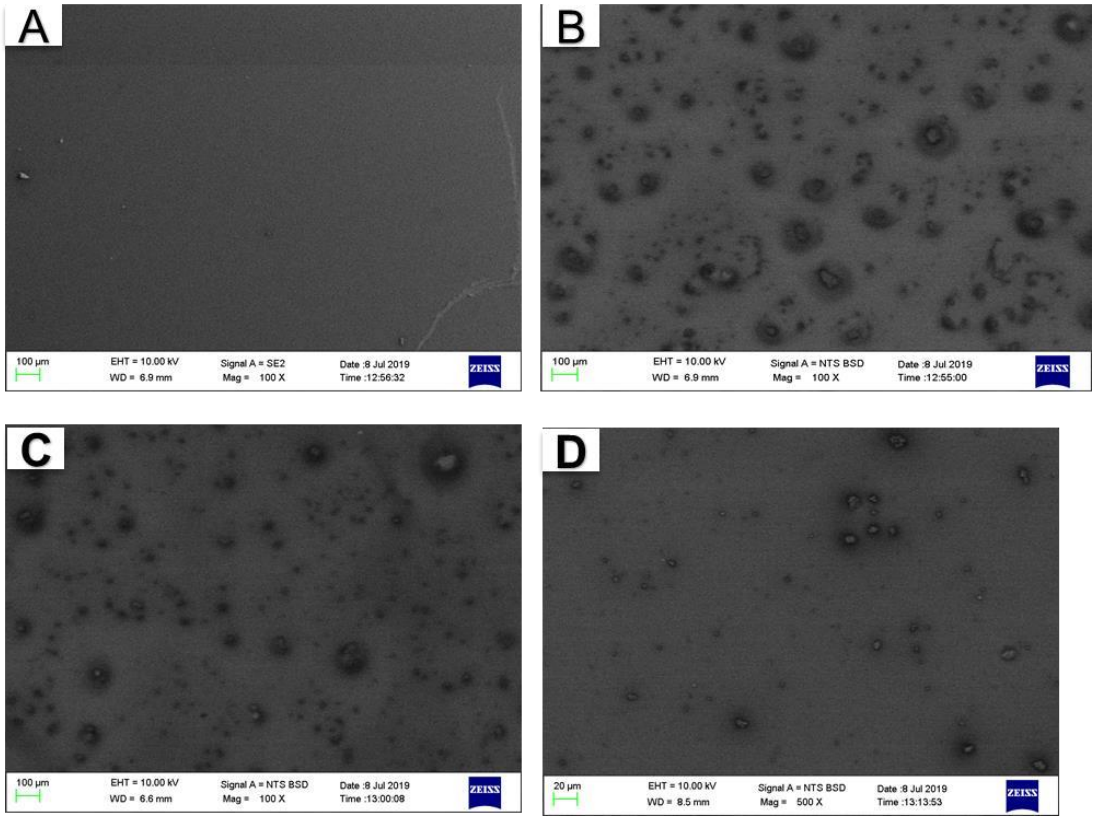


Figure 6-13 Surface morphology of fabricated solar cell devices A) reference cell, F1, B) F2, C) F3, D) F4

6.3.2.2 Atomic force microscopy/ surface roughness

Table 6-4 shows a summary of the AFM analysis of the AFM images in Figure 6-14. The statistical analysis was derived using the height distribution histograms from the AFM analysis software WSxM 4.0. The average roughness (*Ra*) implies the mean height and was derived over the entire measured length/area. It is useful for detecting general variations in overall profile height characteristics and for monitoring an established manufacturing process. The root mean square roughness (R_{rms}) is described as the square root of the distribution of surface height, normally known to be more sensitive than the average roughness for large deviations from the mean line/plane. The R_{rms} was then used to compute the skewness which establishes the profile symmetry

about the mean line. The positive skewness values indicate an asymmetrical height distribution with more peaks than valleys.

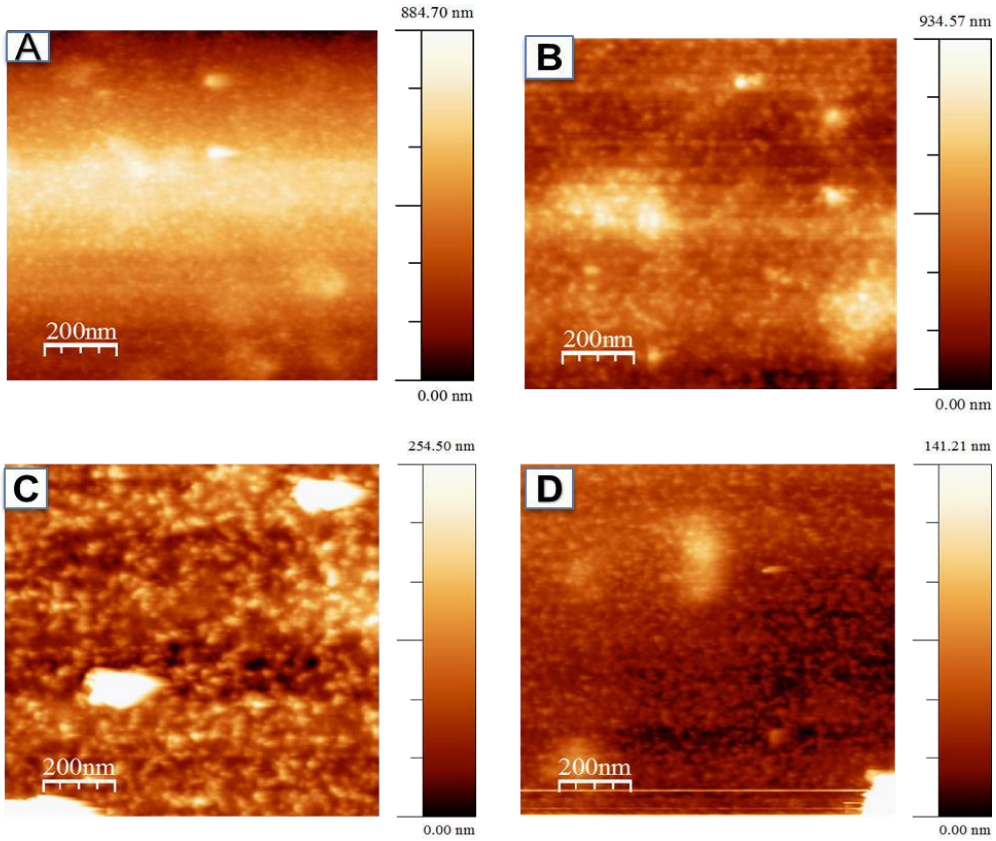


Figure 6-14 AFM images of A) reference B) F2 C) F3 D) F4

Table 6-4 Summary of tapping mode AFM analysis

Sample ID	**R_a (nm)**	**R_{rms} (nm)**	**Skewness (R_{sk})**
F1	3.85	5.95	2.46
F2	9.49	17.92	6.20
F3	10.24	18.85	4.79
F4	8.39	16.99	16.48

Table 6-4 shows a summary of surface topographic parameters; average roughness (R_a), root mean square roughness (R_{rms}) and skewness (R_{sk}). Sample F1 showed a smoother film with R_{rms} of 5.95 nm and skewness of 2.46 nm. Upon incorporation of the sugarcane bagasse ash derived SiNPs, the films became rougher. F3 shows films with highest roughness, R_{rms} =18.85 nm but a low skewness of 4.79. This lower skewness implies that the particles seem to be homogenously distributed in the PEDOT: PSS layer. This homogenous distribution of the SiNPs in PEDOT:PSS with high Rrms is critical for light scattering leading to more time in the active layer. This results into more light absorption experienced using the UV-Vis measurements. Usually the scattering cross-section can be tuned by controlling the size and geometry of the nanostructures such that photons are scattered forward and backward in comparable quantities (Mokkapati et al., 2011). As a result, F3 showed highest current density, see Figure 6-17. Moreover, the increasing anode surface roughness may result in an increased interface area between the anode and the active layer hence providing shorter transport channels for holes to travel to the ITO. These channels potentially will enhance not only hole collection efficiency but also their carrier mobility. This could also have contributed to the high short current density as seen from the *J-V* characteristics.

6.3.2.3 UV-vis spectroscopy

Figure 6-15 shows the UV-Vis measurement of reference device with structure ITO/ PEDOT:PSS/P3HT:PCBM thin film and incorporation of SCBA-derived SiO_2 NPs, SCBA-derived SiNPs and p-type SCBA-derived SiNPs into the PEDOT:PSS layer. Generally, solid state absorption spectra of P3HT: PCBM thin film shows two peaks. The peak at approximately 517 nm and a shoulder at 612 nm are usually attributed to the π–π^* transition in the P3HT molecules while

the hump at 325 nm is due to PCBM excitation characteristics (Shrotriya et al., 2005). The shoulder at 612 is enhanced with incorporation of the nanoparticles; this shows greater light absorption necessary for efficiency enhancement in organic solar cell. The use of SCBA SiNPs in the PEDOT:PSS generated an increase in absorption. For short-wavelength (300–600 nm) light that can efficiently transmit through glass into the active layer of a solar cell, the display of improved light harvesting capability with SCBA SiNPs is quite significant in realizing enhanced device performance.

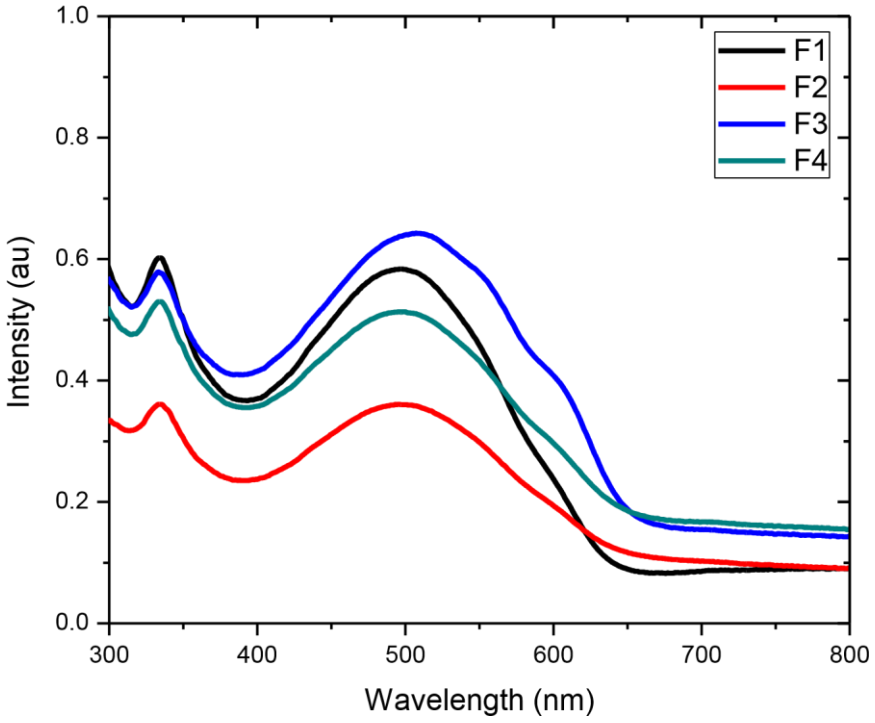


Figure 6-15 Solid-state uv-vis measurements of the thin films F1, F2, F3 and F4

6.3.2.4 J-V characterization

From Table 6-5 the reference device gives an efficiency of 0.83%. Upon incorporation of SCBA SiO_2 NPs and p-type SCBA SiNPs into the PEDOT: PSS layer the device performance reduced.

Table 6-5 Summary of the performance of devices with different structures

Sample ID	J_{sc} (mA)	V_{oc}(V)	FF(%)	PCE(%)
F1	0.13	0.50	38.20	0.83
F2	0.0039	0.21	3.88	0.001
F3	1.61	0.57	15.26	0.14
F4	0.11	0.49	38.62	0.63

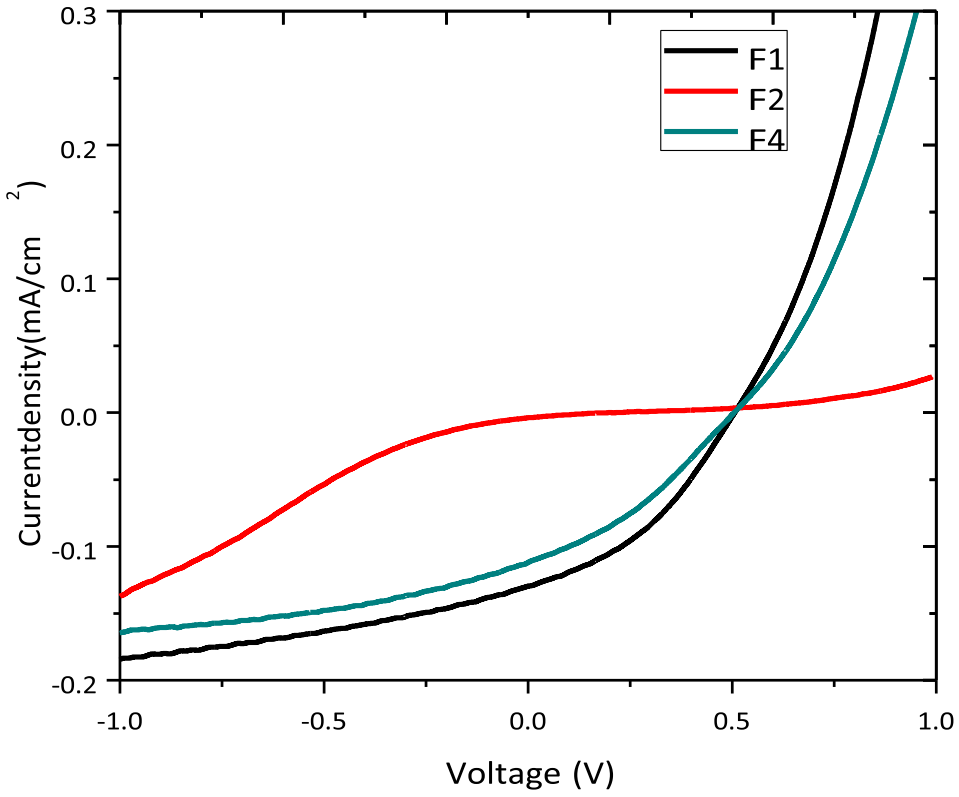


Figure 6-16 J–V characteristics, recorded under illumination at 100 mW cm^{-2} (AM 1.5G) of reference device F1 and devices with SCBA-derived SiO2 NPs and p-type SCBA-derived SiNPs incorporated into the PEDOT: PSS layer.

The profile for F2, as observed in Figure 6-16 is expected since SiO_2-NPs are insulating therefore the series resistance due to the layer may be highest in this device.

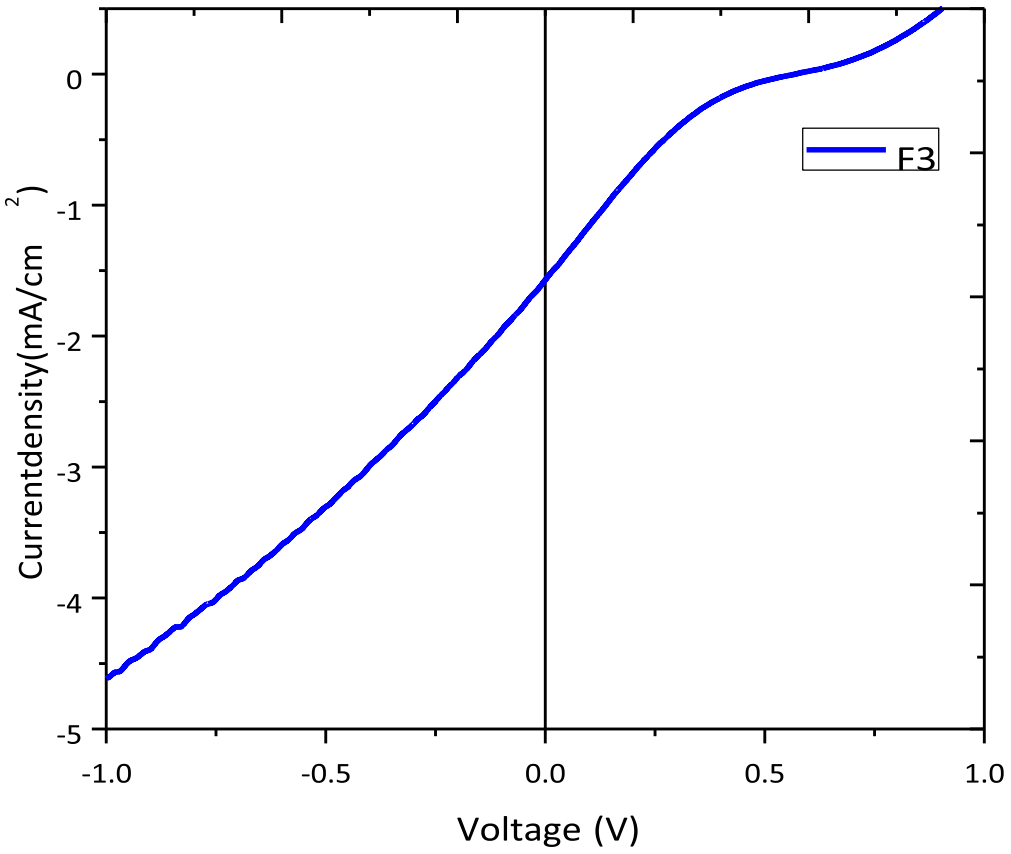


Figure 6-17 J–V characteristics, recorded under illumination at 100 mW cm^{-2} (AM 1.5G) of devices with SCBA SiNPs incorporated into the PEDOT:PSS layer.

Device SCBA SiNPs into the PEDOT:PSS layer showed a remarkable increase of current density of about 42.48%. This increase is in agreement with short wavelength absorption spectra. The increase could also be attributed to cascading energy-level alignment when the energy levels of SCBA SiNPs is combined with those of P3HT and PCBM (Khlyabich et al., 2011) as shown in Figure 6-17. It has been shown that a cascade energy-level alignment (Figure 6-18) may improve the separation of excitons especially when the NPs are incorporated into the active layer as well as the transport of charge carriers upon separation (An et al., 2014; Yang et al., 2013; Zhao et al., 2016) leading to enhanced solar cell efficiency both optically and electronically.

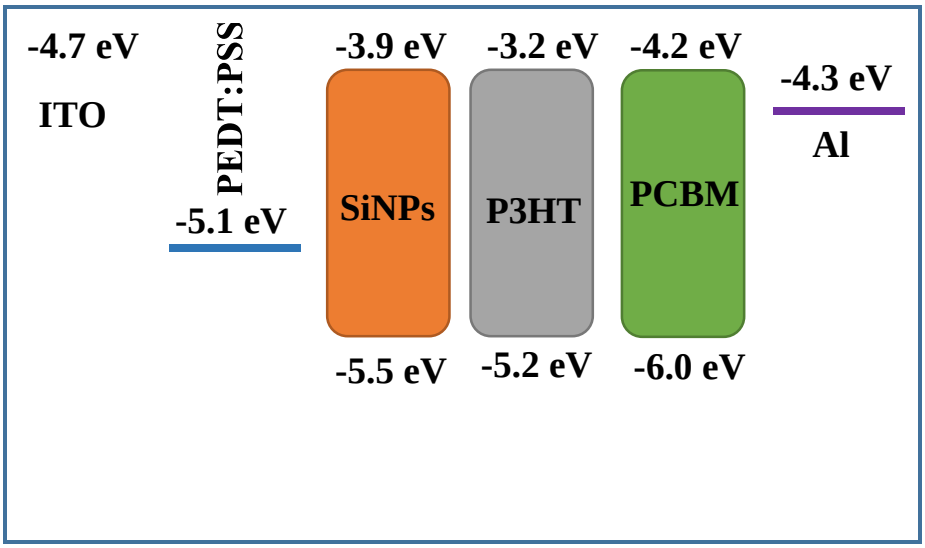


Figure 6-18 Energy-level diagram of a hybrid organic solar cell structure

Compared to the reference device F1, devices with SCBA SiO_2 NPs and p-type SCBA SiNPs incorporated into the PEDOT: PSS layer recorded a slightly low performance. Device F4 with structure ITO/PEDOT: PSS+p-type SCBA SiNPs/P3HT: PCBM/Al recorded a better fill factor of 34.62% since the p type had a better hole transport hence lowering the series resistance. This implies that the holes are effectively collected before much recombination occurs.

6.4 Concluding Remark

The results obtained in this chapter indicate that the protocol presented for the synthesis of nano silicon particles from sugarcane bagasse ash derived nano silica using a magnesiothermic reduction method (MRM) was successful. The MRM reaction was performed at 700^{o}C for 4 hours. The nano silicon washed using 2% HF exhibited a surface area of 30.18 m^2/g compared to the nano silicon etched with aquaregia with surface area of 20.39 m^2/g. However, aquaregia is a promising etching acid for silicon. The nano silicon particles (SiNPs) produced from sugarcane bagasse ash waste were successfully incorporated into organic solar cell device in the hole transport layer where they were mixed with PEDOT: PSS. The non-uniformity film morphologies were expected to reduce

device efficiency. However, despite the limitation, device performance indicated that SCBA SiNPs is a promising candidate for future organic-inorganic hybrid solar cells due to being cheap sourced from waste SCBA and lack of toxicity. The reference film showed a smoother surface with R_{rms} of 5.95 nm which drastically increased upon the incorporation of the nanoparticles. There was an improvement in absorption upon the incorporation of SCBA SiNPs in the PEDOT: PSS which could be attributed to light scattering. This led to a remarkable increase in the current density of about 42.48 %. Other device structure showed a lower current density although device with ptype SCBA SiNPs recorded a better fill factor of 34.62% which could be attributed to it being ptype hence it had a better hole transport which resulted in the lowering of the series resistance. There is still needed to incorporate the nano silicon into the active layer and study their optoelectrical performance.

Chapter 7 : General Conclusions and Recommendations

7.1 Conclusions

As highlighted in Chapter 1 of the thesis, the following objectives have been achieved:

1. Characterization of sugarcane bagasse ash obtained from an ethanol-producing company in Zimbabwe.
2. Proposal and application of an energy-efficient process for the conversion of the extracted silica into pure silicon.
3. Fabrication of a hybrid organic solar cell using the produced pure silicon and the evaluation its performance.

The results obtained from the objectives have produced novel contributions in the area of beneficiation of sugarcane bagasse ash waste into nano silicon for solar cell application. Consequently, the undernoted contributions have been made;

- High purity amorphous nano silica (98.92%) was obtained from an improved sol-gel method in which activated carbon was used to enhance the purity of sodium silicate prior to precipitation of nano silica. The particle size for the nano silica ranged from 6-24 nm and the surface area, pore volume and pore diameter were 240 m^2/g, 0.577 cm^3/g and 10 nm respectively.
- Successfully prepared crystalline nano silicon particles with size ranging from 1-30 nm from sugarcane bagasse ash derived nano silica. The surface area, pore volume and pore diameter were 30.14 m^2/g, 0.194 cm^3/g and 25 nm respectively.
- The produced silicon nano particles were incorporated into the hole transport layer poly(3,4- ethylenedioxythiophene)-poly(styrene sulfonate) (PEDOT:PSS) of an organic solar cell based on blend of poly(3-hexylthiophene) (P3HT) and [6:6]-phenyl-C61butyric

acid (PCBM). From this study, a proof of concept for the application of SCBA-derived SiNPs in solar cells has been established. The PCE of the solar cell was 0.63 % compared with the PCE reference of 0.83%. As far as could be ascertained, this is the first solar cell reported that incorporates nano silicon particles extracted from sugarcane bagasse ash.

In summary, the mentioned novel contributions have been communicated to fellow researchers in the area of bio-waste valorization and solar cell technology as articles in international scientific journals (one book chapter in press, two manuscripts are under review) and in conference proceedings (two proceedings) (See Appendix 2 for copies of the contributions).

7.2 Recommendations

- The purity of nano silica from sugarcane bagasse ash can be enhanced by the optimization of the adsorption method. Thus, future study on the adsorption process of sodium silicate solution prior to the precipitation of nano silica to remove metal impurities is proposed.
- The purity of nano silicon from magnesiothermic reduction is still low and etching with hydrofluoric acid prior to solar cell fabrication was done. However, HF promises to be continuously used in etching of silicon for solar cell application as it proves to be the best compared to other inorganic acids.
- The proof of concept for the use of synthesized nano silicon particles in the organic solar cell has been established. However, the PCE is low therefore future work should be done to optimize the fabrication process. The SiNPs can also be incorporated in the active layer (P3HT: PCBM) to also check the effect on PCE.

- The SiNPs were only tested for an organic solar cell based on the blend of P3HT and PCBM, there is a possibility to incorporate the SiNPs in other solar cells like thin film silicon solar cells and dye-sensitized solar cells to investigate their effectiveness in enhancing PCE.

References

Abbasi, A., and Zargar, A. (2013). Using baggase ash in concrete as pozzolan. Middle East Journal of Scientific Research *13*, 716–719.

Adebisi, J., Agunsoye, J., Bello, S., Ahmed, I., Ojo, O., and Hassan, S. (2017). Potential of producing solar grade silicon nanoparticles from selected agro-wastes: A review. Solar Energy *142*, 68–86.

Adebisi, J.A., Agunsoye, J.O., Bello, S.A., Haris, M., Ramakokovhu, M.M., Daramola, M.O., and Hassan, S.B. (2019). Green Production of Silica Nanoparticles from Maize Stalk. Particulate Science and Technology 1–9.

Adesanya, D., and Raheem, A. (2009). Development of corn cob ash blended cement. Construction and Building Materials *23*, 347–352.

Affandi, S., Setyawan, H., Winardi, S., Purwanto, A., and Balgis, R. (2009). A facile method for production of high-purity silica xerogels from bagasse ash. Advanced Powder Technology *20*, 468–472.

Agostinelli, T., Lilliu, S., Labram, J.G., Campoy-Quiles, M., Hampton, M., Pires, E., Rawle, J., Bikondoa, O., Bradley, D.D., and Anthopoulos, T.D. (2011). Real-Time Investigation of Crystallization and Phase-Segregation Dynamics in P3HT: PCBM Solar Cells During Thermal Annealing. Advanced Functional Materials *21*, 1701–1708.

Agunsoye, J., Adebisi, J., Bello, S., Haris, M., Agboola, J., and Hassan, S. (2018). Synthesis of Silicon Nanoparticles from Cassava Periderm by Reduction Method. The 2018 Materials Science &Technology Conference & Exhibition 701–709.

Ahire, J.H., Wang, Q., Coxon, P.R., Malhotra, G., Brydson, R., Chen, R., and Chao, Y. (2012). Highly Luminescent and Nontoxic Amine-Capped Nanoparticles from Porous Silicon: Synthesis

and Their Use in Biomedical Imaging. ACS Applied Materials & Interfaces *4*, 3285–3292. Ahn, J., Kim, H.S., Pyo, J., Lee, J.-K., and Yoo, W.C. (2016). Variation in crystalline phases: controlling the selectivity between silicon and silicon carbide via magnesiothermic reduction using silica/carbon composites. Chemistry of Materials *28*, 1526–1536.

Aigbodion, V., Hassan, S., Ause, T., and Nyior, G. (2010). Potential utilization of solid waste (bagasse ash). Journal of Minerals and Materials Characterization and Engineering *9*, 67-77. Akram, T., Memon, S.A., and Obaid, H. (2009). Production of low cost self compacting concrete using bagasse ash. Construction and Building Materials *23*, 703–712.

Alayande, O., Dare, O., Ayinde, W.B., Bamigbose, J., Ayedun, P., and Osinkolu, G.A. (2012). Development of ordered and disordered macroporous silica from bagasse ash. African Journal of Pure and Applied Chemistry *6*, 10–14.

Ali, H.H., El-Sadek, M., Morsi, M.B., El-Barawy, K.A., and Abou-Shahba, R.M. (2017). Upgrading of Locally Produced Metallurgical Grade Silicon (MG-Si). Egyptian Journal of Chemistry *61*, 155-161

Al-khazraji, R., Li, Y., and Zhang, L. (2018). Application of slag refining technique to metallurgical grade silicon purification process: A review. Functional Materials *25*, 364–370. Altoe, S.P.S., Sales, A., and Martins, C.H. (2019). Waste tires and the burning of sugarcane bagasse in the manufacture of concrete pavers (pavers). RIEM-IBRACON Structures and Materials Journal *12*, 608-637

Alves, R.H., Reis, T.V. da S., Rovani, S., and Fungaro, D.A. (2017). Green synthesis and characterization of biosilica produced from sugarcane waste ash. Journal of Chemistry *2017*, 1-9

Amri, C., Ouertani, R., Hamdi, A., and Ezzaouia, H. (2018). Enhancement of electrical parameters

in solar grade monocrystalline silicon by external gettering through sacrificial silicon nanowire layer. Materials Research Bulletin *98*, 41–46.

An, Q., Zhang, F., Li, L., Zhuo, Z., Zhang, J., Tang, W., and Teng, F. (2014). Enhanced performance of polymer solar cells by employing a ternary cascade energy structure. Physical Chemistry Chemical Physics *16*, 16103–16109.

Andrews, R.N., and Clarson, S.J. (2015). Pathways to Solar Grade Silicon. Silicon *7*, 303–305.

Antoniadis, H., Jiang, F., Shan, W., and Liu, Y. (2010). All screen printed mass produced silicon ink selective emitter solar cells. 35th IEEE Photovoltaic Specialists Conference, 24-29

Anukam, A.I. (2013). Gasification Characteristics of Sugarcane Bagasse. University of Fort Hare.

Anwar, S. (2010). Determination of moisture content of bagasse of jaggery unit using microwave oven. Journal of Engineering Science and Technology *5*, 472–478.

Arici, E., Sariciftci, N.S., and Meissner, D. (2003). Hybrid solar cells based on nanoparticles of CuInS2 in organic matrices. Advanced Functional Materials *13*, 165–171.

Arif, E., Clark, M.W., and Lake, N. (2017). Sugar cane bagasse ash from a high-efficiency cogeneration boiler as filler in concrete. Construction and Building Materials *151*, 692–703.

Armaroli, N., and Balzani, V. (2007). The future of energy supply: challenges and opportunities. Angewandte Chemie International Edition *46*, 52–66.

ASTM (2007). Standard Test Methods for Moisture, Ash, and Organic Matter of Peat and Other Organic Soils. American Society for Testing Materials International, D2974-07a.

Bahrami, A., Simon, U., Soltani, N., Zavareh, S., Schmidt, J., Pech-Canul, M.I., and Gurlo, A. (2017). Eco-fabrication of hierarchical porous silica monoliths by ice-templating of rice husk ash. Green Chemistry *19*, 188–195.

Bang, B.M., Lee, J., Kim, H., Cho, J., and Park, S. (2012). High-Performance Macroporous Bulk

Silicon Anodes Synthesized by Template-Free Chemical Etching. Advanced Energy Materials *2*, 878–883.

Bao, Z., Weatherspoon, M.R., Shian, S., Cai, Y., Graham, P.D., Allan, S.M., Ahmad, G., Dickerson, M.B., Church, B.C., and Kang, Z. (2007). Chemical reduction of three-dimensional silica micro-assemblies into microporous silicon replicas. 10145-10149 *446*, 172.

Basika, E., Kigozi, J., and Kiggundu, N. (2015). Investigation of sugar cane bagasse ash as a binding material for the construction industry. Journal of Global Ecology and Environment *2*, 205–208.

Basu, P.K., Kumbhar, S., Sreejith, K., Yadav, T.S., Kottantharayil, A., Arora, B., Narasimhan, K., and Sharma, A.K. (2019). Active area cell efficiency (19%) monocrystalline silicon solar cell fabrication using low-cost processing with small footprint laboratory tools. Bulletin of Materials Science *42*, 33.

Batra, V.S., Urbonaite, S., and Svensson, G. (2008). Characterization of unburned carbon in bagasse fly ash. Fuel *87*, 2972–2976.

Benioub, R., Adnane, M., Boucetta, A., Chahtou, A., Kobatake, H., Furuya, Y., and Itaka, K. (2017). Optimization of the Raw Material Input Molar Ratio on the Carbothermal Production of Solar-Grade Silicon. Journal of New Technology and Materials *277*, 1–7.

Bernardini, S., Johnston, S., West, B., Naerland, T.U., Stuckelberger, M., Lai, B., and Bertoni, M.I. (2017). Nano-XRF analysis of metal impurities distribution at grain boundaries during mcsilicon solar cell processing. IEEE J. Photovoltaics *1*, 1–4.

Bernardis, S. (2012). Engineering Impurity Behavior on the Micron-Scale in MetallurgicalGrade Silicon Production. PhD. Massachusetts Institute of Technology.

Bezerra, T.L., and Ragauskas, A.J. (2016). A review of sugarcane bagasse for second-generation bioethanol and biopower production. Biofuels, Bioproducts and Biorefining *10*, 634–647. Bezerra, M.A., Santelli, R.E., Oliveira, E.P., Villar, L.S., and Escaleira, L.A. (2008). Response surface methodology (RSM) as a tool for optimization in analytical chemistry. Talanta *76*, 965– 977.

Bhagiyalakshmi, M., Yun, L.J., Anuradha, R., and Jang, H.T. (2010). Utilization of rice husk ash as silica source for the synthesis of mesoporous silicas and their application to CO2 adsorption through TREN/TEPA grafting. Journal of Hazardous Materials *175*, 928–938.

Bhat, S.V., Govindaraj, A., and Rao, C. (2011). Hybrid solar cell based on P3HT–ZnO nanoparticle blend in the inverted device configuration. Solar Energy Materials and Solar Cells *95*, 2318–2321.

Binod, P., Sindhu, R., Singhania, R.R., Vikram, S., Devi, L., Nagalakshmi, S., Kurien, N., Sukumaran, R.K., and Pandey, A. (2010). Bioethanol production from rice straw: an overview. Bioresource Technology *101*, 4767–4774.

Bizzo, W.A., Lenço, P.C., Carvalho, D.J., and Veiga, J.P.S. (2014). The generation of residual biomass during the production of bio-ethanol from sugarcane, its characterization and its use in energy production. Renewable and Sustainable Energy Reviews *29*, 589–603.

Bley, R.A., Kauzlarich, S.M., Davis, J.E., and Lee, H.W.H. (1996). Characterization of Silicon Nanoparticles Prepared from Porous Silicon. Chem. Mater. *8*, 1881–1888.

Borra, C.R., Blanpain, B., Pontikes, Y., Binnemans, K., and Van Gerven, T. (2016). Recovery of rare earths and other valuable metals from bauxite residue (red mud): a review. Journal of Sustainable Metallurgy *2*, 365–386.

Boulos, M.I., Fauchais, P., and Pfender, E. (2013). Thermal Plasmas: Fundamentals and Applications (Plenum Press).

Boza, A.F., Kupfer, V.L., Oliveira, A.R., Radovanovic, E., Rinaldi, A.W., Meneguin, J.G.,

Domingues, N.L., Moisés, M.P., and Favaro, S.L. (2016). Synthesis of α-aminophosphonates using a mesoporous silica catalyst produced from sugarcane bagasse ash. RSC Advances *6*, 23981–23986.

Braga, A.F.B., Moreira, S.P., Zampieri, P.R., Bacchin, J.M.G., and Mei, P.R. (2008). New processes for the production of solar-grade polycrystalline silicon: A review. Solar Energy Materials and Solar Cells *92*, 418–424.

Cantu, M.L., and Krebs, F.C. (2005). Polymer photovoltaics: From conjugated polymers to hybrid organic-inorganic solar cells. In Recent Research Developments in Applied Physics, Vol. 8, (Research Signpost), pp. 71–98.

Carley, K.M., Kamneva, N.Y., and Reminga, J. (2004). Response Surface Methodology: CASOS Technical Report (Carnegie Mellon University, School of Computer Science, Pittsburgh, PA, 15213).

Castaldelli, V., Akasaki, J., Melges, J., Tashima, M., Soriano, L., Borrachero, M., Monzó, J., and Payá, J. (2013). Use of slag/sugar cane bagasse ash (SCBA) blends in the production of alkaliactivated materials. Materials *6*, 3108–3127.

Channoy, C., Maneewan, S., Punlek, C., and Chirarattananon, S. (2018). Preparation and Characterization of Silica Gel from Bagasse Ash. Advanced Materials Research *1145*, 44–48.

Chen, T.A., and Rieke, R.D. (1992). The first regioregular head-to-tail poly (3-hexylthiophene-2, 5-diyl) and a regiorandom isopolymer: nickel versus palladium catalysis of 2 (5)-bromo-5 (2)(bromozincio)-3-hexylthiophene polymerization. Journal of the American Chemical Society *114*, 10087–10088.

Chen, D., Mei, X., Ji, G., Lu, M., Xie, J., Lu, J., and Lee, J.Y. (2012). Reversible Lithium-Ion Storage in Silver-Treated Nanoscale Hollow Porous Silicon Particles. Angewandte Chemie International Edition *51*, 2409–2413.

Chen, H., Wang, F., Zhang, C., Shi, Y., Jin, G., and Yuan, S. (2010). Preparation of nano-silica materials: The concept from wheat straw. Journal of Non-Crystalline Solids *356*, 2781–2785.

Chen, X., Jiang, J., Yan, F., Tian, S., and Li, K. (2014). A novel low temperature vapor phase hydrolysis method for the production of nano-structured silica materials using silicon tetrachloride. RSC Advances *4*, 8703–8710.

Chi, D., Qu, S., Wang, Z., and Wang, J. (2014). High efficiency P3HT: PCBM solar cells with an inserted PCBM layer. Journal of Materials Chemistry C *2*, 4383–4387.

Cho, S.K., Bard, A.J., and Fan, F.F. (2015). Production of thin film solar grade silicon on metals by electrodeposition from silicon dioxide in a molten salt (University of Texas).

Cho, S.Y., Kim, T.Y., and Sun, P.P. (2019). Recovery of silver from leachate of silicon solar cells by solvent extraction with TOPO. Separation and Purification Technology *215*, 516–520. Chusilp, N., Jaturapitakkul, C., and Kiattikomol, K. (2009). Utilization of bagasse ash as a pozzolanic material in concrete. Construction and Building Materials *23*, 3352–3358.

Coletti, G., Bronsveld, P.C.P., Hahn, G., Warta, W., Macdonald, D., Ceccaroli, B., Wambach, K., Le Quang, N., and Fernandez, J.M. (2011). Impact of Metal Contamination in Silicon Solar Cells. Advanced Functional Materials *21*, 879–890.

Cordeiro, G., Toledo Filho, R., and Fairbairn, E. (2009). Effect of calcination temperature on the pozzolanic activity of sugar cane bagasse ash. Construction and Building Materials *23*, 3301–3303.

Dang, M.T., Hirsch, L., and Wantz, G. (2011). P3HT: PCBM, best seller in polymer photovoltaic research. Advanced Materials *23*, 3597–3602.

Danso, H., Martinson, D.B., Ali, M., and Williams, J. (2015). Effect of fibre aspect ratio on mechanical properties of soil building blocks. Construction and Building Materials *83*, 314–319.

Das, G., Mandal, S., Mukhopadhyay, S., Banerjee, C., and Barua, A.K. (2017). Effect of oxide based graded buffer and bottom n-layer on the performance of the single junction amorphous silicon solar cells. Journal of Materials Science: Materials in Electronics *28*, 16165–16172. Das, P., Ganesh, A., and Wangikar, P. (2004). Influence of pretreatment for deashing of sugarcane bagasse on pyrolysis products. Biomass and Bioenergy *27*, 445–457.

Deng, X., and Schiff, E.A. (2011). Amorphous Silicon-Based Solar Cells. In Handbook of Photovoltaic Science and Engineering, (John Wiley & Sons), pp. 505–565.

Dennler, G., Lungenschmied, C., Neugebauer, H., Sariciftci, N., and Labouret, A. (2005). Flexible, conjugated polymer-fullerene-based bulk-heterojunction solar cells: Basics, encapsulation, and integration. Journal of Materials Research *20*, 3224–3233.

Dietmueller, R., Stegner, A.R., Lechner, R., Niesar, S., Pereira, R.N., Brandt, M.S., Ebbers, A., Trocha, M., Wiggers, H., and Stutzmann, M. (2009). Light-induced charge transfer in hybrid composites of organic semiconductors and silicon nanocrystals. Applied Physics Letters *94*, 83.

Ding, D., Rath, T., Lanzetta, L., Manuel Marin-Beloqui, J., and Haque, S.A. (2018). Efficient Hybrid Solar Cells Based on Solution Processed Mesoporous TiO2/Tin (II) Sulfide Heterojunctions. ACS Applied Energy Materials *1*, 3042–3047.

Dixit, A., Gupta, S., Dai Pang, S., and Kua, H.W. (2019). Waste Valorisation using biochar for cement replacement and internal curing in ultra-high performance concrete. Journal of Cleaner Production 117876.

Dowland, S.A., Reynolds, L.X., MacLachlan, A., Cappel, U.B., and Haque, S.A. (2013). Photoinduced electron and hole transfer in CdS: P3HT nanocomposite films: effect of nanomorphology on charge separation yield and solar cell performance. Journal of Materials Chemistry A *1*, 13896–13901.

Drosg, B., Fuchs, W., Al Seadi, T., Madsen, M., and Linke, B. (2015). Nutrient Recovery by Biogas Digestate Processing (Dublin: IEA Bioenergy Task 37 Report).

Du Preez, P. (1970). The Effect of Silica on Cane Growth. In South African Sugar Technologists' Association-June 1970, (South Africa Sugar Association Experiment Station),183–188.

Duhan, J.S., Kumar, R., Kumar, N., Kaur, P., Nehra, K., and Duhan, S. (2017). Nanotechnology: The new perspective in precision agriculture. Biotechnology Reports *15*, 11–23.

Easther, I.M., Chitopo, R., and Chigumira, M. (2019). The Green Economy Potential in Zimbabwe. The Sustainability Ethic in the Management of the Physical, Infrastructural and Natural Resources of Zimbabwe, 467.

Eisenhawer, B., Zhang, D., Clavel, R., Berger, A., Michler, J., and Christiansen, S. (2011). Growth of doped silicon nanowires by pulsed laser deposition and their analysis by electron beam induced current imaging. Nanotechnology *22*, 705–706.

Embong, R., Shafiq, N., Kusbiantoro, A., and Nuruddin, M.F. (2016). Effectiveness of lowconcentration acid and solar drying as pre-treatment features for producing pozzolanic sugarcane bagasse ash. Journal of Cleaner Production *112*, 953–962.

Embong, R., Shafiq, N., and Kusbiantoro, A. (2016). Silica Extraction and Incineration Process of Sugarcane Bagasse Ash (SCBA) as Pozzolanic Materials: A Review. ARPN Journal of Engineering and Applied Sciences *11*, 7304–7308.

Epstein, E. (1999). Silicon. Annual Review of Plant Physiology and Plant Molecular Biology *50*, 641–664.

Faisal, M., and Muhammad, K. (2016). Synthesis and characterization of geopolymer from bagasse bottom ash, waste of sugar industries and naturally available china clay. Journal of Cleaner Production *129*, 491–495.

Falk, G., Shinhe, G.P., Teixeira, L.B., Moraes, E.G., and de Oliveira, A.P.N. (2019). Synthesis of silica nanoparticles from sugarcane bagasse ash and nano-silicon via magnesiothermic reactions. Ceramics International *45*, 21618–21624.

Fang, Y., Ellis, A., Uchimiya, M., and Strathmann, T.J. (2019). Selective oxidation of colourinducing constituents in raw sugar cane juice with potassium permanganate. Food Chemistry, 125036.

Fardhyanti, D., Putri, R., Fianti, O., Simalango, A., and Akhir, A. (2018). Synthesis of Silica Powder from Sugar Cane Bagasse Ash and Its Application as Adsorbent in Adsorptivedistillation of Ethanol-water Solution. MATEC Web of Conferences *237*, 02002.

Faria, K., Gurgel, R., and Holanda, J. (2012). Recycling of sugarcane bagasse ash waste in the production of clay bricks. Journal of Environmental Management *101*, 7–12.

Farirai, F., Mupa M, Shonhiwa C, and Daramola O. M. (2019). Sol-gel Coupling Adsorption Method for Extraction of High Purity Silica from Sugarcane Bagasse Ash for Solar Cell Application. In Biomass Conversion Technologies for Energy Carriers, Chemicals and Materials, (Lisbon, Portugal), 1436–1438.

Favors, Z., Wang, W., Bay, H.H., Mutlu, Z., Ahmed, K., Liu, C., Ozkan, M., and Ozkan, C.S. (2014). Scalable synthesis of nano-silicon from beach sand for long cycle life Li-ion batteries. Scientific Reports *4*, 5623.

Feng, X., Yang, J., Bie, Y., Wang, J., Nuli, Y., and Lu, W. (2014). Nano/micro-structured Si/CNT/C composite from nano-SiO 2 for high power lithium ion batteries. Nanoscale *6*, 12532–12539.

Ferreira-Leitao, V., Gottschalk, L.M.F., Ferrara, M.A., Nepomuceno, A.L., Molinari, H.B.C., and Bon, E.P. (2010). Biomass residues in Brazil: availability and potential uses. Waste and Biomass Valorization *1*, 65–76.

Fox, R.L., Silva, J.A., Plucknett, D.L., and Teranishi, D.Y. (1969). Soluble and total silicon in sugar cane. Plant and Soil *30*, 81–92.

Frias, M., Villar-Cociña, E., and Valencia-Morales, E. (2007). Characterisation of sugar cane straw waste as pozzolanic material for construction: calcining temperature and kinetic parameters. Waste Management *27*, 533–538.

Frías, M., Villar, E., and Savastano, H. (2011). Brazilian sugar cane bagasse ashes from the cogeneration industry as active pozzolans for cement manufacture. Cement and Concrete Composites *33*, 490–496.

Gadioli, M.C.B., Vieira, C.M.F., Rodríguez, R.J.S., Conte, R.A., Pinatti, D.G., and Monteiro, S.N. (2008). Characterization of granulometric fractions of ash from boiler burnt sugarcane bagasse. (Trans Tech Publ), pp. 471–476.

Ganesan, K., Rajagopal, K., and Thangavel, K. (2007). Evaluation of bagasse ash as supplementary cementitious material. Cement and Concrete Composites *29*, 515–524.

Gangopadhyay, U., Jana, S., and Das, S. (2013). State of Art of Solar Photovoltaic Technology. Journal of Energy *764132*, 1–9.

Georgieva, T.I., Mikkelsen, M.J., and Ahring, B.K. (2008). Ethanol production from wetexploded wheat straw hydrolysate by thermophilic anaerobic bacterium Thermoanaerobacter BG1L1 in a continuous immobilized reactor. Applied Biochemistry and Biotechnology *145*, 99– 110.

Gledhill, S.E., Scott, B., and Gregg, B.A. (2005). Organic and nano-structured composite photovoltaics: An overview. Journal of Materials Research *20*, 3167–3179.

Goher, M.E., Hassan, A.M., Abdel-Moniem, I.A., Fahmy, A.H., Abdo, M.H., and El-sayed, S.M. (2015). Removal of aluminum, iron and manganese ions from industrial wastes using granular activated carbon and Amberlite IR-120H. The Egyptian Journal of Aquatic Research *41*, 155– 164.

Gollu, S.R., Sharma, R., Srinivas, G., Kundu, S., and Gupta, D. (2015). Incorporation of SiO_2 dielectric nanoparticles for performance enhancement in P3HT: PCBM inverted organic solar cells. Organic Electronics *24*, 43–50.

Goyal, A., and Soni, P. (2017). Doping of nano-crystalline silicon powders by mechanical alloying: the process and characterization. Journal of Materials Science: Materials in Electronics *28*, 14720–14727.

Grau, F., Choo, H., Hu, J., and Jung, J. (2015). Engineering behavior and characteristics of wood ash and sugarcane bagasse ash. Materials *8*, 6962–6977.

Gribov, B.G., and Zinov'ev, K.V. (2003). Preparation of High-Purity Silicon for Solar Cells. Inorganic Materials *39*, 653–662.

Groen, J.C., Peffer, L.A., and Pérez-Ramírez, J. (2003). Pore size determination in modified micro- and mesoporous materials. Pitfalls and limitations in gas adsorption data analysis. Microporous and Mesoporous Materials *60*, 1–17.

Gu, K.L., Zhou, Y., Morrison, W.A., Park, K., Park, S., and Bao, Z. (2018). Nanoscale domain imaging of all-polymer organic solar cells by photo-induced force microscopy. ACS Nano *12*, 1473–1481.

Guimarães, J.L., Frollini, E., da Silva, C.G., Wypych, F., and Satyanarayana, K.G. (2009). Characterization of banana, sugarcane bagasse and sponge gourd fibers of Brazil. Industrial Crops and Products *30*, 407–415.

Günes, S., Neugebauer, H., and Sariciftci, N.S. (2007). Conjugated polymer-based organic solar cells. Chemical Reviews *107*, 1324–1338.

Guo, M., Zou, X., Ren, H., Muhammad, F., Huang, C., Qiu, S., and Zhu, G. (2011). Fabrication of high surface area mesoporous silicon via magnesiothermic reduction for drug delivery. Microporous and Mesoporous Materials *142*, 194–201.

Gupta, K., and Gupta, N. (2016). Semiconductor Materials: Their Properties, Applications, and Recent Advances. In Advanced Semiconducting Materials and Devices, (Springer), 3–40.

Gur, I., Fromer, N.A., and Alivisatos, A.P. (2006). Controlled Assembly of Hybrid Bulk−Heterojunction Solar Cells by Sequential Deposition. The Journal of Physical Chemistry B *110*, 25543–25546.

Hames, Y., Alpaslan, Z., Kösemen, A., San, S.E., and Yerli, Y. (2010). Electrochemically grown ZnO nanorods for hybrid solar cell applications. Solar Energy *84*, 426–431.

Hariharan, V., Shanmugam, M., Amutha, K., and Sivakumar, G. (2014). Preparation and Characterization of Ceramic Products Using Sugarcane Bagasse Ash Waste. Research Journal of Recent Sciences *2277*, 2502.

Hassan, A., Abdelghny, A., Elhadidy, H., and Youssef, A. (2014). Synthesis and characterization of high surface area nanosilica from rice husk ash by surfactant-free sol–gel method. Journal of Sol-Gel Science and Technology *69*, 465–472.

Haynes, R.J. (2019). What effect does liming have on silicon availability in agricultural soils? Geoderma *337*, 375–383.

He, J., Hossain, M.A., Lin, H., Wang, W., Karuturi, S.K., Hoex, B., Ye, J., Gao, P., Bullock, J., and Wan, Y. (2019). 15% Efficiency Ultrathin Silicon Solar Cells with Fluorine-Doped Titanium Oxide and Chemically Tailored Poly (3, 4-ethylenedioxythiophene): Poly (styrenesulfonate) as Asymmetric Heterocontact. ACS Nano *3*, 6356–6362.

Heintz, A.S., Fink, M.J., and Mitchell, B.S. (2007). Mechanochemical synthesis of blue luminescent alkyl/alkenyl-passivated silicon nanoparticles. Advanced Materials *19*, 3984–3988.

Hemaprabha, E., Pandey, U.K., Chattopadhyay, K., and Ramamurthy, P.C. (2018). Doped silicon nanoparticles for enhanced charge transportation in organic-inorganic hybrid solar cells. Solar Energy *173*, 744–751.

Hermann, K. (2004). The Impact of Nanotechnology on Energy. Nanotech. L. & Bus. *1*, 242.

Hernández, J.M., Middendorf, B., Gehrke, M., and Budelmann, H. (1998). Use of wastes of the sugar industry as pozzolana in lime-pozzolana binders: study of the reaction. Cement and Concrete Research *28*, 1525–1536.

Holzapfel, M., Buqa, H., Hardwick, L.J., Hahn, M., Würsig, A., Scheifele, W., Novák, P., Kötz, R., Veit, C., and Petrat, F.-M. (2006). Nano silicon for lithium-ion batteries. Electrochimica Acta *52*, 973–978.

Huabcharoen, P., Wimolmala, E., Markpin, T., and Sombatsompop, N. (2017). Purification and characterization of silica from sugarcane bagasse ash as a reinforcing filler in natural rubber composites. BioResources *12*, 1228–1245.

Huan, C., and Shu-Qing, S. (2014). Silicon nanoparticles: Preparation, properties, and applications. Chinese Physics B *23*, 088102.

Huang, C., Edesess, M., Bensoussan, A., and Tsui, K. (2016). Performance analysis of a gridconnected upgraded metallurgical grade silicon photovoltaic system. Energies *9*, 342.

Huang, L., Lai, H., Lu, C., Fang, M., Ma, W., Xing, P., Li, J., and Luo, X. (2016). Enhancement in extraction of boron and phosphorus from metallurgical grade silicon by copper alloying and aqua regia leaching. Hydrometallurgy *161*, 14–21.

Huisken, F., Hofmeister, H., Kohn, B., Laguna, M., and Paillard, V. (2000). Laser production and deposition of light-emitting silicon nanoparticles. Applied Surface Science *154*, 305–313.

Hummelen, J.C., Knight, B.W., LePeq, F., Wudl, F., Yao, J., and Wilkins, C.L. (1995). Preparation and characterization of fulleroid and methanofullerene derivatives. The Journal of Organic Chemistry *60*, 532–538.

Imran, M., and Khan, A.A. (2018). Characterization of Agricultural Waste Sugarcane Bagasse Ash at 1100° C with various hours. Materials Today: Proceedings *5*, 3346–3352.

IEA (2017). Access to Electricity. In Energy Access Outlook 2017: From Poverty to Prosperity, Special Report, (France: International Energy Agency), 39−53.

Islam, M.S., Rhamdhani, M.A., and Brooks, G.A. (2011). Solar-grade silicon: current and alternative production routes. Chemeca 2011: Engineering a Better World: Sydney Hilton Hotel, NSW, Australia, 18-21 September 2011, 1826.

Itaka, K., Ogasawara, T., Boucetta, A., Benioub, R., Sumiya, M., Hashimoto, T., Koinuma, H., and Furuya, Y. (2015). Direct Carbothermic Silica Reduction from Purified Silica to Solar-Grade Silicon. (IOP Publishing), 012-015.

Izdebska, J., and Thomas, S. (2015). Printing on Polymers: Fundamentals and Applications (William Andrew Publishing).

Jagadesh, P., Ramachandramurthy, A., Murugesan, R., and Sarayu, K. (2015). Micro-Analytical studies on sugar cane bagasse ash. Sadhana *40*, 1629–1638.

James, J., and Pandian, P.K. (2017). A Short Review on the Valorisation of Sugarcane Bagasse Ash in the Manufacture of Stabilized/Sintered Earth Blocks and Tiles. Advances in Materials Science and Engineering *2017*, 15.

Jia, G., Plentz, J., Gawlik, A., Azar, A., Stokkan, G., Syvertsen, M., Carvalho, P., Dellith, J., Dellith, A., Andrä, G., et al. (2018). Silicon Powder-Based Wafers for Low-Cost Photovoltaics: Laser Treatments and Nanowire Etching. International Journal of Photoenergy *2018*, 7. Jose, S.K., Soman, M., and Evangeline, S. (2019). Foamed concrete using waste materials: A review. (CRC Press), 153.

Joshaghani, A., and Moeini, M.A. (2017). Evaluating the effects of sugar cane bagasse ash (SCBA) and nanosilica on the mechanical and durability properties of mortar. Construction and Building Materials *152*, 818–831.

Joshaghani, A., Ramezanianpour, A.A., and Rostami, H. (2016). Effect of incorporating Sugarcane Bagasse Ash (SCBA) in mortar to examine durability of sulfate attack. 13–15.

Jovanov, V., Yumnam, N., Müller, A., Gruber, M., and Wagner, V. (2017). Determining

Material-Specific Morphology of Bulk-Heterojunction Organic Solar Cells Using AFM Phase Imaging. The Journal of Physical Chemistry C *121*, 9173–9180.

Kale, P.G., and Solanki, C.S. (2010). Synthesis of Si nanoparticles from freestanding porous silicon (PS) film using ultrasonication. (Institute of Electrical and Electronics Engineers), 003692–003697.

Kamath, S.R., and Proctor, A. (1998). Silica gel from rice hull ash: preparation and characterization. Cereal Chemistry *75*, 484–487.

Kang, H., Kim, W., and Lavoie, A. (2017). Methods for Depositing Silicon Oxide. Lam Research Corporation, Fremont, CA (US)

Katare, V., and Madurwar, M. (2017). Experimental characterization of sugarcane biomass ash – A review. Construction and Building Materials *152*.

Kauldhar, B.S., and Yadav, S.K. (2018). Turning waste to wealth: A direct process for recovery of nano-silica and lignin from paddy straw agro-waste. Journal of Cleaner Production *194*, 158– 166.

Kawade, U., Rathi, V., and Girge, V. (2013). Effect of use of Bagasse Ash on Strength of Concrete. International Journal of Innovative Research in Science, Engineering and Technology *2*, 2997–3000.

Kaygusuz, K. (2012). Energy for sustainable development: A case of developing countries. Renewable and Sustainable Energy Reviews *16*, 1116–1126.

Kazmi, S.M., Abbas, S., Saleem, M.A., Munir, M.J., and Khitab, A. (2016). Manufacturing of sustainable clay bricks: Utilization of waste sugarcane bagasse and rice husk ashes. Construction and Building Materials *120*, 29–41.

Kharissova, O.V., Dias, H.R., Kharisov, B.I., Pérez, B.O., and Pérez, V.M.J. (2013). The greener synthesis of nanoparticles. Trends in Biotechnology *31*, 240–248.

Khlyabich, P.P., Burkhart, B., and Thompson, B.C. (2011). Efficient ternary blend bulk heterojunction solar cells with tunable open-circuit voltage. Journal of the American Chemical Society *133*, 14534–14537.

Kiel, J.W., Eberle, A.P., and Mackay, M.E. (2010). Nanoparticle agglomeration in polymerbased solar cells. Physical Review Letters *105*, 168701.

Kim, H., Han, B., Choo, J., and Cho, J. (2008). Three-dimensional porous silicon particles for use in high-performance lithium secondary batteries. Angewandte Chemie International Edition *47*, 10151–10154.

Kim, K., Liu, J., Namboothiry, M.A., and Carroll, D.L. (2007). Roles of donor and acceptor nanodomains in 6% efficient thermally annealed polymer photovoltaics. Applied Physics Letters *90*, 163511.

Kim, K.H., Lee, D.J., Cho, K.M., Kim, S.J., Park, J.-K., and Jung, H.-T. (2015). Complete magnesiothermic reduction reaction of vertically aligned mesoporous silica channels to form pure silicon nanoparticles. Scientific Reports *5*, 9014.

Klafehn, G.W. (2016). Silicon nanoparticle optimization and integration into amorphous silicon via PECVD for use in photovoltaics. Thesis. Colorado School of Mines.

Ko, D.-H., Tumbleston, J.R., Gadisa, A., Aryal, M., Liu, Y., Lopez, R., and Samulski, E.T. (2011). Light-trapping nano-structures in organic photovoltaic cells. Journal of Materials Chemistry *21*, 16293–16303.

Kuang, D., Klein, C., Ito, S., Moser, J., Humphry-Baker, R., Evans, N., Duriaux, F., Graetzel, C., Zakeeruddin, S.M., and Grätzel, M. (2007a). High-efficiency and stable mesoscopic dyesensitized solar cells based on a high molar extinction coefficient ruthenium sensitizer and nonvolatile electrolyte. Advanced Materials *19*, 1133–1137.

Kuang, D., Klein, C., Ito, S., Moser, J., Humphry-Baker, R., Evans, N., Duriaux, F., Graetzel, C., Zakeeruddin, S.M., and Grätzel, M. (2007b). High-efficiency and stable mesoscopic dyesensitized solar cells based on a high molar extinction coefficient ruthenium sensitizer and nonvolatile electrolyte. Advanced Materials *19*, 1133–1137.

Kudo, N., Shimazaki, Y., Ohkita, H., Ohoka, M., and Ito, S. (2007). Organic–inorganic hybrid solar cells based on conducting polymer and SnO2 nanoparticles chemically modified with a fullerene derivative. Solar Energy Materials and Solar Cells *91*, 1243–1247.

Kumar, T.S., Balaji, K., and Rajasekhar, K. (2016). Assessment of Sorptivity and Water Absorption of Concrete with Partial Replacement of Cement by Sugarcane Bagasse Ash (SCBA) and Silica Fume. International Journal of Applied Engineering Research *11*, 5747–5752. Kuo, C., Tang, W., Gau, C., Guo, T.-F., and Jeng, D. (2008). Ordered bulk heterojunction solar cells with vertically aligned TiO_2 nanorods embedded in a conjugated polymer. Applied Physics Letters *93*, 263.

Le Blond, J.S., Horwell, C.J., Williamson, B.J., and Oppenheimer, C. (2010). Generation of crystalline silica from sugarcane burning. Journal of Environmental Monitoring *12*, 1459–1470.

Lee, J.H., Kwon, J.H., Lee, J.-W., Lee, H., Chang, J.H., and Sang, B.-I. (2017). Preparation of high purity silica originated from rice husks by chemically removing metallic impurities. Journal of Industrial and Engineering Chemistry *50*, 79–85.

Lee, W., Shin, S., Han, S.-H., and Cho, B.W. (2008). Manipulating interfaces in a hybrid solar cell by in situ photosensitizer polymerization and sequential hydrophilicity/hydrophobicity control for enhanced conversion efficiency. Applied Physics Letters *92*, 173.

Lei, Y., Ma, W., Lv, G., Wei, K., Li, S., and Morita, K. (2017). Purification of metallurgicalgrade silicon using zirconium as an impurity getter. Separation and Purification Technology *173*, 364–371.

Lei, Y., Ma, W., Ma, X., Wu, J., Wei, K., Li, S., and Morita, K. (2017c). Leaching behaviors of impurities in metallurgical-grade silicon with hafnium addition. Hydrometallurgy *169*, 433–439.

Leite-Rossi, L., Saulino, H., Shimabukuro, E., Cunha-Santino, M., and Trivinho-Strixino, S. (2019). Shredder chironomid diets are influenced by decomposition rates of different leaf litter species. Neotropical Entomology *48*, 38–49.

Li, B., Yu, D., and Zhang, S.-L. (1999). Raman spectral study of silicon nanowires. Physical Review B *59*, 1645.

Li, G., Shrotriya, V., Yao, Y., and Yang, Y. (2005). Investigation of annealing effects and film thickness dependence of polymer solar cells based on poly (3-hexylthiophene). Journal of Applied Physics *98*, 043704.

Li, G., Shrotriya, V., Huang, J., Yao, Y., Moriarty, T., Emery, K., and Yang, Y. (2011). Highefficiency solution processable polymer photovoltaic cells by self-organization of polymer blends. In Materials for Sustainable Energy: A Collection of Peer-Reviewed Research and Review Articles from Nature Publishing Group, (World Scientific), 80–84.

Li, J., Ban, B., Li, Y., Bai, X., Zhang, T., and Chen, J. (2017). Removal of impurities from metallurgical grade silicon during Ga-Si solvent refining. Silicon *9*, 77–83.

Li, M., Dai, Y., Ma, W., Yang, B., and Chu, Q. (2017). Review of new technology for preparing crystalline Silicon solar cell materials by metallurgical method. 012016.

Liang, J., Li, X., Zhu, Y., Guo, C., and Qian, Y. (2015). Hydrothermal synthesis of nano-silicon from a silica sol and its use in lithium ion batteries. Nano Research *8*, 1497–1504.

Lim, E.L., Yap, C.C., Teridi, M.A.M., Teh, C.H., bin Mohd Yusoff, A.R., and Jumali, M.H.H. (2016). A review of recent plasmonic nanoparticles incorporated P3HT: PCBM organic thin film solar cells. Organic Electronics *36*, 12–28.

Liu, C., Holman, Z.C., and Kortshagen, U.R. (2010). Optimization of Si NC/P3HT hybrid solar cells. Advanced Functional Materials *20*, 2157–2164.

Liu, C.-Y., Holman, Z.C., and Kortshagen, U.R. (2008). Hybrid solar cells from P3HT and silicon nanocrystals. Nano Letters *9*, 449–452.

Liu, J., Chen, S., Qian, D., Gautam, B., Yang, G., Zhao, J., Bergqvist, J., Zhang, F., Ma, W., and Ade, H. (2016). Fast charge separation in a non-fullerene organic solar cell with a small driving force. Nature Energy *1*, 16089.

Liu, K., Qu, S., Zhang, X., Tan, F., and Wang, Z. (2013). Improved photovoltaic performance of silicon nanowire/organic hybrid solar cells by incorporating silver nanoparticles. Nanoscale Research Letters *8*, 88.

Liu, N., Huo, K., McDowell, M.T., Zhao, J., and Cui, Y. (2013). Rice husks as a sustainable source of nanostructured silicon for high performance Li-ion battery anodes. Scientific Reports *3*, 1919.

Liu, X., Gao, Y., Jin, R., Luo, H., Peng, P., and Liu, Y. (2014). Scalable synthesis of Si nanostructures by low-temperature magnesiothermic reduction of silica for application in lithium ion batteries. Nano Energy *4*, 31–38.

Liu, Y., Guo, Y., Gao, W., Wang, Z., Ma, Y., and Wang, Z. (2012). Simultaneous preparation of silica and activated carbon from rice husk ash. Journal of Cleaner Production *32*, 204–209.

Liu, Z., Chang, X., Wang, T., Li, W., Ju, H., Zheng, X., Wu, X., Wang, C., Zheng, J., and Li, X. (2017). Silica-derived hydrophobic colloidal nano-Si for lithium-ion batteries. ACS Nano *11*, 6065–6073.

Loh, Y., Sujan, D., Rahman, M.E., and Das, C.A. (2013). Sugarcane bagasse-The future composite material: A literature review. Resources, Conservation and Recycling *75*, 14–22. Lu, H., Wei, K., Ma, W., Xie, K., Wu, J., Lei, Y., and Dai, Y. (2017). Effect of acetic acid on the leaching behavior of impurities in metallurgical grade silicon. Separation Science and Technology *52*, 1257–1264.

Lopez-Delgado, R., Higuera, H., Zazueta-Raynaud, A., Ramos-Carrazco, A., Ceja, J.E., Berman-Mendoza, D., Álvarez, E., and Ayon, A. (2016). Enhancing the Power Conversion Efficiency of Solar Cells Employing down-Shifting Silicon Quantum Dots. Journal of Physics: Conference Series *773*, 012087.

Lund, C., Zhang, W., Jennings, P., and Singh, P. (2000). New Methods for Producing Low Cost Silicon for Solar Cells. In Solar 2000: Renewable Energy Transforming Business, 38th Annual Conference of the Australian and New Zealand Solar Energy Society, 421-429

Luo, D. (2017). Study on the Preparation of Solar Grade Silicon by Metallurgical Method. In New Research on Silicon-Structure, Properties, Technology, (IntechOpen)

Luo, W., Wang, X., Meyers, C., Wannenmacher, N., Sirisaksoontorn, W., Lerner, M.M., and Ji, X. (2013). Efficient fabrication of nanoporous Si and Si/Ge enabled by a heat scavenger in magnesiothermic reactions. Scientific Reports *3*, 2222.

Machado, G., Santos, F., Faria, D., de Queiroz, T.N., Zinani, F., de Queiroz, J.H., and Gomes, F. (2018). Characterization and Potential Evaluation of Residues from the Sugarcane Industry of Rio Grande do Sul in Biorefinery Processes. Natural Resources *9*, 175.

MacLachlan, A.J., Rath, T., Cappel, U.B., Dowland, S.A., Amenitsch, H., Knall, A., Buchmaier, C., Trimmel, G., Nelson, J., and Haque, S.A. (2015). Polymer/nanocrystal hybrid solar cells: influence of molecular precursor design on film nanomorphology, charge generation and device performance. Advanced Functional Materials *25*, 409–420.

Makhanda, G., Pwaka, O., and Mafini, C. (2019). Liquid Petroleum Gas Supply Chain Challenges in Rural Medical Facilities in Zimbabwe. (Springer), 288–301.

Makonese, T. (2016). Renewable energy in Zimbabwe. (Institute of Electrical and Electronics Engineers), 1–9.

Makonese, T., Ifegbesan, A.P., and Rampedi, I.T. (2018). Household cooking fuel use patterns and determinants across southern Africa: Evidence from the demographic and health survey data. Energy & Environment *29*, 29–48.

Marchal, J.C., Krug III, D.J., McDonnell, P., Sun, K., and Laine, R.M. (2015). A low cost, low energy route to solar grade silicon from rice hull ash (RHA), a sustainable source. Green Chemistry *17*, 3931–3940.

Martines-Filho, J., Burnquist, H.L., and Vian, C.E. (2006). Bioenergy and the rise of sugarcanebased ethanol in Brazil. Choices *21*, 91–96.

Matichenkov, V., and Calvert, D. (2002). Silicon as a beneficial element for sugarcane. Journal American Society of Sugarcane Technologists *22*, 21–30.

Medina, C., Banfill, P.F.G., de Rojas, M.S., and Frías, M. (2013). Rheological and calorimetric behaviour of cements blended with containing ceramic sanitary ware and construction/demolition waste. Construction and Building Materials *40*, 822–831.

Modani, P.O., and Vyawahare, M.R. (2013). Utilization of Bagasse Ash as a Partial Replacement of Fine Aggregate in Concrete. Procedia Engineering *51*, 25–29.

Mohanraj, K., Kannan, S., Barathan, S., and Sivakumar, G. (2012). Preparation and Characterization of Nano SiO2 from Corn Cob Ash by Precipitation Method. Material Science 186–252.

Mohomane, S.M., Motaung, T.E., and Revaprasadu, N. (2017). Thermal degradation kinetics of sugarcane bagasse and soft wood cellulose. Materials *10*, 1246.

Mokkapati, S., Beck, F., De Waele, R., Polman, A., and Catchpole, K. (2011). Resonant nanoantennas for light trapping in plasmonic solar cells. Journal of Physics D: Applied Physics *44*, 185101.

Mongstad, T., Klette, H., Nordseth, Ø., Preston, T.J., Wyller, G.M., and Filtvedt, W.O. (2016). New technologies for silicon production from monosilane; Pilot testing and on-line process monitoring aiding the development. Silicon Chem. Sol. Ind. XIII 1–10.

Mor, S., Manchanda, C.K., Kansal, S.K., and Ravindra, K. (2017). Nanosilica Extraction from Processed Agricultural Residue Using Green Technology. Journal of Cleaner Production *143*, 1284–1290.

Moraes, J., Tashima, M., Akasaki, J.L., Melges, J., Monzó, J., Borrachero, M., Soriano, L., and Payá, J. (2016). Increasing the sustainability of alkali-activated binders: the use of sugar cane straw ash (SCSA). Construction and Building Materials *124*, 148–154.

Moretti, J.P., Nunes, S., and Sales, A. (2018). Self-compacting concrete incorporating sugarcane bagasse ash. Construction and Building Materials *172*, 635–649.

Morgenstern, F.S., Böhm, M.L., Kist, R.J., Sadhanala, A., Gélinas, S., Rao, A., and Greenham, N.C. (2016). Charge generation and electron-trapping dynamics in hybrid nanocrystal-polymer solar cells. The Journal of Physical Chemistry C *120*, 19064–19069.

Mudima, K. (2002). Socio-economic impact of smallholder irrigation development in Zimbabwe: A case study of five successful irrigation schemes. (International Water Management Institute), 21–30.

Muhumuza, R., Zacharopoulos, A., Mondol, J.D., Smyth, M., and Pugsley, A. (2018). Energy consumption levels and technical approaches for supporting development of alternative energy technologies for rural sectors of developing countries. Renewable and Sustainable Energy Reviews *97*, 90–102.

Musariri, B. (2015). Estimating Potential Output Per Capita for Zimbabwe. Masters. University of Namibia.

Mutolo, K.L., Mayo, E.I., Rand, B.P., Forrest, S.R., and Thompson, M.E. (2006). Enhanced open-circuit voltage in subphthalocyanine/C60 organic photovoltaic cells. Journal of the American Chemical Society *128*, 8108–8109.

Muzari, W., Nyamushamba, G., and Soropa, G. (2016). Climate Change Adaptation in Zimbabwe‟ s Agricultural Sector. International Journal of Science and Research *5*, 1762–1768.

Nayfeh, A.H., Younis, M.I., and Abdel-Rahman, E.M. (2007). Dynamic pull-in phenomenon in MEMS resonators. Nonlinear Dynamics *48*, 153–163.

Muzenda, E., Ntuli, F., and Pilusa, T.J. (2012). Waste management, strategies and situation in South Africa: an overview. International Journal of Environmental and Ecological Engineering *6*, 552–555.

Nazriati, N., Setyawan, H., Affandi, S., Yuwana, M., and Winardi, S. (2014). Using bagasse ash as a silica source when preparing silica aerogels via ambient pressure drying. Journal of Non-Crystalline Solids *400*, 6–11.

Nhiwatiwa, T., Dalu, T., and Brendonck, L. (2017). Impact of irrigation based sugarcane cultivation on the Chiredzi and Runde Rivers quality, Zimbabwe. Science of the Total Environment *587*, 316–325.

Nielsen, H., Baxter, L., Sclippab, G., Morey, C., Frandsen, F., and Dam-Johansen, K. (2000). Deposition of Potassium Salts on Heat Transfer Surfaces in Straw-Fired Boilers: A Pilot-Scale Study. Fuel *79*, 131–139.

Nielsen, H.P., Frandsen, F., Dam-Johansen, K., and Baxter, L. (2000). The Implications of Chlorine-Associated Corrosion on the Operation of Biomass-Fired Boilers. Progress in Energy and Combustion Science *26*, 283–298.

Nordtröm, E. (2012). Design and Development Process of Solar Panels. Thesis. KTH Royal Institute of Technology.

Norsuraya, S., Fazlena, H., and Norhasyimi, R. (2016). Sugarcane bagasse as a renewable source of silica to synthesize Santa Barbara Amorphous-15 (SBA-15). Procedia Engineering *148*, 839–846.

National Renewable Energy Laboratory (2020). Thin Film Photovoltaic Partnership Project | Photovoltaic Research | NREL.

Onojah, A., Amah, A., and Ayomanor, B. (2012). Comparative studies of silicon from rice husk ash and natural quartz. American Journal of Scientific and Industrial Research *3*, 146–149.

Orgil, K. (2018). Comparison of Organic and Inorganic Solar Photovoltaic Systems. Thesis. California Polytechnic State University.

Ostraat, M.L., De Blauwe, J.W., Green, M.L., Bell, L.D., Atwater, H.A., and Flagan, R.C. (2001). Ultraclean two-stage aerosol reactor for production of oxide-passivated silicon nanoparticles for novel memory devices. Journal of The Electrochemical Society *148*, G265– G270.

Otieno, F.O. (2015). Enhancement of photo-conversion efficiency of organic solar cells by plasmon resonance effect. Masters. University of the Witwatersrand.

Otieno, F., Airo, M., Ranganathan, K., and Wamwangi, D. (2016). Annealed silver-islands for enhanced optical absorption in organic solar cell. Thin Solid Films *598*, 177–183.

Otoko, G.R., and Precious, K. (2014). Stabilization of Nigerian Deltaic Clay (Chikoko) With Groundnut Shell Ash. International Journal of Engineering and Technology Research *2*, 1–11.

Otuoze, H., Amartey, Y., Sada, B., Ahmed, H., Sanni, M., and Suleiman, M. (2012). Characterization of Sugar Cane Bagasse Ash and Ordinary Portland Cement Blends in Concrete. In 4th West Africa Built Environment Research (WABER) Conference, (Nigeria: West Africa Built Environment Research (WABER) Conference), 1231–1237.

Oudenhoven, S., Westerhof, R.J.M., and Kersten, S.R. (2015). Fast pyrolysis of organic acid leached wood, straw, hay and bagasse: Improved oil and sugar yields. Journal of Analytical and Applied Pyrolysis *116*, 253–262.

Oudenhoven, S., Lievens, C., Westerhof, R.J.M., and Kersten, S.R. (2016). Effect of temperature on the fast pyrolysis of organic-acid leached pinewood; the potential of low temperature pyrolysis. Biomass and Bioenergy *89*, 78–90.

Oudenhoven, S., van der Ham, A.G., van den Berg, H., Westerhof, R.J.M., and Kersten, S.R. (2016). Using pyrolytic acid leaching as a pretreatment step in a biomass fast pyrolysis plant: Process design and economic evaluation. Biomass and Bioenergy *95*, 388–404.

Owusu, P., and Asumadu-Sarkodie, S. (2016). A Review of Renewable Energy Sources, Sustainability Issues and Climate Change Mitigation. Cogent Engineering *3*, 1167990.

Pa, F.C., Chik, A., and Bari, M.F. (2016). Palm Ash as an Alternative Source for Silica Production. MATEC Web of Conferences *78*, 01062.

Paci, B., Spyropoulos, G.D., Generosi, A., Bailo, D., Albertini, V.R., Stratakis, E., and Kymakis, E. (2011). Enhanced structural stability and performance durability of bulk heterojunction

photovoltaic devices incorporating metallic nanoparticles. Advanced Functional Materials *21*, 3573–3582.

Pal, U.B., Basu, S.N., Jiang, Y., and Xu, J. (2015). Method and apparatus for producing solar grade silicon using a som electrolysis process (Boston, United States Patents Office).

Pandey, A., Soccol, C.R., Nigam, P., and Soccol, V.T. (2000). Biotechnological potential of agro-industrial residues. I: sugarcane bagasse. Bioresource Technology *74*, 69–80.

Park, S.H., Wang, Y., Zhang, J., Wang, A., and Ingle, N.K. (2018). Differential silicon oxide etch.

Patcharin, W., Sriamporn, K., and Kanokkan, A. (2012). Utilization biomass from bagasse ash for phillipsite zeolite synthesis. (Trans Tech Publ), 4038–4042.

Patel, K.G., Shettigar, R.R., and Misra, N.M. (2017). Recent Advance in Silica Production Technologies from Agricultural Waste Stream. Journal of Advanced Agricultural Technologies Vol *4*, 274-279

Payá, J., Monzó, J., Borrachero, M.V., Díaz-Pinzón, L., and Ordonez, L.M. (2002). Sugar-cane bagasse ash (SCBA): studies on its properties for reusing in concrete production. Journal of Chemical Technology & Biotechnology: International Research in Process, Environmental & Clean Technology *77*, 321–325.

Peng, K.-Q., Wang, X., Li, L., Wu, X.-L., and Lee, S.-T. (2010). High-performance silicon nanohole solar cells. Journal of the American Chemical Society *132*, 6872–6873.

Persson, H., Kantarelis, E., Evangelopoulos, P., and Yang, W. (2017). Wood-derived acid leaching of biomass for enhanced production of sugars and sugar derivatives during pyrolysis: Influence of acidity and treatment time. Journal of Analytical and Applied Pyrolysis *127*, 329– 334.

Pfadler, T., Coric, M., Palumbiny, C.M., Jakowetz, A.C., Strunk, K.-P., Dorman, J.A., Ehrenreich, P., Wang, C., Hexemer, A., and Png, R.-Q. (2014). Influence of interfacial area on exciton separation and polaron recombination in nanostructured bilayer all-polymer solar cells. ACS Nano *8*, 12397–12409.

Pizzini, S., Acciarri, M., and Binetti, S. (2005). From electronic grade to solar grade silicon: chances and challenges in photovoltaics. Physica Status Solidi (A) *202*, 2928–2942.

Pode, R. (2016). Potential applications of rice husk ash waste from rice husk biomass power plant. Renewable and Sustainable Energy Reviews *53*, 1468–1485.

Powell, D.M., Winkler, M.T., Choi, H., Simmons, C.B., Needleman, D.B., and Buonassisi, T. (2012). Crystalline silicon photovoltaics: a cost analysis framework for determining technology pathways to reach baseload electricity costs. Energy & Environmental Science *5*, 5874–5883.

Praneetha, S., and Murugan, A.V. (2015). Development of sustainable rapid microwave assisted process for extracting nanoporous Si from earth abundant agricultural residues and their carbonbased nanohybrids for lithium energy storage. ACS Sustainable Chemistry & Engineering *3*, 224–236.

Prasad, K.S., Gandhi, P., and Selvaraj, K. (2014). Synthesis of green nano iron particles (GnIP) and their application in adsorptive removal of As (III) and As (V) from aqueous solution. Applied Surface Science *317*, 1052–1059.

Purnomo, C.W., Salim, C., and Hinode, H. (2012). Synthesis of pure Na–X and Na–A zeolite from bagasse fly ash. Microporous and Mesoporous Materials *162*, 6–13.

Quirino, W. (2005). Calorific power of wood and ligno-cellulosic materials. Revista Da Madeira *15*, 100–106.

Rafiee, E., Shahebrahimi, S., Feyzi, M., and Shaterzadeh, M. (2012). Optimization of synthesis and characterization of nanosilica produced from rice husk (a common waste material). International Nano Letters *2*, 29.

Rahman, N.A., Widiyastuti, W., Sigit, D., Ajiza, M., and Sujana, W. (2018). The Effect of Various Acids to the Gelation Process to the Silica Gel Characteristic Using Organic Silica. IOP Conference Series: Materials Science and Engineering *299*, 012049.

Rahman, N.A., Widhiana, I., Juliastuti, S.R., and Setyawan, H. (2015). Synthesis of mesoporous silica with controlled pore structure from bagasse ash as a silica source. Colloids and Surfaces A: Physicochemical and Engineering Aspects *476*, 1–7.

Ramos, A., Filtvedt, W., Lindholm, D., Ramachandran, P., Rodríguez, A., and Del Cañizo, C. (2015). Deposition reactors for solar grade silicon: A comparative thermal analysis of a Siemens reactor and a fluidized bed reactor. Journal of Crystal Growth *431*, 1–9.

Reis, A.A. dos, Protásio, T. de P., Melo, I.C.N.A. de, Trugilho, P.F., and Carneiro, A. de C.O. (2012). Wood composition and charcoal of Eucalyptus urophylla in different planting locations. Pesquisa Florestal Brasileira *32*, 277–299.

Ren, J., Kong, W., and Sun, R. (2014). Preparation of sugarcane bagasse/poly (acrylic acid-coacrylamide) hydrogels and their application. BioResources *9*, 3290–3303.

Reyes-Reyes, M., Kim, K., and Carroll, D.L. (2005). High-efficiency photovoltaic devices based on annealed poly (3-hexylthiophene) and 1-(3-methoxycarbonyl)-propyl-1-phenyl-(6, 6) C 61 blends. Applied Physics Letters *87*, 083506.

Rodríguez-Machín, L., Arteaga-Pérez, L.E., Pérez-Bermúdez, R.A., Casas-Ledón, Y., Prins, W., and Ronsse, F. (2018). Effect of citric acid leaching on the demineralization and thermal degradation behavior of sugarcane trash and bagasse. Biomass and Bioenergy *108*, 371–380.

Rodríguez-Machín, L., Arteaga-Pérez, L.E., Pala, M., Herregods-Van De Pontseele, K., PérezBermúdez, R.A., Feys, J., Prins, W., and Ronsse, F. (2019). Influence of citric acid leaching on the yield and quality of pyrolytic bio-oils from sugarcane residues. Journal of Analytical and Applied Pyrolysis *137*, 43–53.

Rovani, S., Santos, J.J., Corio, P., and Fungaro, D.A. (2018). Highly pure silica nanoparticles with high adsorption capacity obtained from sugarcane waste ash. ACS Omega *3*, 2618–2627.

Rovani, S., Santos, J.J., Coriob, P., and Fungaroa, D.A. (2019). An Alternative and Simple Method for the Preparation of Bare Silica Nanoparticles Using Sugarcane Waste Ash, an Abundant and Despised Residue in the Brazilian Industry. J. Braz. Chem. Soc *30*, 1524–1533.

Sadare, O.O. (2018). Development and Evaluation of Adsorption Coupling Biodesulphurization (ad/Bds) Process for the Desulphurization of South African Petroleum Distillates. PhD. University of the Witwatersrand.

Safarian, J., Tranell, G., and Tangstad, M. (2012). Processes for Upgrading Metallurgical Grade Silicon to Solar Grade Silicon. Energy Procedia *20*, 88–97.

Sales, A., and Lima, S.A. (2010). Use of Brazilian sugarcane bagasse ash in concrete as sand replacement. Waste Management *30*, 1114–1122.

Salinas, J., Salto, C., Maldonado, J., Ramos-Ortíz, G., Rodríguez, M., Meneses-Nava, M., Barbosa-García, O., Farfán, N., and Santillan, R. (2011). Organic solar cells under the BHJ approach using conventional/inverted architectures. (International Society for Optics and Photonics), p. 80117.

San, N.O., Kurşungöz, C., Tümtaş, Y., Yaşa, Ö., Ortac, B., and Tekinay, T. (2014). Novel onestep synthesis of silica nanoparticles from sugarbeet bagasse by laser ablation and their effects on the growth of freshwater algae culture. Particuology *17*, 29–35.

Sangster, A., Hodson, M., and Tubb, H. (2001). Silicon deposition in higher plants. In Studies in

Plant Science, (Elsevier), 85–113.

Santos, I., Goncalves, A., Santos, C.S., Almeida, M., Afonso, M., and Cruz, M.J. (1990). Purification of metallurgical grade silicon by acid leaching. Hydrometallurgy *23*, 237–246.

dos Santos, R.M.M., Gonçalves, R.G.L., Constantino, V.R.L., Santilli, C.V., Borges, P.D., Tronto, J., and Pinto, F.G. (2017). Adsorption of Acid Yellow 42 dye on calcined layered double hydroxide: Effect of time, concentration, pH and temperature. Applied Clay Science *140*, 132–139.

Sarti, D., and Einhaus, R. (2002). Silicon feedstock for the multi-crystalline photovoltaic industry. Solar Energy Materials and Solar Cells *72*, 27–40.

Savant, N.K., Korndörfer, G.H., Datnoff, L.E., and Snyder, G.H. (1999). Silicon nutrition and sugarcane production: a review. Journal of Plant Nutrition *22*, 1853–1903.

Scharber, M.C., and Sariciftci, N.S. (2013). Efficiency of bulk-heterojunction organic solar cells. Progress in Polymer Science *38*, 1929–1940.

Schettino, M.A.S., and Holanda, J.N.F. (2015). Characterization of Sugarcane Bagasse ash Waste for Its Use in Ceramic Floor Tile. Procedia Materials Science *8*, 190–196.

Scoones, I., Mavedzenge, B., and Murimbarimba, F. (2017). Sugar, People and Politics in Zimbabwe's Lowveld. Journal of Southern African Studies *43*, 567–584.

Şerbănoiu, A.A., Bărbuţă, M., Burlacu, A., and Grădinaru, C.M. (2017). Fly Ash Cement Concrete with Steel Fibers-Comparative Study. Environmental Engineering & Management Journal *16*, 1123–1128.

Shao, Y., Wang, J., Preto, F., Zhu, J., and Xu, C. (2012). Ash Deposition in Biomass Combustion or Co-Firing for Power/Heat Generation. Energies *5*, 5171–5189.

Shen, Y. (2017). Rice husk silica derived nanomaterials for sustainable applications. Renewable and Sustainable Energy Reviews *80*, 453–466.

Shi, L., Wang, W., Wang, A., Yuan, K., and Yang, Y. (2016). Understanding the impact mechanism of the thermal effect on the porous silicon anode material preparation via magnesiothermic reduction. Journal of Alloys and Compounds *661*, 27–37.

Shi, Y., Zhang, F., Hu, Y.-S., Sun, X., Zhang, Y., Lee, H.I., Chen, L., and Stucky, G.D. (2010). Low-temperature pseudomorphic transformation of ordered hierarchical macro-mesoporous SiO_2/C nanocomposite to SiC via magnesiothermic reduction. Journal of the American Chemical Society *132*, 5552–5553.

Shim, J., Velmurugan, P., and Oh, B.-T. (2015). Extraction and physical characterization of amorphous silica made from corn cob ash at variable pH conditions via sol gel processing. Journal of Industrial and Engineering Chemistry *30*, 249–253.

Shrotriya, V., Ouyang, J., Tseng, R.J., Li, G., and Yang, Y. (2005). Absorption spectra modification in poly (3-hexylthiophene): methanofullerene blend thin films. Chemical Physics Letters *411*, 138–143.

Sika, M., and Hardie, A. (2014). Effect of pine wood biochar on ammonium nitrate leaching and availability in a S outh A frican sandy soil. European Journal of Soil Science *65*, 113–119. Silva, D.A. (2019). The linear interdependence of superior calorific value as a function of immediate analysis in lignocellulosic materials. Dissertation. Federal University of São Carlos.

Sirirat, J., and Supaporn, W. (2010). Pozzolanic Activity of Industrial Sugar Cane Bagasse Ash. Suranaree Journal of Science and Technology *17*, 349–357.

Smith, D.D., Cudzinovic, M.J., McIntosh, K.R., and Mehta, B.G. (2006). Use of Doped Silicon Dioxide in the Fabrication of Solar Cells (Australia National University, Canberra).

Somorin, T., Sowale, A., Shemfe, M., Ayodele, A.S., and Kolios, A. (2019). Clean Technologies and Innovation in Energy. In Energy in Africa, (Springer), 149–197.

Souza, A., Teixeira, S., Santos, G., Costa, F., and Longo, E. (2011). Reuse of sugarcane bagasse ash (SCBA) to produce ceramic materials. Journal of Environmental Management *92*, 2774– 2780.

Stefanidis, S.D., Heracleous, E., Patiaka, D.T., Kalogiannis, K.G., Michailof, C.M., and Lappas, A.A. (2015). Optimization of bio-oil yields by demineralization of low quality biomass. Biomass and Bioenergy *83*, 105–115.

Streetman, B.G., and Banerjee, S. (1995). Solid state electronic devices (Englewood Cliffs, New Jersey: Prentice Hall International Editions).

Su, J., Gao, B., Chen, Z., Fu, J., An, W., Peng, X., Zhang, X., Wang, L., Huo, K., and Chu, P.K. (2016). Large-scale synthesis and mechanism of β-SiC nanoparticles from rice husks by lowtemperature magnesiothermic reduction. ACS Sustainable Chemistry & Engineering *4*, 6600–6607.

Takanezawa, K., Tajima, K., and Hashimoto, K. (2008). Efficiency enhancement of polymer photovoltaic devices hybridized with ZnO nanorod arrays by the introduction of a vanadium oxide buffer layer. Applied Physics Letters *93*, 297.

Tan, Z., Zhu, T., Thein, M., Gao, S., Cheng, A., Zhang, F., Zhang, C., Su, H., Wang, J., and Henderson, R. (2009). Integration of planar and bulk heterojunctions in polymer/nanocrystal hybrid photovoltaic cells. Applied Physics Letters *95*, 063510.

Tao, M. (2008). Inorganic photovoltaic solar cells: silicon and beyond. The Electrochemical Society Interface *17*, 30–35.

Tchakouté, H.K., Rüscher, C.H., Hinsch, M., Djobo, J.N.Y., Kamseu, E., and Leonelli, C.

(2017). Utilization of sodium waterglass from sugar cane bagasse ash as a new alternative hardener for producing metakaolin-based geopolymer cement. Chemie Der Erde-Geochemistry *77*, 257–266.

Teixeira, S.R., De Souza, A.E., de Almeida Santos, G.T., Vilche Pena, A.F., and Miguel, A.G. (2008). Sugarcane bagasse ash as a potential quartz replacement in red ceramic. Journal of the American Ceramic Society *91*, 1883–1887.

Teixeira, S.R., Magalhaes, R. da S., Arenales, A., Souza, A.E. de, Romero, M., and Rincón, Jm. (2014). Valorization of sugarcane bagasse ash: producing glass-ceramic materials. Journal of Environmental Management *134*, 15–19.

Temuujin, J., Okada, K., and MacKenzie, K.J. (2003). Preparation of porous silica from vermiculite by selective leaching. Applied Clay Science *22*, 187–195.

Thuc, C.N.H., and Thuc, H.H. (2013). Synthesis of silica nanoparticles from Vietnamese rice husk by sol–gel method. Nanoscale Research Letters *8*, 58.

To, T.Q., Kenny, C., Cheong, S., and Aldous, L. (2017). Carbon dioxide as a pH-switch antisolvent for biomass fractionation and pre-treatment with aqueous hydroxide solutions. Green Chemistry *19*, 2129–2134.

Torres-Agredo, J., Mejía de Gutiérrez, R., Escandón Giraldo, C., and González Salcedo, L. (2014). Characterization of sugar cane bagasse ash as supplementary material for Portland cement. Ingeniería e Investigación *34*, 5–10.

Tress, W., Leo, K., and Riede, M. (2011). Influence of hole-transport layers and donor materials on open-circuit voltage and shape of I–V curves of organic solar cells. Advanced Functional Materials *21*, 2140–2149.

Tripathi, D.K., Singh, V.P., Ahmad, P., Chauhan, D.K., and Prasad, S.M. (2016). Silicon in

Plants: Advances and Future Prospects (India: CRC Press).

Tsang, S., Fu, H., Wang, R., Lu, J., Yu, K., and Tao, Y. (2009). Highly efficient cross-linked PbS nanocrystal/C 60 hybrid heterojunction photovoltaic cells. Applied Physics Letters *95*, 183505.

Tsuboi, Y., Ura, S., Takahiro, K., Henmi, T., Okada, A., Wakasugi, T., and Kadono, K. (2017). Magnesiothermic reduction of silica glass substrate—Chemical states of silicon in the generated layers. Journal of Asian Ceramic Societies *5*, 341–349.

Tuck, C.O., Pérez, E., Horváth, I.T., Sheldon, R.A., and Poliakoff, M. (2012). Valorization of biomass: deriving more value from waste. Science *337*, 695–699.

Ulum, S., Holmes, N., Darwis, D., Burke, K., Kilcoyne, A.D., Zhou, X., Belcher, W., and Dastoor, P. (2013). Determining the structural motif of P3HT: PCBM nanoparticulate organic photovoltaic devices. Solar Energy Materials and Solar Cells *110*, 43–48.

Umamaheswaran, K., and Batra, V.S. (2008). Physico-chemical characterisation of Indian biomass ashes. Fuel *87*, 628–638.

Usman, A., Raji, A., Waziri, N., and Hassan, M. (2014). A study on silica and alumina potential of the savannah bagasse ash. IOSR Journal of Mechanical and Civil Engineering *11*, 48–52.

Uzum, A., Kanda, H., Fukui, H., Izumi, T., Harada, T., and Ito, S. (2017). Totally Vacuum-Free Processed Crystalline Silicon Solar Cells over 17.5% Conversion Efficiency. (Multidisciplinary Digital Publishing Institute), 42.

Vaibhav, V., Vijayalakshmi, U., and Roopan, S.M. (2015). Agricultural waste as a source for the production of silica nanoparticles. Spectrochimica Acta Part A: Molecular and Biomolecular Spectroscopy *139*, 515–520.

Van Bavel, S.S., Bärenklau, M., de With, G., Hoppe, H., and Loos, J. (2010). P3HT/PCBM bulk heterojunction solar cells: impact of blend composition and 3D morphology on device performance. Advanced Functional Materials *20*, 1458–1463.

Venkateswaran, S., Yuvakkumar, R., and Rajendran, V. (2013). Nano silicon from nano silica using natural resource (RHA) for solar cell fabrication. Phosphorus, Sulfur, and Silicon and the Related Elements *188*, 1178–1193.

Vieira, A. (2012). Caracterização Da Biomassa Proveniente De Resíduos Agrícolas. Dissertation. Western State University of Paraná.

Villar-Cociña, E., Morales, E.V., Santos, S.F., Savastano Jr, H., and Frías, M. (2011). Pozzolanic behavior of bamboo leaf ash: Characterization and determination of the kinetic parameters. Cement and Concrete Composites *33*, 68–73.

VonderHaar, G. (2017). Efficiency of Solar Cell Design and Materials. Missouri S&T's Peer to Peer *1*, 7.

Vons, V.A., de Smet, L.C., Munao, D., Evirgen, A., Kelder, E.M., and Schmidt-Ott, A. (2011). Silicon nanoparticles produced by spark discharge. Journal of Nanoparticle Research *13*, 4867.

Wang, L., Lu, A., Wang, C., Zheng, X., Zhao, D., and Liu, R. (2006). Nano-fibriform production of silica from natural chrysotile. Journal of Colloid and Interface Science *295*, 436–439.

Wang, L., Liu, Y., Jiang, X., Qin, D., and Cao, Y. (2007). Enhancement of photovoltaic characteristics using a suitable solvent in hybrid polymer/multiarmed CdS nanorods solar cells. The Journal of Physical Chemistry C *111*, 9538–9542.

Wang, T., Zhu, J., Chen, Y., Yang, H., Qin, Y., Li, F., Cheng, Q., Yu, X., Xu, Z., and Lu, B. (2017). Large-scale production of silicon nanoparticles@ graphene embedded in nanotubes as ultra-robust battery anodes. Journal of Materials Chemistry A *5*, 4809–4817.

Wang, Z.-M., Wang, W., Coombs, N., Soheilnia, N., and Ozin, G.A. (2010). Graphene oxide−periodic mesoporous silica sandwich nanocomposites with vertically oriented channels. Acs Nano *4*, 7437–7450.

Woodhouse, M.A., Smith, B., Ramdas, A., and Margolis, R.M. (2019). Crystalline Silicon Photovoltaic Module Manufacturing Costs and Sustainable Pricing: 1H 2018 Benchmark and Cost Reduction Road Map (National Renewable Energy Lab.(NREL), Golden, CO (United States)).

Worathanakul, P., Payubnop, W., and Muangpet, A. (2009). Characterization for post-treatment effect of bagasse ash for silica extraction. World Academy of Science, Engineering and Technology *3*, 339–341.

Wu, H., Zheng, G., Liu, N., Carney, T.J., Yang, Y., and Cui, Y. (2012). Engineering empty space between Si nanoparticles for lithium-ion battery anodes. Nano Letters *12*, 904–909.

Würfel, U., Neher, D., Spies, A., and Albrecht, S. (2015). Impact of charge transport on current–voltage characteristics and power-conversion efficiency of organic solar cells. Nature Communications *6*, 6951.

Xi, F., Li, S., Ma, W., Ding, Z., Lei, Y., Chen, Z., Wei, K., Xie, K., and Wu, J. (2018). Removal of impurities from metallurgical grade silicon with metal assisted chemical leaching. Hydrometallurgy *178*, 250–255.

Xie, J., Wang, G., Huo, Y., Zhang, S., Cao, G., and Zhao, X. (2014). Nanostructured silicon spheres prepared by a controllable magnesiothermic reduction as anode for lithium ion batteries. Electrochimica Acta *135*, 94–100.

Xing, A., Tian, S., Tang, H., Losic, D., and Bao, Z. (2013). Mesoporous silicon engineered by the reduction of biosilica from rice husk as a high-performance anode for lithium-ion batteries. RSC Advances *3*, 10145–10149.

Xu, Q., Ji, T., Gao, S.-J., Yang, Z., and Wu, N. (2019). Characteristics and Applications of Sugar Cane Bagasse Ash Waste in Cementitious Materials. Materials *12*, 39.

Yan, D., Phang, S.P., Wan, Y., Samundsett, C., Macdonald, D., and Cuevas, A. (2019). High efficiency n-type silicon solar cells with passivating contacts based on PECVD silicon films doped by phosphorus diffusion. Solar Energy Materials and Solar Cells *193*, 80–84.

Yang, J., Tang, A., Zhou, R., and Xue, J. (2011). Effects of nanocrystal size and device aging on performance of hybrid poly (3-hexylthiophene): CdSe nanocrystal solar cells. Solar Energy Materials and Solar Cells *95*, 476–482.

Yang, L., Yan, L., and You, W. (2013). Organic solar cells beyond one pair of donor–acceptor: ternary blends and more. The Journal of Physical Chemistry Letters *4*, 1802–1810.

Yang, Y.M., Chen, W., Dou, L., Chang, W.-H., Duan, H.-S., Bob, B., Li, G., and Yang, Y. (2015). High-performance multiple-donor bulk heterojunction solar cells. Nature Photonics *9*, 190.

Yao, X., Zhou, H., Xu, K., Xu, Q., and Li, L. (2019). Evaluation of the Fusion and Agglomeration Properties of Ashes from Combustion of Biomass, Coal and Their Mixtures and the Effects of K_2CO_3 Additives. Fuel *255*, 115829.

Yao, X., Zhou, H., Xu, K., Xu, Q., and Li, L. (2020). Investigation on the Fusion Characterization and Melting Kinetics of Ashes from Co-Firing of Anthracite and Pine Sawdust. Renewable Energy *145*, 835–846.

Yasar, A., Shabbir, S.A., Tabinda, A.B., Nazar, M., Rasheed, R., Malik, A., and Mukhtar, S. (2019). Refuse-derived fuels as a renewable energy source in comparison to coal, rice husk, and

sugarcane bagasse. Energy Sources, Part A: Recovery, Utilization, and Environmental Effects *41*, 564–572.

Yasuda, K., Nohira, T., Kobayashi, K., Kani, N., Tsuda, T., and Hagiwara, R. (2013). Improving Purity and Process Volume During Direct Electrolytic Reduction of Solid SiO_2 in Molten $CaCl_2$ for the Production of Solar-Grade Silicon. Energy Technology *1*, 245–252.

Yin, C.Y., Aroua, M.K., and Daud, W.M.A.W. (2007). Review of modifications of activated carbon for enhancing contaminant uptakes from aqueous solutions. Separation and Purification Technology *52*, 403–415.

Yoon, W.-J., Jung, K.-Y., Liu, J., Duraisamy, T., Revur, R., Teixeira, F.L., Sengupta, S., and Berger, P.R. (2010). Plasmon-enhanced optical absorption and photocurrent in organic bulk heterojunction photovoltaic devices using self-assembled layer of silver nanoparticles. Solar Energy Materials and Solar Cells *94*, 128–132.

Yoshikawa, K., Kawasaki, H., Yoshida, W., Irie, T., Konishi, K., Nakano, K., Uto, T., Adachi, D., Kanematsu, M., and Uzu, H. (2017). Silicon heterojunction solar cell with interdigitated back contacts for a photoconversion efficiency over 26%. Nature Energy *2*, 17032.

Yu, P., Wu, J., Liu, S., Xiong, J., Jagadish, C., and Wang, Z.M. (2016). Design and fabrication of silicon nanowires towards efficient solar cells. Nano Today *11*, 704–737.

Zamani, A., Marjani, A.P., and Mousavi, Z. (2019). Agricultural Waste Biomass-Assisted Nanostructures: Synthesis and Application. Green Processing and Synthesis *8*, 421–429. Zhang, J., Wang, A., and Ingle, N.K. (2017). Selective Etch for Silicon Films (Applied Materials, Inc., California).

Zhang, S., Shao, J., Hoi, L., Wu, S., Zhu, B., Fan, S., Li, H., and Yu, D. (2005). Amorphousnesslike nature of nano-crystalline polar semiconductors. Physica Status Solidi (c) *2*, 3090–3095. Zhao, S.,

Pi, X., Mercier, C., Yuan, Z., Sun, B., and Yang, D. (2016). Silicon-nanocrystalincorporated ternary hybrid solar cells. Nano Energy *26*, 305–312.

Zhao, C.-X., Huang, Y., Wang, J.-Q., Niu, C.-Y., and Jia, Y. (2019). Prediction of a new direct-gap silicon phase: T36 silicon. Physics Letters A *383*, 125903.

Zhou, Y., Eck, M., Veit, C., Zimmermann, B., Rauscher, F., Niyamakom, P., Yilmaz, S., Dumsch, I., Allard, S., and Scherf, U. (2011). Efficiency enhancement for bulk-heterojunction hybrid solar cells based on acid treated CdSe quantum dots and low bandgap polymer PCPDTBT. Solar Energy Materials and Solar Cells *95*, 1232–1237.

Zhu, L., Wang, L., Pan, C., Chen, L., Xue, F., Chen, B., Yang, L., Su, L., and Wang, Z.L. (2017). Enhancing the efficiency of silicon-based solar cells by the piezo-phototronic effect. ACS Nano *11*, 1894–1900.

Zhu, X., Monahan, N.R., Gong, Z., Zhu, H., Williams, K.W., and Nelson, C.A. (2015). Charge transfer excitons at van der Waals interfaces. Journal of the American Chemical Society *137*, 8313–8320.

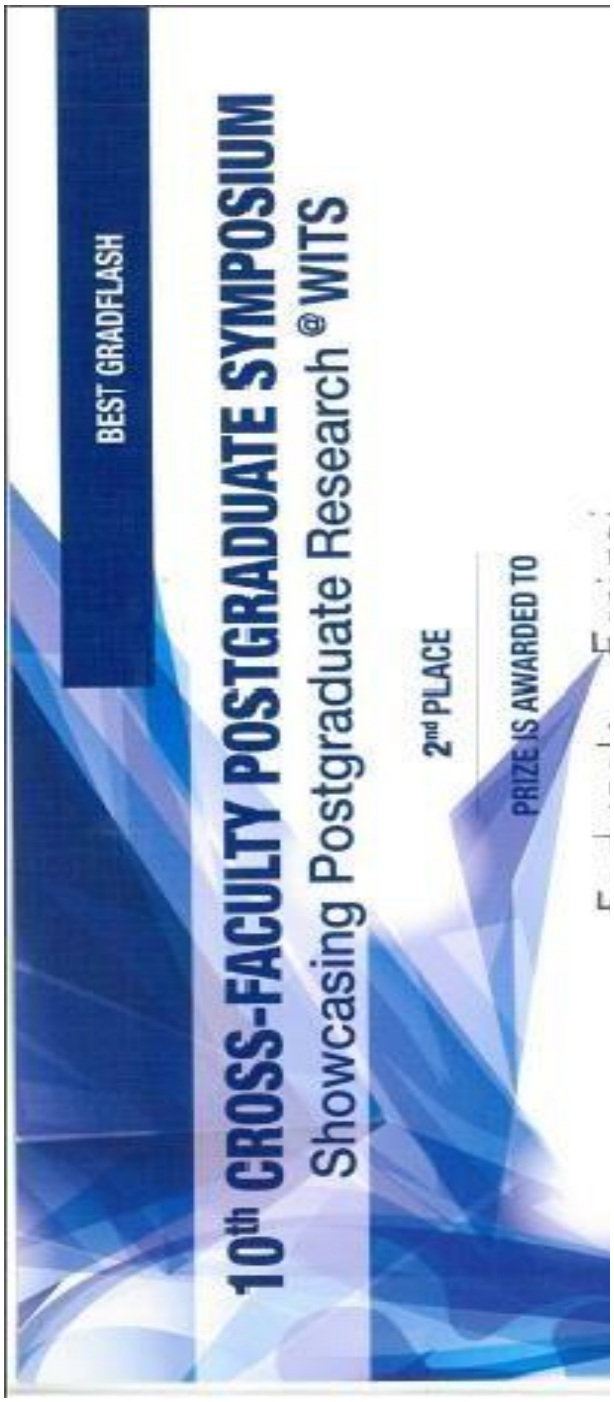
Zong, L., Zhu, B., Lu, Z., Tan, Y., Jin, Y., Liu, N., Hu, Y., Gu, S., Zhu, J., and Cui, Y. (2015). Nanopurification of silicon from 84% to 99.999% purity with a simple and scalable process. Proceedings of the National Academy of Sciences *112*, 13473–13477.

Zulehner, W. (2000). Historical overview of silicon crystal pulling development. Materials Science and Engineering: B *73*, 7–15.

Zulehner, W., Neuer, B., and Rau, G. (2000). Silicon. In Ullmann's Encyclopedia of Industrial Chemistry, (Germany: Wiley-VCH Verlag GmbH & Co. KGaA)

Appendices

8.1 Appendix 1



1660060:PRODUCTION_OF_NANO_SILICON_PARTICLES_FR.

ORIGINALITY REPORT

19%	12%	10%	7%
SIMILARITY INDEX	INTERNET SOURCES	PUBLICATIONS	STUDENT PAPERS

PRIMARY SOURCES

1	Elangovan Hemaprabha, Upendra K. Pandey, Kamanio Chattopadhyay, Praveen C. Ramamurthy. "Doped silicon nanoparticles for enhanced charge transportation in organic-inorganic hybrid solar cells", Solar Energy, 2018 Publication	2%
2	www.etaflorence.it Internet Source	1%
3	www.tandfonline.com Internet Source	1%
4	repository.up.ac.za Internet Source	1%
5	mobile.wiredspace.wits.ac.za Internet Source	1%
6	Kui-Qing Peng, Xin Wang, Li Li, Xiao-Ling Wu, Shuit-Tong Lee. "High-Performance Silicon Nanohole Solar Cells", Journal of the American Chemical Society, 2010 Publication	<1%